The expression pattern, prognostic significance and pharmacologic targeting of the eukaryotic translation initiation factor 2α in head and neck squamous cell carcinoma

Inauguraldissertation
zur Erlangung des Grades eines Doktors der Medizin des Fachbereichs Medizin
der Justus-Liebig-Universität Gießen

vorgelegt von Cyran, Anna Maria aus Kattowitz, Polen

Gießen, 2024

Aus dem Fachbereich Medizin der Justus-Liebig-Universität Gießen

Zentrum für Hals-, Nasen- und Ohrenheilkunde

Betreuer: Univ.-Prof. Dr. med. habil. Christoph Arens

Gutachterin: Prof. Dr. med. Ulrike Bockmühl

Tag der Disputation: 01.04.2025

List of Contents

1.0 Introduction 1
1.1 Epidemiology and Survival Trends 2
1.2 Risk Factors 6
1.2.1 Alcohol and Tobacco Consumption 6
1.2.2. HPV Infection 7
1.2.3 Other Oncogenic Viruses 9
1.2.4 Other Risk Factors 9
1.3 Pathophysiology of Carcinogen-Associated HNSCC 10
1.3.1 Cytogenetic Model of HNSCC Progression 12
1.4 HPV-Driven Carcinogenesis 13
1.4.1. The Genetic Landscape of HPV+ HNSCC 14
1.5 Staging of HNSCC 15
1.6 Therapy of HNSCC 16
1.6.1 Treatment of Early Disease 16
1.6.2 Treatment of Locoregionally Advanced Disease (Stages III and IV) 17
1.6.3 Treatment of Recurrent and Metastatic Disease 18
1.6.4. Treatment of HPV+ OPSCC 18
1.7 Selected Therapeutic Agents 19
1.7.1 Cisplatin 19
1.7.2 Paclitaxel 19
1.7.3 5-Fluorouracil 20
1.8 Non-Oncogene Addiction of Cancers as a Potential Strategy for Drug Development 20
1.8.1 The Eukaryotic Initiation Factor 2α- the Integrator of Stress Signaling and Translation 21
1.9 Study Aim 23
2.0 Material and Methods 24
2.1 Collection of Samples and Ethics statement 24
2.2 Bioinformatic Analysis of *EIF2S1* Expression 24
2.2.1 RNA Expression Analysis 24
2.2.2. The Analysis of Protein Expression 27
2.3 Histological assessment and Immunohistochemistry (IHC) 27
2.4 Western Blot 29

2.4.1 Preparation of Lysates from Intraoperative Tissue Samples 29
2.4.2 Preparation of Cell Culture Lysates..... 30
2.4.3 Gel Electrophoresis and Protein Transfer onto PVDF Membranes..... 30
2.4.4 Chemiluminescent Detection and Analysis of Western Blot Images 32
2.5 Cell Culture and Preparation of Stock Solutions..... 32
2.6 Viability Testing and Calculation of Drug Synergies 33
2.7 Colony Formation Assay 34
2.8 Cell Death and Cell Cycle Analysis with Flow Cytometry 34
2.9 Chemosensitivity Testing of HNSCC Patient-Derived 3D Spheroids (PD3DS).. 34
3.0 Results..... 36
3.1 mRNA Transcripts of EIF2 Complex Members are Overexpressed in HNSCC.. 36
3.2 Elevated *EIF2S1* Gene Expression is Associated with Shorter OS and DFS Survival in HNSCC 42
3.3 Elevated *EIF2S1* Expression in HNSCC is Associated with Clinicopathological Features Indicating Disease Aggressiveness and Severity 45
3.4 eIF2S1 Expression in HPV-Positive and -Negative HNSCC 46
3.5 Drivers of *EIF2S1* Overexpression in HNSCC 49
3.5.1 Structural Gene Alterations 49
3.5.2 Chromosomal Co-localization Determines EIF Cluster Expression in HNSCC 50
3.5.3 DNA Methylation 53
3.6 Protein Levels of EIF2 Complex Members are Elevated in HNSCC..... 55
3.7 eIF2α Protein Abundance is Elevated in Immunohistochemically Stained HNSCC Tissue Samples 61
3.8 eIF2α Protein Expression in Relation to HPV Infection..... 63
3.9 eIF2α Abundance Increases with Malignant Progression 64
3.10 eIF2α Abundance and Phosphorylation in Freshly Frozen Intraoperative Patient Samples..... 68
3.11 EIF2 Complex Members are Essential for HNSCC Survival *in vitro* 70
3.12 Treatment with an eIF2α Phosphorylation Inhibitor Decreases Cell Viability and Clonogenic Survival *in vitro* by Disrupting Cell Cycle Progression..... 71
3.13 Salubrinal Decreases the Viability of Patient-Derived 3D Tumor Spheroids (PD3DS) and Enhances the Cytotoxicity of Selected Chemotherapeutics..... 77

4.0 Discussion 84
4.1 Characterization of *EIF2S1* Gene and Protein Expression 84
4.2 Drivers of *EIF2S1* Expression 84
4.3 The effects of eIF2α expression and phosphorylation on carcinogenesis 85
4.4 Pharmacological Modification of EIF2α Phosphorylation 86
4.5 The Effects of eIF2α Hyperphosphorylation on Cell Cycle 87
4.6 Salubrinal Synergizes with Genotoxic Drugs in HNSCC 88
4.7 Cytoprotective Properties of Salubrinal in Cisplatin-Induced Ototoxicity 90
5.0 Conclusion 91
Zusammenfassung 93
List of Tables 95
List of Figures 96
List of Abbreviations and Symbols: 99
References: 105
Supplement List: i

1.0 Introduction

Head and neck squamous cell carcinoma (HNSCC) is a heterogeneous group of tumors arising from the mucosal epithelium of the oral cavity, nasopharynx (epipharynx), oropharynx, larynx and hypopharynx (Chow, 2020). Over 90% of cancers in this anatomic region are squamous and arise from the stratified epithelium (Gatta et al., 2015). Figure 1 illustrates the anatomical sites of HNSCC development and its typical histological features. Briefly, the oral cavity is subdivided into the following locations: the lip and buccal mucosa, the hard palate, the anterior tongue, the floor of the mouth and the retromolar trigone. The oropharynx includes the lingual and palatine tonsils, the base of the tongue, the soft palate, the uvula and the posterior pharyngeal wall, while the hypopharynx extends from the hyoid bone to the cricoid cartilage. (Johnson et al., 2020). Most structures of the upper aerodigestive tract are lined with stratified squamous epithelium supported by lamina propria and the contiguous basement membrane, which determines differentiation, migration, and serves as a barrier for tumor invasion.

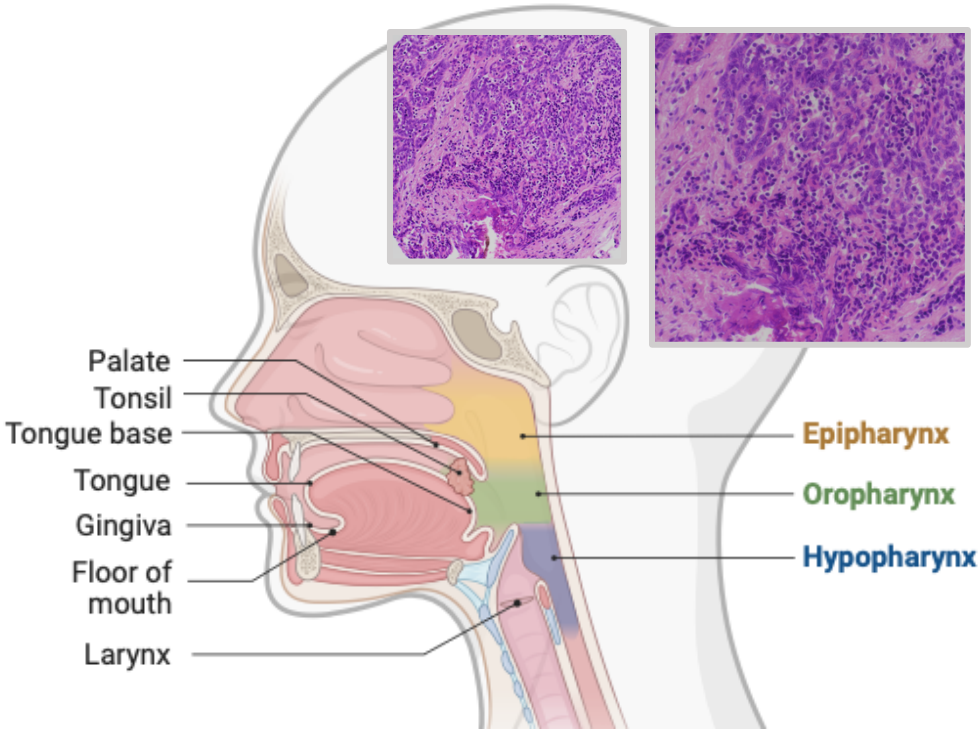

Figure 1. Schematic illustration of the anatomical sites of HNSCC development. The photomicrographs of H&E sections (20x and 40x magnification respectively) shown in the insets represent the typical histopathological features of HNSCC- nests of squamous cells with pink cytoplasm and keratinization set against fibrous stroma.

A noteworthy exception is the tonsillar mucosa, situated in close proximity to the lymphoid tissue of the Waldeyer's ring, which serves as the first line of protection against antigens. The tonsillar epithelium has multiple crypts lined with unique reticulated squamous epithelium, facilitating the transport of antigens to the lymphoid tissue. Its basal cell layer is incomplete, and the supporting basement membrane is porous, allowing the passage of immune cells. Such cytoarchitecture of tonsillar epithelium renders it particularly vulnerable to viral infection, as discussed in greater detail in a dedicated section below (Pai & Westra, 2009). Typical HNSCC is characterized by nests of squamous cells with pink cytoplasm and sparse intercellular bridges, keratin pearls, surrounded fibrous stroma, although different histological variants exist (verrucous, basaloid and spindle-cell). The microscopic appearance varies with the degree of differentiation, yet prototypic HNSCC is moderately differentiated (Pai & Westra, 2009). Nasopharyngeal squamous cell carcinomas are characterized by distinct clinical and epidemiological features (Wong et al., 2021). They are included in the statistical and epidemiological overview presented below but are not discussed in the body of this work.

1.1 Epidemiology and Survival Trends

HNSCC ranks as the 8th most common cancer entity worldwide, with an annual incidence of 878 348 new cases; it is also the 9th deadliest cancer overall, leading to 444 347 deaths each year (Sung et al., 2021). Table 1 summarizes the number of deaths and newly diagnosed cases in each anatomic site within the head and neck and relates it to the total number of deaths and new cancer cases worldwide. The incidence risk of HNSCC is three to four times higher in men than in women for most sites and a staggering seven times higher for laryngeal cancer. Table 2 provides a global overview of the incidence and mortality of HNSCC in both sexes. The incidence of HNSCC is projected to continue to rise and reach 1.29 million new cases between 2020 and 2040. The reasons for this trend are twofold. In North America and Europe, the prevalence of human papillomavirus-(HPV) associated cancers is surging. While, in countries with low human development index, carcinogen-induced HNSCC are expected to increase in prevalence with a disproportionately higher rise in mortality. The risk of HNSCC increases with age and the median age at diagnosis for carcinogen-related HNSCC is 66. HPV-related disease is seen in younger patients with a median age of 53 (Johnson et al., 2020). Figure 2 illustrates projected trends in HNSCC incidence worldwide; Figure 3 describes the projections in more detail for selected European countries.

The survival rates vary significantly depending on the tumor site, stage at diagnosis and geographic location. According to the data collected by the American National Cancer Institute (NCI), in the early 2000s, the 5-year overall survival (OS) for all HNSCC has improved from 54.7% to 65.9%.

The OS increased drastically for locally advanced disease, especially cancers originating in the tonsil, tongue and oral cavity, reaching 69.8, 64.9 and 62.9%, respectively. However, little to no improvement was observed in the large groups of patients with cancers localized in the oropharynx, hypopharynx and larynx. Lip cancer was the most prognostically favorable, with an OS rate consistently exceeding 90% (Pulte & Brenner, 2010). In Europe in the early 2000s, the 5-year OS was poorest for hypopharyngeal cancers- 25% and best for larynx- 59%. The outcomes were better in women than men. Between 1999-2007 the survival rates improved for all cancer sites except the larynx where they remained unchanged (Gatta et al., 2015). The described improvement in patient outcomes is, at least in part, attributed to the emergence of HPV-associated cancers, which are seen in a younger population with fewer comorbidities and respond well to radiotherapy. In Germany, in 2012, the adjusted survival rate (ASR) per 100 000 of HNSCC amounted to 20.4 among men, placing it as the 6th most common cancer overall. The same statistical measure among women equaled 7.09, making it the 12th most common malignancy (Pulte & Brenner, 2010). In addition to the disease-specific mortality, HNSCC is associated with a significant negative impact on patient quality of life and a very high suicide rate among survivors (Osazuwa-Peters, Simpson, et al., 2018).

	New cases annually (%)	Deaths annually (%)
Lip/Oral cavity	377 713 (2)	177 757 (1.8)
Larynx	184 615 (1)	99 840 (1)
Nasopharynx	133 354 (0.7)	80 008 (0.8)
Oropharynx	98 412 (0.5)	48 143 (0.5)
Hypopharynx	84 254 (0.4)	38 599 (0.4)
HNSCC all sites	**878 348 (4.85)**	**444 347 (4.49)**
All cancers	18 094 716 (100)	9 894 402 (100)

Table 1. Global incidence and mortality of HNSCC with subdivision into anatomic sites, excluding non-melanoma skin cancer. Data extracted from GLOBOCAN 2020*

	Incidence		Mortality	
	Women	**Men**	**Women**	**Men**
Lip/Oral cavity	113 502	264 211	52 735	125 022
Larynx	24 350	160 265	14 489	85 351
Nasopharynx	36 983	96 371	21 914	58 094
Oropharynx	19 367	79 045	8 553	39 590
Hypopharynx	14 000	70 254	6 296	32 303
HNSCC all sites	**208 202**	**670 146**	**103 987**	**340 360**
All cancers	8 751 759	9 342 957	4 403 188	5 491 214

Table 2. Global incidence and mortality of HNSCC among men and women, with subdivision into individual anatomic sites, excluding non-melanoma skin cancer. Data extracted from GLOBOCAN 2020*.

* Global Cancer Observatory: Cancer Today. Lyon, France: International Agency for Research on Cancer. Retrieved 23 October 2023 from: https://gco.iarc.fr/today.

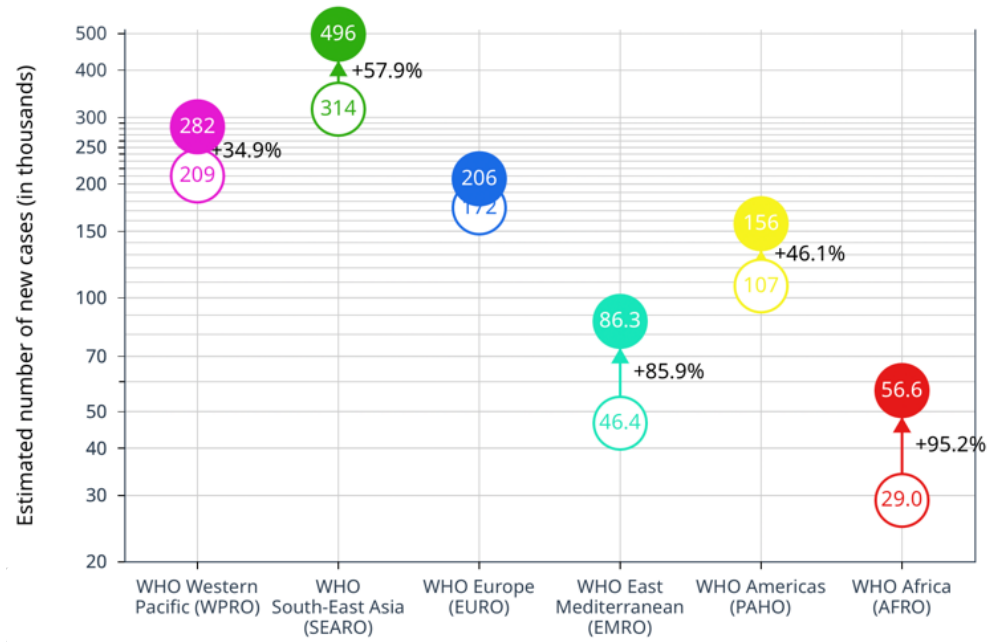

Figure 2. Projected increase in the incidence of HNSCC worldwide from 2020 to 2040. The estimated number of new cases is represented in thousands. Data extracted from GLOBOCAN 2020*.

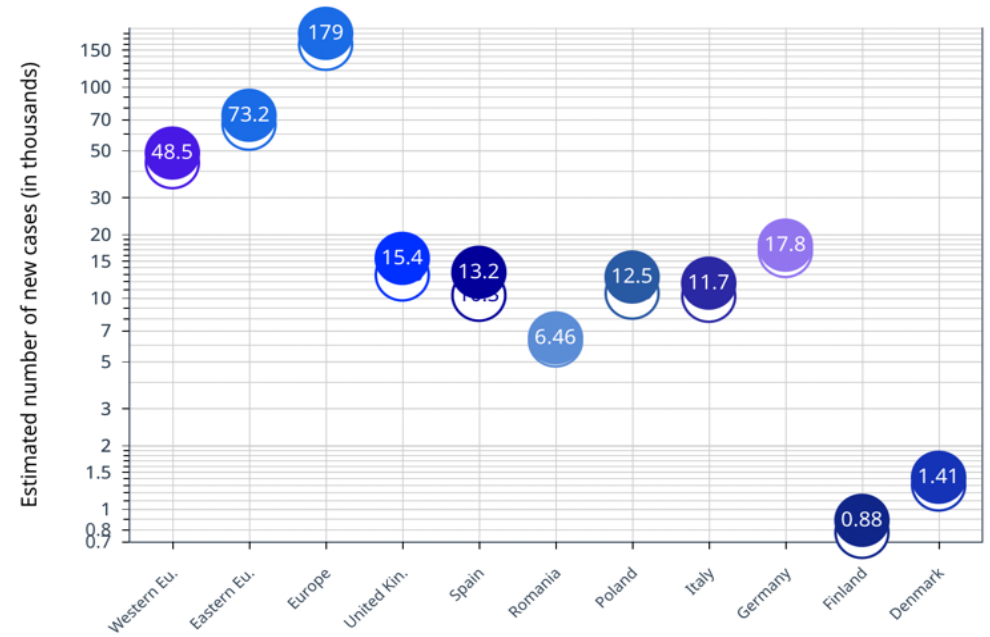

Figure 3. Projected increase in the incidence of HNSCC in selected European countries from 2020 to 2040. The estimated number of new cases is represented in thousands. Data extracted from GLOBOCAN 2020*.

1.2 Risk Factors

The most common risk factors for HNSCC are tobacco use, alcohol consumption and viral infection with oncogenic subtypes of HPV in oral and oropharyngeal cancers, as well as Epstein-Barr Virus (EBV) in nasopharyngeal cancers. These 4 factors are classified by the International Agency for Research on Cancer (IARC) as carcinogenic to humans (group 1 carcinogens) (Cogliano et al., 2011).

1.2.1 Alcohol and Tobacco Consumption

Alcohol is metabolized to acetaldehyde, which binds DNA, proteins and other cellular components, exerting both mutagenic and carcinogenic effects. The process of alcohol metabolism *per se* also increases oxidative stress, further amplifying DNA damage. All types of alcoholic beverages increase the risk of cancer, and the effects are dose-dependent. Ethanol also increases mucosal permeability to other toxicants (LoConte et al., 2017). The risk is highest for tissues directly exposed. In dedicated studies, even low alcohol consumption was associated with an elevated cancer risk (Bagnardi et al., 2013). Moderate alcohol use increased the relative risk of HNSCC in the oral cavity and oropharynx (1.83x) and larynx (1.44x). Heavy drinking increased the risk further to 5.13x and 2.65x for the same anatomic sites, respectively (Bagnardi et al., 2013). In a series of studies, Hashibe (Hashibe et al., 2007, 2009) reached similar conclusions: alcohol consumption exceeding three drinks per day independently increases the risk of HNSCC development with an odds ratio of 2 and has a potentiating effect with tobacco. Frequent and prolonged use of alcohol-based mouthwash was also reported to increase the risk of oral and oropharyngeal cancer marginally (Boffetta et al., 2016; Wilson & Conway, 2016).

Smoking tobacco in various forms (including cigarettes, cigars, pipes, waterpipes), as well as consumption of smokeless forms (e. g. snuff, chew) is carcinogenic. Polycyclic aromatic hydrocarbons, nitrosamines, other toxins and their metabolites are proteo- and genotoxic (United States Centers for Disease Control and Prevention et al., 2010). The dose-response effect is best illustrated by data on cigarette smoking. Accordingly, the risk of developing HNSCC increases with the number of cigarettes per day and the number of smoking years. Heavy smoking exceeding 10 cigarettes/day for over 30 years increases the odds ratio more than fourfold, yet even moderate cigarette consumption of 1- 3 cigarettes/day over 30 years leads to an increased cancer risk (Berthiller et al., 2016). The same trend was seen for chewing of different tobacco preparations (Gholap et al., 2023).

Both alcohol consumption and smoking continue to be negative prognostic factors in patients with a diagnosed HNSCC and increase the mortality rate (Beynon et al., 2018; Giraldi et al., 2017; Osazuwa-Peters, Adjei Boakye, et al., 2018). Conversely, smoking cessation upon diagnosis improves therapy response, reduces the risk of recurrence and prolongs survival (Krutz et al., 2022).

A pooled analysis of data by the International Head and Neck Cancer Epidemiology Consortium revealed carcinogenic effects of passive smoking, with an odds ratio of 1.55-1.6 in individuals exposed to smoke for over 15 years (Lee et al., 2008). Similar results were obtained in a large case-control study on a US-American population, whereby exposure to passive smoke in childhood was associated with an increased risk of HNSCC (odds ratio: 1.28) (Troy et al., 2013).

While users of electronic cigarettes are exposed to fewer toxicants than smokers and likely experience a lower risk of cancer, the long-term health effects of electronic cigarettes are underexplored. Several *in vitro* studies have suggested mutagenic, cytotoxic and carcinogenic effects of substances in e-cigarettes. There is a lack of evidence on human subjects with a long follow-up to evaluate the cancer risk in e-cigarette users versus non-users (Szukalska et al., 2020).

1.2.2. HPV Infection

The viral infection is sexually transmitted via orogenital contact. The resulting subtype of oropharyngeal cancer develops mostly in the tonsils, tongue base, soft palate and uvula, is biologically distinct and has a favorable prognosis (Chow, 2020). The WHO currently classifies 14 HPV types as high risk (hrHPV): 16, 18, 31, 33, 35, 39, 45, 51, 52, 56, 58, 59, 66 and 68 (Lechner et al., 2022). The assessment of HPV status is possible with various methods, including techniques based on the polymerase chain reaction (PCR) characterized by high sensitivity but a high rate of false-positive results due the detection of endemic infections and more specific but less sensitive *in situ* hybridization methods. A clinically useful, indirect method for HPV detection is immunohistochemical staining of P16 protein in tissue samples (Hayes et al., 2015).

An analysis of over 5000 specimens from 60 geographically diverse studies revealed an overall HPV prevalence of 25.9% across all HNSCC sites. This proportion was higher in oropharyngeal cancer 35.6%. HPV+ oropharyngeal squamous cell carcinoma (OPSCC) is seen much more frequently in men than in women, owing to a higher incidence of persistent HPV infections. Almost 87% of HPV+ OPSCC are caused by HPV16. In

contrast, HPV18 was rare in the oropharynx (2.8%) and relatively more common in the oral cavity and larynx (17% and 13%, respectively) (Kreimer et al., 2005). Occasionally, other types- HPV 31, 33, 45, 52 and 58, were identified (de Sanjosé et al., 2018).

The prevalence of HPV-associated HNSCC outside of the oropharynx reported in the literature varies significantly. Most studies describe small groups and so fail to accurately depict the disease characteristics and a possible difference in prognosis. A systematic review of the literature revealed the following weighted prevalence of HPV infections (based on HPV DNA detection): oral cavity 20.2%; larynx 23,6% and ca. 30% in sinonasal and nasopharyngeal cancers (Isayeva et al., 2012). A study by Zhou *et al.* (Zhu et al., 2019) on 1539 Chinese patients with HPV16+ non-oropharyngeal HNSCC reported better OS and disease-free survival (DFS) in laryngeal cancers but not other anatomical sites. Two US-American studies utilizing information from the National Cancer Database on HPV16/18+ HNSCC recorded more favorable outcomes in the larynx and hypopharynx than in the oral cavity (Tian et al., 2019). Since HPV testing is only clinically relevant in OPSCC, conducting large-scale, multicentric studies assessing the involvement of HPV in tumorigenesis at other sites within the head and neck is difficult.

1.2.2.1 HPV Vaccine

The European Medicines Agency (EMA) and its American equivalent, the Food and Drug Agency (FDA), authorized 3 vaccines containing virus-like particles (VLPs): the bivalent Cervarix, the quadrivalent Gardasil v4 and the most recent Gardasil v9 directed against HPV types 6, 11, 16, 18, 31, 33, 45, 52 and 58 (European Medicines Agency a, b, c; United States Food and Drug Administration a, b, c). The vaccines induce neutralizing antibodies in higher titers than natural infections (Zhou et al., 2021). Initially, the vaccines were registered for the prevention of warts, dysplasia and neoplasia in the anogenital region. Currently, the FDA recommends Gardasil v9 for both male and female patients aged 9- 45 years for the prevention of dysplasia and cancer in the genital, and head and neck regions, preferably prior to sexual contact.

Immunization with the bivalent vaccine, in the context of a clinical trial on the cervical disease, protected against oral infections in 93% at 4 years follow-up (Herrero et al., 2013). In the United States, the first effects of immunization of young people are seen as lower (though not statistically significant) incidence of oral HPV+ cancers in vaccine recipients (Chaturvedi et al., 2017; Hirth et al., 2017). In many countries, HPV vaccination is only offered to girls and precipitated a significant decrease in the incidence

of cervical cancer. However, herd immunity protecting boys from HPV infections did not come to an effect. In the United States and several European countries (among others, in Germany), the vaccination program was extended to boys, yet reversal of the trend in OPSCC prevalence will likely be a decade-long process. Much attention is dedicated to the development of therapeutic vaccines, as well as the therapeutic use of the existing ones. Clinical observations speak in favor of this approach- inoculation triggers a faster viral clearance from premalignant lesions and is beneficial as a therapy adjunct in recurrent respiratory papillomatosis (Goon et al., 2023). Adjuvant vaccination of previously unvaccinated patients following surgical treatment of cervical intraepithelial neoplasia was associated with a reduced recurrence risk (Lichter et al., 2020).

1.2.3 Other Oncogenic Viruses

Epstein-Barr Virus (EBV; Human herpesvirus 4, HHV4), a group 1 carcinogen according to the IARC, is the primary etiologic agent in nasopharyngeal carcinoma, common in Southeast Asia. The causative relationship is well-defined, as DNA and viral gene expression are present in tumor and precursor cells. The key oncogenic drivers are latent membrane protein 1 (LMP1), EBV-encoded small RNAs and Epstein-Barr nuclear antigen 1 (EBNA1), which influence a range of oncogenic pathways (Goon et al., 2022). Hepatitis C virus (HCV), a causative factor in the development of hepatocellular carcinoma, was shown in multiple studies to be associated with an increased risk of HNSCC (Borsetto et al., 2020; Mahale et al., 2016). Less well-documented is the association with other potentially oncogenic viruses, for example, some Herpesviridae (Parker et al., 2006; Wołącewicz et al., 2020).

1.2.4 Other Risk Factors

Other risk factors for developing HNSCC include poor oral hygiene, periodontal diseases, immunodeficiencies (Hashim et al., 2016) and prior irradiation (Baker et al., 2019). Multiple other chemicals increase the risk of the disease, among the most frequent are occupational exposures to polycyclic aromatic hydrocarbons (Paget-Bailly et al., 2012), asbestos (Clin et al., 2022; Khetan et al., 2019; Langevin et al., 2013), pesticides (Leonel et al., 2021), cement (Dietz et al., 2004; Khetan et al., 2019) and the dry-cleaning agent perchloroethylene (Barul et al., 2017; Carton et al., 2017). Opium, a known carcinogen when inhaled or ingested, was shown to increase the risk of HNSCC, with an odds ratio of around 4. This relationship was not confirmed for other opioid compounds, including heroin and analgesics (Mohebbi et al., 2021; Singh et al., 2021).

While no genetic alterations are known to cause the disease specifically, patients with mutations in pathways contributing to carcinogenesis in general have an increased risk of HNSCC development. Examples include dysfunctions in DNA damage and repair mechanisms, such as in Fanconi anemia. (Kutler et al., 2003). Genome-wide association studies have identified several susceptibility loci, suggesting the role of human leukocyte antigen (HLA) genes in the development of HNSCC, especially in the oropharynx (Shete et al., 2020). Further research on this subject could explain the development of cancer in some patients following HPV infection but not in others. The role of polymorphisms in genes related to alcohol, tobacco and toxin metabolism, such as aldehyde dehydrogenase 2 (*ALDH2*), is also suspected (Druesne-Pecollo et al., 2009). Diet and other lifestyle factors are currently considered to have a modest impact on the disease risk (Gormley et al., 2022).

1.3 Pathophysiology of Carcinogen-Associated HNSCC

The pathogenesis of HNSCC is stepwise, starting with epithelial dysplasia, progressing to carcinoma *in situ*, and finally, invasive cancer. Histologically, the term squamous dysplasia describes an abnormal cellular organization, increased mitotic activity, nuclear pleomorphism and an enlargement of the epithelium prior to invasion of the underlying connective tissue. Such alterations are graded depending on the relative thickness of the epithelium involved. Carcinoma *in situ* denotes severe dysplastic changes throughout the entire thickness of the epithelial layer. Invasive cancers break through the basement membrane and infiltrate the subepithelial connective tissue (Pai & Westra, 2009).

These phenotypic changes correspond to the accumulating genetic and epigenetic alterations in molecular pathways responsible for proliferation, differentiation, migration and other processes corresponding to the hallmarks of cancer (Johnson et al., 2020). Carcinogens and their metabolites form covalent bonds with DNA and cellular components, impairing their function. Of particular significance are DNA-adducts which, unless promptly repaired, lead to accumulating mutations. Smoking and tobacco typically induce an exchange of a purine nucleotide for another purine, and a pyrimidine to another pyrimidine, precipitating a characteristic mutational signature (Hayes et al., 2015).

Most patients present with *de novo* tumors arising from macroscopically normal-appearing mucosa (Johnson et al., 2020). The concept of field cancerization was first introduced by Slaughter (Slaughter et al., 1953) in 1953 and predicts that contact with carcinogens affecting large areas of mucosa increases the risk of cancer development in

the entire exposed area. Field cancerization is a frequent cause of local recurrence and second primary tumors in tissues with contiguous epithelium, such as the head and neck region, bladder and cervix (Dakubo et al., 2007). Indeed, studies show that 62.5% of local recurrences originate from the exposed field (Tabor et al., 2004). Field cancerization implies an anaplastic tendency of a group of neighboring cells. It is, therefore, conceivable that multiple cells could give rise to tumors, yet molecular data examining pre-cancer cell clonality strongly suggest a single-cell origin. Consequently, the most plausible model of progression proposes a carcinogen-dependent accumulation of genetic and epigenetic alterations in a patch of contiguous cells, once a single precursor cell gains proliferative advantage, it expands clonally, passing over genetic alterations to its offspring. Such pre-conditioned epithelium undergoes further modifications, ultimately acquiring characteristics of invasive cancer (Leemans et al., 2018). Sequential cytogenetic events occurring in this process are discussed in section 1.3.1 Cytogenetic Model of HNSCC Progression.

Alternatively, HNSCC arises from areas of macroscopically altered mucosa, often described as premalignant lesions. A recent consensus report issued by a WHO-led collaboration proposes the term *oral potentially malignant disorders* (OPMD), instead of the traditionally used terms precancerosis and premalignancy. The disorders are heterogeneous; the common denominator is the increased risk of cancer formation. The latest report published in 2020 encompasses 11 entities, including leukoplakia, erythroplakia, oral submucous fibrosis and oral lichen planus. On average, 7.9% (Iocca et al., 2020) of OPMDs progress to cancer, but the proportion varies between 1.4% and 49.5%. Initial biopsy of OPMDs often features microinvasion (Aguirre-Urizar et al., 2021). Leukoplakia is the most common OPMD, its estimated prevalence is around 2% (Petti, 2003). It presents as a thick white plaque overlying the mucosa of the upper aerodigestive tract and cannot be easily rubbed off, as forced removal causes bleeding from the underlying tissue. Between 7.2 and 9.8% of all cases undergo malignant transformation. Non-homogenous leukoplakia (seen in almost two-thirds of cases) transforms more readily than homogenous (Aguirre-Urizar et al., 2021; Guan et al., 2023; Iocca et al., 2020). Erythroplakia presents as an intense red mucosal thickening, its risk of malignant transformation is significantly higher, varying between 19.9% (Lorenzo-Pouso et al., 2022) and 33% (Iocca et al., 2020). Histologically, erythroplakia consists of highly dysplastic cells. Histopathological examination identifies focal carcinoma in over 40% of samples with erythroplakia (Lorenzo-Pouso et al., 2022). Both leukoplakia and

erythroplakia are often present in surgical margins of evident carcinomas (Warnakulasuriya et al., 2021). Clinically, the most important parameter predicting progression to malignancy is the degree of dysplasia ranging from mild to severe (Ranganathan & Kavitha, 2019). Retrospective analyses also indicate the prognostic significance of lesion size (>4cm) and ploidy assessment (Brouns et al., 2014; Ranganathan & Kavitha, 2019).

1.3.1 Cytogenetic Model of HNSCC Progression

HNSCC is characterized by a high degree of genomic instability with numerous chromosomal losses and amplifications. This section outlines the key genetic events in HNSCC formation and progression. A classical model of histological progression entails early loss of 3p, 9p and 17p, as seen in hyperplasia and dysplasia. Progression to carcinoma *in situ* is associated with 11q13, 13q21 and 14q32 loss. In invasive carcinoma, the inactivation of genes localized to 6p, 4q27 and 10q23 is frequent (Johnson et al., 2020). The locus 9p21 hosts the tumor suppressor gene *CDKN2A* encoding the protein P16, which halts the cell cycle by disrupting CDK4/6-cyclin D complexes. Loss of P16 coupled with amplifications in cyclin D1 gene- also frequent in HNSCC- leads to a loss of the G_1/S checkpoint. While normally, such excessive DNA replication activates TP53, the majority of HNSCC also feature allelic losses or missense mutations in this gene (locus 17p13) (Leemans et al., 2018). The list of gene mutations in HNSCC is dominated by tumor suppressors. Frequently mutated in association with smoking are members of the WNT- ß-catenin signaling pathway (*FAT1*, *AJUBA*, *NOTCH1*), which promotes tumor aggressiveness and helps maintain a stem-like cell phenotype (Alamoud & Kukuruzinska, 2018). Other examples include genes involved in epigenetic regulation (*KMT2D* and *NSD1*) and *TGFB2R*, whose function is to regulate proliferation, differentiation and epithelial-mesenchymal transition (EMT) (Pang et al., 2018). Two notable exceptions are the oncogenes *EGFR* and *PIK3CA*. EGFR belongs to a family of receptor tyrosine kinases; it is overexpressed in as many as 90% of HNSCC patients and is associated with poor outcomes. These observations lead to the development of the first targeted molecular therapy in HNSCC- cetuximab. EGFR triggers the activation of MAPK and PIK3-AKT, stimulating the transcription of genes involved in proliferation, angiogenesis, invasion and metastasis (Psyrri et al., 2013). The downstream effects of *PIK3CA*- mutated in almost 20% of HNSCC- are mediated by the protein kinase B (PKB, also known as AKT1), which activates mTOR, ultimately resulting in the upregulation of

translation, cell cycle progression and cell growth (Psyrri et al., 2013). Deregulation of the PIK3/AKT/mTOR pathway and its negative regulator PTEN in HNSCC is a consequence of both mutations and structural alterations of these genes (Gao et al., 2013; Mroz et al., 2015). Finally, typical for carcinogen-induced HNSCC are mutations in genes involved in the regulation of oxidative stress (*NFE2L2* and *KEAP1*) (Hayes et al., 2015; Lawrence et al., 2015).

Newest studies utilizing single-cell RNA sequencing, a powerful technique particularly well-suited to answer the question of cancer origin and development, confirm much of the previous findings and continue to describe new candidate genes involved in tumor progression. Interestingly, many genes related to hypoxia, glycolysis, as well as *NFκB*, *TNFα* and the PIK3/AKT/mTOR axis, are already highly expressed in carcinoma *in situ* but become further amplified in cancer (Choi et al., 2023).

Based on the frequently occurring cytogenetic alterations, HPV- HNSCC can be classified as CNA-rich or CAN-silent tumors. The CNA-rich HNSCC constitutes the majority of cases and can be further subdivided into classical, basal and mesenchymal subtypes. The classical subtype is characterized by alterations in genes involved in defense against oxidative stress. The CNA-silent tumors are less frequent and feature otherwise uncommon *HRAS* mutations. The clinical relevance of such genetic subtyping is unclear, yet as data accumulates, it may once dictate therapeutic choices.

1.4 HPV-Driven Carcinogenesis

The latency from HPV exposure to cancer development exceeds 10 years (Kreimer et al., 2013). In HPV+ HNSCC, the progression from dysplasia to invasive cancer is often less evident and surface dysplasia may be absent. HPV+ HNSCC are often poorly differentiated. Due to their weak keratinization and high nucleus-to-cytoplasm ratio, the tumors may resemble basaloid squamous cell carcinoma- an aggressive variant of HPV-HNSCC. Typical are tumor-infiltrating lymphocytes and central necrosis, frequently described as cystic degeneration, especially prominent in metastatic lymph nodes (Westra, 2012). HPV+HNSCC feature fewer fibroblasts and a higher degree of infiltration with immune cells- NK/T and plasma B cells- than HPV- tumors (Choi et al., 2023).

HPV+ HNSCC arises predominantly in the oropharynx, where the immunotolerant environment of the palatine and tonsillar crypts was postulated to be permissive towards the development of persistent infections, necessary for viral carcinogenesis. Viral

integration does not appear to be a *sine qua non* condition for malignant transformation but likely increases its risk and more research is needed to determine its nature and true rate. Available data shows HPV18 integration in nearly all cases of HNSCC, while the more prevalent type HPV16 in 76% (Koneva et al., 2018; Lawrence et al., 2015; Network et al., 2017).

The viral genome encodes seven early (E1- E7) and two late capsid proteins (L1, L2). While E1- E5 are primarily involved in viral replication; E6 and E7 are the key drivers of viral oncogenesis. The canonical function of E6 and E7 is to foster viral replication in the basal epithelial cells by initiating cell cycle entry. Increased expression of E6 and E7 conveys a higher risk of HPV infection leading to transformation (Koneva et al., 2018). In the context of viral carcinogenesis, E6 forms complexes with the host's ubiquitination proteins and causes proteasomal degradation of TP53. The protein E7 has a high binding affinity to RB1, which leads to its degradation and the release of E2F transcription factors (E2F1), driving the cell past the restriction checkpoint (G_1/S) (Rampias et al., 2014). Additional interactions and downstream effects of E6 and E7 are still being discovered. E6 can bind to and influence the function of other transcriptional activators such as EP300, CBP, Bak and hTERT (Ghittoni et al., 2015) and induce telomerase activity (Münger et al., 2004). E7 stimulates cell cycle progression by interacting with cyclin-CDK complexes, mitigating CDK-inhibitors, and participates in chromatin remodeling. Its targets also include P107 and P130, which are similar in structure and function to RB1 (Rampias et al., 2014). In response to RB1 ablation, HPV+ tumors highly upregulate P16, which, in the clinical setting is an indirect indicator of the presence of HPV in the examined tissue. Inactivation of these two pathways is an early 'hit' in the HPV-induced carcinogenesis and is equivalent to cell immortalization *in vitro* (Smeets et al., 2011).

1.4.1. The Genetic Landscape of HPV+ HNSCC

The uncontrolled replication of DNA resulting from the degradation of two key tumor suppressors leads to genomic instability and resistance to apoptosis. E6 and E7 may trigger tumorigenesis, but further genetic alterations are required to sustain the process. Of particular importance are the activating mutations and amplifications of *PIK3CA*. The gene is localized to 3q26, the locus most frequently amplified in HPV+ HNSCC and activates many pathways contributing to cell proliferation, survival and motility (Bader et al., 2005). Noteworthy alterations present predominantly in viral HNSCC include 14q32 deletions harboring the tumor suppressor *TRAF3*, 11q deletions containing the

tumor suppressor *ATM1,* and 20q11 amplifications augmenting the transcriptional activator *E2F1*. The former is inactivated in approximately 20% of these tumors and is implicated in innate immunity, interferon response and activation of NFκB-dependent transcription factors (Lawrence et al., 2015). Other genes frequently mutated in HPV+ HNSCC are involved in epidermal differentiation (*ZNF750*, *NOTCH1*, *EP300*) and evasion of immune response (*TRAF3*, *NFKBIA*) (Hayes et al., 2015). Moreover, HPV+ and HPV- HNSCC share multiple genomic alterations: amplifications at 1q, 3q, 5p and 8q, as well as deletions in 3p, 5q and 11q (Hayes et al., 2015). Interestingly, HPV+ tumors do not feature the focal amplification of 7p, involving the *EGFR* gene locus, an alteration frequently seen in HPV-HNSCC. The therapeutic implications of this are not yet fully understood (Choi et al., 2023).

Despite different mutational signatures, the overall mutational rate is similar in HPV+ and HPV- HNSCC. The mutational burden seen in HPV+ HNSCC may partly explain the heightened activity of the APOBEC3 enzymes, developed by host cells to eradicate viral infections. The enzymes suppress viral replication by deaminating cytosine bases in single-strand nucleic acids, producing a stop codon. APOBEC3A and APOBEC3B were shown to be involved in response directed against HPV. Their editing activity introduces point mutations. Such genome-wide cytosine mutations may account for different mutational variants in e.g., *PIK3CA* depending on etiology (Riva et al., 2021).

1.5 Staging of HNSCC

The TNM staging system, developed by the American Joint Committee on Cancer (AJCC) /International Union Against Cancer (IUAC) is the most widely used system used to estimate prognosis, plan treatment, and evaluate outcomes. It is applicable for clinical assessment prior to treatment (cTNM), pathological assessment following tumor resection (pTNM) and for recurring tumors (rTNM). The staging system entails three categories: T describes the primary tumor dimensions from carcinoma *in situ* (Tis) to T4, defined for each anatomic subsite within the head and neck region. The N stage is assigned based on the cervical lymph node involvement- their number, size and laterality. Depending on the presence or absence of distant metastasis, the M1 or M0 category is assigned. In 2017, the staging system was updated to include the depth of invasion (DOI) for cancers of the oral cavity, extracapsular nodal extension (ENE) in HPV- HNSCC and a novel staging for HPV+ cancers of the oropharynx. Hence, the staging of oropharyngeal tumors requires information on the viral status obtained by means of IHC assessment of

P16 abundance in tumor tissue. Because the nodal involvement in HPV-associated tumors has a lesser negative prognostic impact than in non-viral HNSCC, any number of ipsilateral metastatic lymph nodes <6cm are classified as N1. Primary tumor staging for HPV+ HNSCC remains similar but excludes Tis and T4b. Once the TNM categories are defined, their combination is summarized as cancer group stage ranging from I to IV. The changes outlined above resulted in the downstaging of many stage III and IV HPV+ tumors to stage I and II (Amin et al., 2017; Edge & Compton, 2010).

1.6 Therapy of HNSCC

Anatomical location, stage, disease characteristics, patient preference, available expertise and experience dictate the type of treatment. Whenever possible, a curative approach is assumed, aimed at organ-sparing and optimizing functionality.

1.6.1 Treatment of Early Disease

Thirty to forty percent of patients are diagnosed with stage I and II HNSCC. In this group, a single modality- either surgery or definitive radiotherapy- is sufficient to provide long-term oncologic control in 70- 90% (Chow, 2020). For easily accessible tumors, such as in the oral cavity, surgery is preferred as it yields histological information on the depth of invasion and the status of surgical margins, leaving no significant functional and cosmetic impairment. In the oropharynx, surgery and radiation yield similar outcomes (Worden & Ha, 2008). External beam source 3D-conformal radiotherapy is currently the minimum standard. Intensity-modulated radiotherapy (IMRT) uses different beam intensities throughout the irradiated volume to maximize the dose delivered to the tumor mass, minimizing normal tissue exposure. This approach is complemented by image-guided radiotherapy (IGRT), which uses frequent pre-treatment imaging to account for variations in patient positioning and changes in anatomy between sessions, thus reducing irradiation margins. Both approaches are now widely accepted as standard and allow the reduction of toxicity to healthy tissue (Anderson et al., 2021). Surgical morbidity can be reduced by laser microsurgery or transoral robotic surgery (Weinstein et al., 2012). The approach to laryngeal tumors differs depending on anatomic localization. Endoscopic laser microsurgery and radiotherapy are good options for voice preservation (Aaltonen et al., 2014). For patients undergoing surgery, the goal is to achieve negative surgical margins; if needed, re-resection should be pursued. Elective neck dissection for clinically negative lymph nodes should be considered, as *a priori* surgery gives better outcomes than excision after relapse (D'Cruz et al., 2015). A sentinel lymph node biopsy may be a less

morbid option, providing non-inferior OS in selected cases (Argiris et al., 2008; Hasegawa et al., 2019). The laterality and extent of lymph node removal is dictated by the primary tumor site, associated risk of recurrence and metastatic spread (Argiris et al., 2008). Carcinomas of the lip often do not require lymph node excision. In contrast, oropharyngeal, hypopharyngeal as well as supra- and subglottic tumors carry a high risk of occult metastasis. Similarly, in patients treated with definitive radiotherapy, prophylactic irradiation of cervical lymph nodes may be indicated (Anderson et al., 2021). For patients treated surgically, histological risk features for disease recurrence are evaluated. These features include: the presence of two or more positive lymph nodes, perineural invasion, ENE, lymphvascular invasion and positive or close surgical margins. The most significant factors for locoregional control and OS, include ENE and positive surgical margins. Histological high-risk features warrant adjuvant therapy to eradicate microscopic cancer foci, which would otherwise lead to disease recurrence (National Comprehensive Cancer Network, 2023). The RTOG 9501 and EORTC 22931 clinical studies established chemoradiation with high-dose cisplatin as the standard of care in this group of patients. The addition of cisplatin to conventionally fractionated radiation improves progression-free survival (PFS), OS and locoregional oncologic control (Bernier et al., 2005).

1.6.2 Treatment of Locoregionally Advanced Disease (Stages III and IV)

Over 60% of patients with HNSCC present with stage III and IV disease, and 10% present initially with distant metastasis (Argiris et al., 2008; Braakhuis et al., 2012). Surgery is preferred for cancers of the oral cavity and lip and remains an option for smaller, accessible tumors at other localizations, deemed to give acceptable functional outcomes. Therapeutic or elective treatment of cervical lymph nodes is also warranted. After surgery, the histopathological report determines the extent of adjuvant therapy. Inoperable tumors are treated with concurrent chemoradiation. Non-surgical therapy is preferred in the management of tumors arising in the larynx, oropharynx and hypopharynx. For locally advanced disease the preferred regimen is high-dose cisplatin with radiotherapy. Alternatives include carboplatin with 5-fluorouracil (5FU), or

paclitaxel and cetuximab [2] (National Comprehensive Cancer Network, 2023). Nonetheless, the management strategies in these patients are highly individualized and sequential therapy, including chemotherapy and irradiation is possible. Where appropriate, patients may be enrolled in clinical studies.

1.6.3 Treatment of Recurrent and Metastatic Disease

More than half of patients initially diagnosed with locally advanced HNSCC relapse within 2 years (Argiris et al., 2008). Few patients are candidates for salvage surgery. Re-irradiation may be possible, but tissue toxicity is very limiting. For years, the cornerstone of treatment was systemic chemotherapy with a platinum compound, taxanes, 5FU and cetuximab. The development of immune checkpoint inhibitors (ICI) marks a significant shift in the management of advanced HNSCC. ICI target immune checkpoint proteins: CTLA-4 and PD-1, primarily present on T cells, but also other types of immune cells, as well as PD-L1 frequently expressed by tumors. By blocking the downstream inhibitory signaling, ICI facilitate T-cell activation and stimulate the immune system to unleash an effective antitumor response (Ettl et al., 2022). PD-1 inhibitors pembrolizumab[3] and nivolumab[4] improve the OS of patients with recurrent and metastatic disease pretreated with platinum-based chemotherapy and are an established therapeutic option in this group of patients. Overall, the choice of drug or therapy regimen depends on patient's prior treatment and is tailored to overall fitness and comorbidities. In each case, the enrollment in clinical trials should be considered.

1.6.4. Treatment of HPV+ OPSCC

As previously outlined, HPV+ HNSCC are associated with a better prognosis and are especially responsive to irradiation. Patients with locally advanced disease have very good survival rates, which is why treatment morbidity and post-cancer quality of life have

---

[2] A monoclonal antibody targeting the epidermal growth factor receptor (EGFR), introduced to the clinical practice alongside 5FU and platinum following the EXTREME trial, since successfully combined with irradiation (Rivera et al., 2009).

[3] The initial accelerated FDA approval of pembrolizumab was based on a phase 1 study KEYNOTE-012. Following phase 2 and 3 studies (KEYNOTE-055 and -040) showed durable responses and good safety profiles. Recently, an important phase 3 trial KEYNOTE-048 showed improved OS in patients with PD-L1 expressing tumors treated with pembrolizumab alone or in combination with 5FU and cisplatin, in comparison to the EXTREME regimen (5FU, cisplatin, cetuximab).

[4] The approval of nivolumab was predicated on the phase 3 trial CheckMate 141, demonstrating an improved OS and a favorable safety profile in patients pre-treated with platinum-based therapy, as compared to investigator's choice of chemotherapy.

come to focus, prompting a discussion about treatment deintensification. To date, there is insufficient data to recommend a therapy de-escalation for patients with HPV+ HNSCC. Multiple clinical trials aiming to address this question are underway (NCT03396718, NCT05600842, NCT01706939, NCT05119036, NCT02281955, NCT05268614, NCT03215719, NCT03323463).

1.7 Selected Therapeutic Agents

In the following paragraphs, selected standard-of-care therapeutics are discussed with a focus on the molecular aspects relevant to the experimental data presented in this thesis.

1.7.1 Cisplatin

Cisplatin is one of the oldest chemotherapeutics and remains a component of the first-line therapies for many malignancies, including HNSCC. Once the molecule enters the cell, its chloride groups are replaced by water molecules, rendering it strongly electrophilic. It then binds to the electron-rich purine residues in the DNA, forming intra-strand crosslinks and inhibiting DNA synthesis. Strong genotoxicity of cisplatin activates TP53, which interacts with a variety of proteins– including P38, MAPK, JNK, Bax- and activates caspases via multiple pathways. Caspase-mediated apoptosis is the primary mechanism of cell death induced by cisplatin (Brown et al., 2019). Cisplatin also increases oxidative stress by binding to sulfhydryl groups of mitochondrial proteins, increases the production of reactive oxygen species (ROS) and modulates calcium signaling (Dasari & Tchounwou, 2014). Significant toxicity and resistance, especially in relapsed patients, have prompted the development of other platinum-based therapies, such as carboplatin and oxaliplatin.

1.7.2 Paclitaxel

Paclitaxel is a plant-derived alkaloid compound that stabilizes the microtubule cytoskeleton and causes cancer cells to accumulate disorganized microtubule arrays. Initially, the suspected mechanism of cytotoxicity was mitotic arrest (Schrijvers & Vermorken, 2000). Later studies have shown that the induction of a spindle assembly checkpoint requires high drug concentrations, which are challenging to achieve *in vivo*. Clinically relevant concentrations exert antitumor effects by disrupting spindle formation and cytokinesis, leading to the formation of aneuploid cells (Weaver, 2014). The drug also induces apoptosis via intrinsic and extrinsic pathways due to the elevation of ROS production, disruption of mitochondrial function and stimulation of anticancer immunity (Guigay et al., 2019; Zhao et al., 2022).

1.7.3 5-Fluorouracil

5-fluorouracil (5FU) is an antimetabolite drug and an analog of uracil with C^5-Hydrogen atom substituted with Fluorine. The drug is transported into the cell by the same transporters as uracil and is converted into several active metabolites: fluorouridine triphosphate (FUTP), fluorodeoxyuridine mono- and triphosphate (FdUMP, FdUTP). 5FU exerts its cytotoxic effects via two main mechanisms. For one, FdUMP stably binds to the enzyme thymidylate synthase and inactivates it. In response, different feedback mechanisms are invoked and result in an imbalance in the deoxynucleotide triphosphate (dNTP) pool within the cell, which impairs downstream DNA synthesis and repair (Chalabi-Dchar et al., 2021; Longley et al., 2003). Elevated substrate levels are genotoxic as they become triphosphorylated and misincorporated into the DNA and RNA. Attempts to repair the DNA are ineffective, and only lead to further nucleotide misincorporations, DNA strand breaks and finally, cell death (Ghafouri-Fard et al., 2021). The second major mechanism of 5FU toxicity involves the misincorporation of FUTP into RNA. This process occurs across all RNA species- from ribosomal, messenger, small nuclear and transfer RNA- at all stages of maturity and has profound consequences for cell viability (Chalabi-Dchar et al., 2021). Data obtained on cancer cell lines suggests that 5FU may also induce mitochondrial ROS, influence the cell cycle and inhibit angiogenesis (Zhang et al., 2008).

1.8 Non-Oncogene Addiction of Cancers as a Potential Strategy for Drug Development

The genetic heterogeneity of HNSCC makes the development of targeted therapies difficult (Lawrence et al., 2015). An alternative approach is targeting other cellular pathways cancer cells rely on for survival. As these pathways are also present in normal cells but do not determine their survival, this phenomenon has been dubbed non-oncogene addiction (Luo et al., 2009; Nagel et al., 2016). An example of such an approach is targeting protein synthesis. Translation is a fundamental process, playing a key role in gene expression. Its dysregulation is a hallmark of cancer and leads to abnormal proliferation, angiogenesis, metabolic changes, and aberrant survival patterns (Bhat et al., 2015). There is ample evidence for altered expression of eukaryotic translation initiation factors (eIF) in human cancers. Robust proliferation of malignant cells precipitates an increased demand for proteins, suggesting there may be a therapeutic window for pharmacologic interventions in cancer treatment (Hao et al., 2020a). In fact, modulating

translation through pharmacological means has favorable safety profiles in several cancer types (Bhat et al., 2015).

1.8.1 The Eukaryotic Initiation Factor 2α- the Integrator of Stress Signaling and Translation

Translation is a fundamental biological process, consuming a significant proportion of cells' resources. It is divided into 4 phases: initiation, elongation, termination and recycling of translational components. Initiation is the rate-limiting step subject to tight regulation (Leprivier et al., 2015). Under normal growth conditions, translation initiation is cap-dependent and entails the formation of the ternary complex (TC), composed of the heterotrimeric eIF2, GTP and Met-tRNAi. Aided by eIF1, eIF1A, eIF5 and eIF3, the TC binds to the 40S ribosomal subunit, forming the 43S preinitiation complex (PIC) (Spilka et al., 2013). In parallel, the eIF4F complex, comprising multiple initiation factors, binds the 7-methylguanosine cap structure of mRNA and uncoils it. The 43S PIC is then recruited to the activated mRNA and scanning in the 5'-3' direction proceeds. Once the initiator tRNA recognizes the AUG start codon, scanning is arrested, elongation and recycling steps follow (Robichaud et al., 2018).

As tumor cells endure elevated proteotoxic, mitotic, metabolic, and oxidative stress levels, the α subunit of the eukaryotic initiation factor 2 (eIF2α) is an important regulatory node integrating cells' homeostatic needs and environmental stimuli (Payne, 2022). It is regulated by phosphorylation of serine 51 by four kinases, each responding to a specific type of stress. The protein kinase R (PKR) responds to dsRNA in viral infections, PKR-like ER kinase (PERK) acts to counter endoplasmic reticulum (ER) and oxidative stress, general control nonderepressible 2 (GCN2) senses nutrient depletion, while heme-regulated EIF2α kinase (HRI)- heme deprivation, drugs, and toxicants (Joshi et al., 2013; Wek, 2018). Phosphorylation of eIF2α at serine 51 initiates the integrated stress response (ISR) and stalls global translation by locking it in a stable complex with its guanine-nucleotide-exchange factor eIF2B (Figure 4). This crucial regulatory mechanism allows time for repair following diverse insults before the cell continues proliferation (Sharma et al., 2016). At the same time, ISR promotes the translation of mRNA harboring upstream open reading frames (uORF) and internal ribosome entry site (IRES) in the 5'UTR (Thakor & Holcik, 2012), most prominently ATF and CHOP (Koromilas, 2015). These genes are often inefficiently translated in normal conditions and serve the adaptation to stress. The ISR is designed to counteract noxious stimuli

rapidly. Once cellular homeostasis is restored, the signal is extinguished, and eIF2α is dephosphorylated by GADD34, which it preferentially translates. However, the effects of eIF2α phosphorylation may be cytoprotective or deleterious, depending on the context: the type of environmental cue, its duration, and concomitant signaling. Extensive data show that prolonged activation of this pathway can lead to programmed cell death or growth arrest (Kojima et al., 2003; Novoa et al., 2003).

Figure 4. Schematic representation of translation regulation in the initiation phase by stress. Four stress-responsive kinases phosphorylate eIF2α at Ser51 residue, locking it in an inactive state, bound to the nucleotide exchange factor eIF2B. Inactivation of eIF2, depletes the availability of the ternary complex, restricting canonical translation initiation. Abbreviations: eukaryotic initiation factor (eIF), protein kinase R (PKR), PKR-like ER kinase (PERK), general control nonderepressible 2 (GCN2) and heme-regulated kinase (HRI), endoplasmic reticulum (ER), double strand RNA (dsRNA), phosphate residue (P).

1.9 Study Aim

The aim of this study was to describe the expression patterns of EIF2 complex members on transcript and protein levels in HNSCC. Given the particular importance of the regulatory subunit, eIF2α, the study sought to characterize its protein abundance in more detail in metastasis, invasive carcinoma and premalignant epithelial lesions, as well as to relate its expression to clinical and histopathological parameters.

In the light of the described expression patterns and prognostic significance of the *EIF2S1* gene and its protein product, eIF2α, the second goal of the study was to evaluate the effects of pharmacological targeting of eIF2α by the small-molecule inhibitor- salubrinal. The therapeutic potential of the inhibitor was tested *in vitro* alone and in combination with standard-of-care drugs. Lastly, salubrinal was evaluated on patient-derived 3D tumor spheroids.

The overarching aim of research carried out in this area is to establish the feasibility and potential translational implications of using non-oncogene addiction of cancers for therapy. In the context HNSCC, a prominent example of malignancy arising on the background of exposure to toxicants and viral infection, prolonged hyperactivation of stress response is an especially promising target.

2.0 Material and Methods

2.1 Collection of Samples and Ethics statement

The study was conducted in accordance with the Declaration of Helsinki and received the approval of the local Ethics Committee (114/17 approved on 20.07.2017). The retrospective arm of the study uses histological slides from 83 patients diagnosed with HNSCC at the Otto-von-Guericke University Magdeburg, Germany and the Medical University of Graz, Austria. Sixteen patients undergoing a tumor resection at Otto-von-Guericke University Magdeburg consented to an intraoperative collection of tissue fragments, which were not necessary for diagnostic histopathology. The harvested tumor fragments were frozen in liquid nitrogen and used for protein isolation. All samples have been pseudonymized before processing for research purposes.

2.2 Bioinformatic Analysis of *EIF2S1* Expression

2.2.1 RNA Expression Analysis

Publicly available mRNA expression data provided by the Cancer Genome Atlas initiative (TCGA; RNASeq V2 RSEM) (Lawrence et al., 2015) were used for the analysis. The patient cohort is characterized in Table 3. The data was accessed and analyzed via the UALCAN web platform (Chandrashekar et al., 2017, 2022). The RNA expression expressed in transcripts per million bases (TPM) in tumor samples (n=522) was compared against normal controls (n=44). Descriptive statistics were performed to obtain mean, median, range and quartile values in tumors, non-tumorous tissue, as well as across cancer grades and stages for all genes of interest. The interquartile ranges between groups were compared by the Welch's t-test; p-value< 0.05 was assumed as the level of statistical significance. The HPV status used for this analysis was determined using DNA sequencing and PathSeq methods by the Broad Institute (Campbell et al., 2018; Kostic et al., 2011). The TP53 mutation status was obtained from the TCGA whole-genome sequencing data. Information on DNA methylation in the TCGA cohort was also accessed via the UALCAN web platform. The data was experimentally generated using bisulfite modification of DNA and array hybridization (Illumina Infinium HumanMethylation450 BeadChip, Illumina). This high-throughput method detects methylation up to 1500 base pairs upstream of the gene transcription start site (TSS) at multiple CpG sites simultaneously. The list of probes is provided in the Supplement S1. The degree of promoter methylation is represented as the Beta-value equal to the ratio of methylated probe intensity to total probe intensity.

The Kaplan-Meier survival analysis of TCGA data was performed via the GEPIA (Tang et al., 2017) web server. Patients were divided into groups with high and low gene expression in TPM, with the cut-off value set at median. The OS in months was compared between the groups by log-rank test; significance level: p-value< 0.05. The survival map includes TCGA data for 33 cancer types. Analogously, patients were divided into two groups based on expression levels of the genes of interest and the survival compared by log-rank test, followed by false-detection rate (FDR) adjustment; significance level: FDR-adjusted p-value< 0.05. The color-coded heatmap represents $\log_{10}$ values of hazard ratios for each gene/cancer type pair.

Gene expression alterations and clinicopathological characteristics in relation to *EIF2S1* transcript expression were analyzed via cBioPortal (Cerami et al., 2012; Gao et al., 2013) using the HNSCC TCGA, Firehose Legacy dataset (n=530). The mRNA expression Z-scores for the individual genes represent the number of standard deviations from the mean across all samples, normalized to diploid samples. Differences in distribution between groups were tested with X^2 test; significance level: p-value< 0.05. Information on mutations were obtained with whole-genome sequencing. Copy-number alterations (CNA) are inferred from DNA sequencing data with the use of the Genomic Identification of Significant Targets in Cancer (GISTIC) algorithm. The resulting putative copy-number values reflect the amplitude and recurrence of given alterations compared to a reference. GISTIC 2.0 delineates the following putative copy-number categories corresponding to computed values in brackets: homozygous deletion (-2); hemizygous deletion (-1); no change (0); gain (1); high-level amplification (2).

Correlations of transcript expression Z-scores across the 24 eIF genes were calculated, the obtained Spearman's rho values were color-coded and represent positive and negative correlations in the form of a heatmap. The Euclidian distance between Spearman's rho values was calculated and used to define clusters of eIF expression. The heatmap and dendrogram graphically depicting expression clusters were computed using Python programming language. With the kind permission of Dr. Piotr Swierczynski, the source code is provided in Supplement S2.

Gene dependency data obtained from the large-scale CRISPR-Cas9 knockdown screen performed by the Broad Institute on 81 HNSCC cell lines were used to bioinformatically assess the ablation effect of the genes of interest. Detailed information on the processing of the data and the dependency score are provided in the original publications (Dempster et al., 2019, 2021; Meyers et al., 2017; Pacini et al., 2021).

Number of patients (%)	Total Male Female	522 (100%) 382 (73,9%) 135 (26,1%)
Diagnosis age (years)	Mean (min- max)	60.8 (19-90)
Primary Tumor Site	Alveolar ridge Base of Tongue Buccal mucosa Floor of mouth Hard Palate Hypopharynx Larynx Lip Oral Cavity Oral Tongue Oropharynx Tonsil	18 (3,5%) 27 (5,2%) 22 (4,2%) 62 (11,9%) 7 (1,3%) 10 (1,9%) 116 (22,3%) 3 (0,6%) 73 (14,1%) 127 (24,5%) 9 (1,7%) 43 (8,3%)
Tumor Stage	T1 T2 T3 T4 TX Not available	35 (6,8%) 150 (29,0%) 134 (25,9%) 179 (34,5%) 3 (29,8%) 16 (3,0%)
Lymph node Stage	N0 N1 N2 N3 NX Not Available	243 (47,0%) 82 (15,9%) 161 (3,1%) 9 (1,7%) 18 (3,5%) 4 (0,8%)
Metastasis Stage	M0 M1 MX Not Available	486 (94,0%) 6 (1,2%) 20 (3,9%) 5 (1,0%)
Clinical Group Stage	Stage I Stage II Stage III Stage IV Not Available	20 (3,9%) 97 (18,8%) 104 (20,1%) 282 (54,5%) 14 (2,7%)
Tumor Grade	G1 G2 G3 G4 GX Not available	62 (11,9%) 301 (58,0%) 125 (24,1%) 7 (1,4%) 18 (3,5%) 4 (0,8%)

Table 3. The characteristics of the patient cohort used for the RNA transcript analysis. Data availability: The Cancer Genome Atlas initiative (TCGA, Firehose legacy; RNASeq V2 RSEM), downloaded via the cBioPortal.com.

2.2.2. The Analysis of Protein Expression

The Clinical Proteomic Tumor Analysis Consortium (CPTAC) (Edwards et al., 2015) protein expression data was analyzed via the UALCAN web platform (Chandrashekar et al., 2017, 2022). Protein expression in normal tissues (n=71) and HNSCC (n=108) is expressed as Z-values, representing the number of standard deviations from the median across samples in each cancer entity. Z-values are calculated from Log_2 spectral count ratios obtained via the CPTAC, normalized to the sample profile, and across the dataset. Descriptive statistics were performed to obtain mean, median, range and quartile values in tumors, non-tumorous tissue, as well as across cancer grades and stages for all genes of interest. The interquartile ranges between groups were compared by Welch's t-test, significance level: p-value< 0.05. Table 4 provides an overview of the patient cohort used for the protein expression analysis.

2.3 Histological assessment and Immunohistochemistry (IHC)

Tissue specimens were fixed in formalin, embedded in paraffin (FFPE), and stained with hematoxylin and eosin (H&E) according to the standard methods. Sections (4 μm) of FFPE blocks were mounted on adhesive-coated glass slides. In each case, the presence of a tumor or premalignant lesion was confirmed by a pathologist on an H&E slide and the tumor grade was assigned. The tumor stage was extracted from patient files. IHC was performed automatically using a Ventana Immunostainer XT and ultraView Universal DAB detection kit (both Ventana Medical Systems, Tucson, USA). Briefly, the procedure included deparaffinization, 30-minute conditioning, heat-induced epitope retrieval (HIER), primary antibody incubation for 30 minutes, and the addition of a peroxidase-labeled secondary antibody. Information on antibodies and dilutions is provided in Table 5. Two pathologists independently scored slides using light microscopy. The eIF2α tissue abundance was evaluated using the intensity score (IS; 0 no staining; 1 weak; 2 moderate and 3 strong staining) and proportion score defined as: <20% of cells= 1; 21- 50%= 2; 51- 80%=3 >80%= 4. (PS). The total immunostaining (TIS) score was calculated by multiplying IS x PS. HPV infection was determined by immunostaining for P16 protein, and HPV 16/18 early antigen 6 (E6). Secondary reagents used for P16 and HPV16/18 evaluation: BIOLOGO Universal Staining System DAB (Art. No DA005, Exalpha Biologicals Inc., USA).

Number of patients (%)	Total Male Female	110 96 (87) 14 (13)
Diagnosis age (years)	Mean (min- max)	61.3 (23.4- 81.5)
Primary Tumor Site	Larynx Oral cavity Oropharynx Lip Hypopharynx	49 (44.5) 49 (44.5) 6 (5.5) 4 (3.6) 2 (1.8)
Tumor Stage	T1 T2 T3 T4	9 (8.2) 41 (37.3) 29 (26.4) 31 (28.2)
Lymph node Stage	N0 N1 N2 N3 NX	36 (32.7) 20 (18.2) 23 (20.9) 5 (4.5) 26 (23.6)
Metastasis Stage	M0 M1 MX Not Available	101 (91.8) 0 (0) 3 (2.7) 6 (5.5)
Clinical Group Stage	Stage I Stage II Stage III Stage IV	7 (6.4) 25 (22.7) 32 (29.1) 46 (41.8)
Tumor Grade	G1 G2 G3	20 (18.2) 79 (71.8) 11 (10)

Table 4. The characteristics of the patient cohort used for the protein expression analysis. The protein expression data generated by the Clinical Proteomic Tumor Analysis Consortium (CPTAC) (Edwards et al., 2015) and was analyzed via the UALCAN web platform (Chandrashekar et al., 2017, 2022).

Antibody		Manufacturer (Cat. No)	Dilution	Species of origin
eIF2**α**	monoclonal	Cell Signaling (#5324)	1:2000	Rabbit
E6 HPV 16/18	monoclonal	Exalpha Biologicals (HP305) Secondary reagents: BIOLOGO Universal Staining System DAB (# DA005)	Ready to use	Mouse
P16	monoclonal	Exalpha Biologicals (P16002) Secondary reagents: BIOLOGO Universal Staining System DAB (# DA005)	1:10	Mouse

Table 5. Antibodies used for immunohistochemical staining of tissue samples.

2.4 Western Blot

2.4.1 Preparation of Lysates from Intraoperative Tissue Samples

Intraoperative specimens were immediately frozen in liquid nitrogen and stored at -80ºC. Cryosections were prepared to confirm or exclude the presence of a tumor. Tissue samples were homogenized (MagNa Lyser, Roche Diagnostics, Switzerland), NP-40 lysis buffer and phosphatase inhibitor (PhosSTOP, Millipore Sigma, Germany) were added (Supplement S3A). The lysates were then centrifuged at 10 000 rpm, 4ºC for 10 minutes, placed in new Eppendorf tubes and stored at -20ºC overnight. The following day, protein quantification was performed with Bradford assay (Protein Assay Dye Reagent, 500-006; Bio-Rad Laboratories Inc., Germany) according to the manufacturer's instructions. The protein concentration in samples was determined by colorimetric measurement of optical density (GloMax®-Multi Detection System (Promega, USA). Sample concentration was compared to the standard curve obtained by a concurrent measurement of bovine serum albumin (BSA) serial dilutions at the following concentrations: 0; 0.1; 0.25; 0.5; 1.0; 1.5 μg/μl. Lysates and BSA standard samples were stored at -20ºC.

2.4.2 Preparation of Cell Culture Lysates

The following steps were carried out on ice, reagents, devices and all plastic utensils were pre-cooled at 4ºC. Cells cultured on 100mm plates were mechanically detached with a scraper, transferred to a test tube and centrifuged (1 000 rpm x 5 minutes at 4ºC). The supernatant was discarded, pellets washed with cold PBS and transferred to Eppendorf tubes and centrifuged again (10 000 rpm x 10 minutes at 4ºC). The pellets were dissolved in the SDS lysis buffer supplemented with protease and phosphatase inhibitors- PMSF (CAS 329-98-6, Sigma Millipore) and PhosSTOP immediately before usage (Supplement S3B). The volume of complete lysis buffer added was matched to the size of each pellet. The samples were then placed on a thermal mixer (Thermomixer R, Eppendorf, Germany) at 99ºC for 10 minutes. The protein quantification and long-term storage were the same as described above.

2.4.3 Gel Electrophoresis and Protein Transfer onto PVDF Membranes

Proteins were separated by gel electrophoresis on 10% polyacrylamide gels, except P21 and RB1, for which 12% and 8% gels were used (Supplement S4). Lysates were diluted with dH_2O to obtain uniform concentrations and 5x loading buffer (Supplement S3C) was added to each sample containing 20 µg protein in a total volume of 20µl. Samples were then placed on a thermal mixer (Thermomixer R, Eppendorf, Germany) at 99ºC for 10 minutes. Following gel electrophoresis (80- 100 Volts) in running buffer (Supplement 3D), proteins were transferred onto a PVDF membrane (Immobilin-P transfer membrane, Merck Millipore, Darmstadt, Germany), which was previously activated in methanol and rinsed in dH_2O and 1x transfer buffer (Supplement S3E). Proteins whose molecular weight exceeded 80kDa were transferred overnight (50 Volts, 14- 16h). For smaller proteins, semi-dry transfer was used (15 Volts; 13 minutes), using a semi-dry blotting unit (TransBlot Turbo Transfer System, Bio-Rad, Munich, Germany) (1-Step Transfer Buffer, ThermoScientific Pierce, USA). Once proteins were transferred, the membrane was rinsed in TBST buffer (Supplement S3F). Non-specific signal was blocked with 5% non-fat milk for 1h at room temperature. The membrane was then incubated with primary antibodies diluted in 5% bovine serum albumin (BSA) or 5% non-fat milk overnight at 4ºC (Table 6). The next day, the membrane was washed three times for 5 minutes with TBST buffer and a secondary antibody (HRP-conjugated) was added for 1 hour at room temperature. The secondary antibody was then removed, and the membrane was washed three times in TBST for 5 minutes in preparation for chemiluminescent detection.

Antibody		Manufacturer (Cat. No)	Dilution	Species of origin
eIF2**α**	monoclonal	Cell Signaling (#5324)	1:1000	Rabbit
phospho-eIF2**α** (Ser51)	monoclonal	Cell Signaling (#3398)	1:1000	Rabbit
GAPDH (14C10)	monoclonal	Cell Signaling (#2118)	1:3000	Rabbit
α-Tubulin	monoclonal	SantaCruz sc-5286	1:1000	Mouse
Cyclin A	monoclonal	SantaCruz sc-271682	1:500	Mouse
Cyclin D1	monoclonal	SantaCruz sc-8396	1:500	Mouse
CDK2	monoclonal	SantaCruz sc-6248	1:500	Mouse
E2F1	polyclonal	Cell Signaling (##3742)	1:1000	Rabbit
p21	monoclonal	Cell Signaling (#2947)	1:1000	Rabbit
Rb1	monoclonal	Invitrogen (SY63-03)	1:1000	Rabbit
pRb1 (Ser780)	polyclonal	Invitrogen (PA5-114632)	1:1000	Rabbit
pRb1 (Ser807/811)	monoclonal	Invitrogen (13H27L9)	1:500	Rabbit
Anti-Rabbit	HRP-linked	Cell Signaling (#7074)	1:2000	Goat
Anti-mouse	HRP-linked	Cell Signaling (#7076)	1:2000	Horse

Table 6. Primary and secondary antibodies used for western blots.

2.4.4 Chemiluminescent Detection and Analysis of Western Blot Images

For the visualization of proteins obtained from cryo-samples Image Quant Chemiluminescent Imaging System, LAS 500, Cytiva (Avantor, USA) and Chemiluminescence Detection Reagent Kit (MERCK Millipore, Darmstadt, Germany) were used. Visualization of western blots from cell culture was performed using Pierce ECL Western Blotting Substrate (#32106; Thermo Fischer Scientific, USA); Blue Autoradiography and Western Blotting Film (*#1968-3810;* USA Scientific, USA) and Agfa CP1000 Developer (Agfa, Belguim). The densitometric quantification of western blot images was performed with Image J (U. S. National Institutes of Health, Bethesda, Maryland, USA). On each membrane, the samples were normalized to the non-treated control or the non-neoplastic control tissue, then to the loading control. The resulting relative adjusted band density is presented as a ratio whereby 1.0 equals the control in the experiment. All statistical analyses of western blot images were performed with GraphPad Prism Software, version 9.0 (GraphPad Prism Inc., La Jolla, USA). The statistical significance of differences between tumor and non-tumor samples was determined with the Wilcoxon test; significance level $p<0.05$.

2.5 Cell Culture and Preparation of Stock Solutions

Human hypopharyngeal (FaDu, CSC-C9379L) and oral (SCC4) squamous cell carcinoma cells were purchased from Creative Bioarray (New York, USA). The cells were cultured according to the supplier's instructions in EMEM (FaDu) and DMEM:F12 (SCC4) supplemented with 10% fetal bovine serum (FBS) and 1% P/S (all supplied by Gibco, Life Technologies, USA). For passaging, 0.05% trypsin solution with EDTA (Gibco, Life Technologies, USA) was used. The cells were incubated at 37°C in a humidified atmosphere with 5% CO_2. Salubrinal (CAS No 405060-95-9; Cayman Chemical, USA) was dissolved in dimethyl sulfoxide (DMSO). Table 7 provides information on other chemicals and solvents used. The stock solutions were stored at -20°C. Further dilutions were made with cell culture media immediately before each experiment. The solvents used: sterile water (UltraPure DNase/RNase-Free Distilled Water, ThermoFischer Scientific) and DMSO (CAS 136321-15-8, Sigma Aldrich).

Agent	CAS number	Manufacturer	Solvent
cisplatin	15663-27-1	Sigma Millipore	water
5-fluorouracil	51-21-8	Sigma Millipore	DMSO
paclitaxel	33069-62-4	Sigma Millipore	DMSO
bortezomib	179324-69-7	Sigma Millipore	DMSO
MG-132	13340-82-67	Sigma Millipore	DMSO

Table 7. Cytotoxic agents used for co-treatment with salubrinal *in vitro*. Dimethyl sulfoxide (DMSO).

2.6 Viability Testing and Calculation of Drug Synergies

Cell viability was assessed by the colorimetric measurement of the conversion of 3-(4,5-dimethylthiazol-2-yl)-2,5-diphenyltetrazolium bromide (MTT) to formazan in mitochondria. Cells were seeded onto a 96-well plate (2000 cells/well). The next day, the desired concentrations of tested chemicals and solvent controls were added. Cells were treated for 24h, 48h, and 72h. At each timepoint, 10µl of MTT (#M6499, ThermoFischer Scientific) solution in PBS was added per 100µl of total well volume. Plates were incubated at 37ºC for 2h. The supernatant was discarded, and 100µl DMSO (CAS 136321-15-8, Sigma Aldrich) was added to each well. Following a 15-minute incubation on a shaker, the optical density was measured at 562nm with GloMax®-Multi Detection System (Promega, USA). Each experiment was performed in triplicates.

The viability data for drug combinations were analyzed via a web-based platform the SynergyFinder (Ianevski et al., 2022), which relies on the MuSyC consensus framework for multi-drug synergy assessment and combinatorial drug discovery (Wooten et al., 2021). The in-built outlier detection algorithm was used for single- and dual-agent response measurements. Single-agent curve fitting follows a 4-parameter logistic regression algorithm (LL4). The dose-response matrices were generated for all co-treatments. The observed response to the drug combinations was compared to the predicted response, assuming no interaction between the two substances. The reference null model used is the HSA (highest single agent). The obtained synergy scores are defined as the average excess response resulting from a given drug interaction. An HSA

score of 15 corresponds to a 15% excess response of the drug combination in comparison to the activity of each drug alone. The following interpretation of HSA synergy scores was assumed in this analysis:

- >10 synergistic interaction;
- <-10 antagonistic interaction;
- -10 to 10 additive effect possible.

2.7 Colony Formation Assay

Cells were seeded onto a 6-well plate, 200 cells per plate. The next day, the desired concentrations of tested chemicals were added. On day 10 of the experiment, cells were washed with PBS, fixed in methanol, and stained for 1h in 1:10 Giemsa solution (Dr. K. Hollborn & Soehne, Germany). Plates were washed with distilled water, the colonies formed were counted manually.

2.8 Cell Death and Cell Cycle Analysis with Flow Cytometry

Asynchronous cells were harvested by trypsinization and resuspended in ice-cold PBS. Seventy percent ethanol was gradually added while vortexing, for overnight fixation at 4^{o}C. To ensure exclusive staining of the DNA, the cells were washed twice, suspended in 1ml PBS and incubated with 50 µl RNase (working solution 100 µg/ml; Qiagen, Cat. No. 19101). Next, 50 µl propidium iodide (PI) (50 µg/ml; Sigma-Aldrich P4864) was added for 30 minutes at room temperature. Percentages of cells in each phase of the cell cycle were determined with the FACS-Calibur flow cytometer (BD Biosciences, San Jose, CA, USA) and the CellQuest Pro software (version 5.1 for Mac OS, BD Biosciences, San Jose, CA, USA). The analysis of the results was performed with the FlowLogic software (version 8.1, Invai Technologies, Sydney, Australia), statistical analysis and graphic representation of results- GraphPad Prism software, version 9.0 (GraphPad Prism Inc., La Jolla, USA).

2.9 Chemosensitivity Testing of HNSCC Patient-Derived 3D Spheroids (PD3DS)

The protocol used was based on previously published work by Boehnke *et al*. (Boehnke et al., 2016). The mechanical and enzymatic tissue dissociation was adjusted every time to individual tissue characteristics. Cryosections from intraoperative tissue samples were performed to confirm the presence of a tumor. Tumor fragments were immersed in the complete medium (EMEM, 10% FBS, 1% P/S) with 2.0 µg/ml amphotericin B (E3789-1g, Sigma Millipore, Germany) overnight. The following day, the tissue was

mechanically fragmented with sterile scalpels (Cat. No. 22-079-707, ThermoFischer Scientific, USA), enzymatically digested with collagenase IV (C4-BIOC, SigmaAldrich, Germany), DNase I solution (#07900, Stemcell Technologies, USA) and 5 U/ml dispase solution (#07913, Stemcell Technologies, USA). The resulting suspension was passed through a 70 μM pore strainer (#27216, Stemcell Technologies, USA). The residue was discarded, and the aggregates in the flow-through were passed through a 37 μM strainer (#27250, Stemcell Technologies, USA). This time, the flow-through was discarded, while residual aggregates were washed off with the complete medium into a test tube and centrifuged. The obtained cells were suspended in the supplemented medium, seeded as an adherent monolayer in 12-well plates, and expanded for 2-3 passages at 37°C, 5% CO_2. Once 70- 80% confluence was achieved, the cells were harvested enzymatically (TrypLE Express Enzyme, #12604013, ThermoFisher Scientific, USA), centrifuged, and resuspended in the supplemented medium. For chemosensitivity testing, 5000 cells per well were suspended in a 1:2 mixture of Matrigel and medium and seeded onto a 384-well plate with an automated liquid handler (Biomek FX P Liquid Handler, Beckman Coulter, USA). On day 4, the test substances were added. Salubrinal concentrations used: 0.4, 2, 20 and 50 μM.

After 4 days of incubation, an ATP-based viability assay was performed according to the manufacturer's instructions (CellTiterGlo, #G9241, Promega, USA). The wells containing Matrigel only were used for background subtraction. DMSO was used as a solvent for all substances and controls. Four replicates were prepared for each dose. Percentage viability was determined as follows:

$$\%\ \text{viability} = 100 \times \frac{\text{Luminescence}_{\text{READOUT}} - \text{Luminescence}_{\text{BLANK}}}{\text{Luminescence}_{\text{DMSO}} - \text{Luminescence}_{\text{BLANK}}}.$$

3.0 Results

The following pages include the original research article published in the journal *Cancers*, entitled: "Inhibition of EIF2α dephosphorylation decreases cell viability and synergizes with standard-of-care chemotherapeutics in head and neck squamous cell carcinoma" (Cyran et al., 2023).

3.1 mRNA Transcripts of EIF2 Complex Members are Overexpressed in HNSCC

Firstly, the expression patterns of genes encoding members of the EIF2 heterotrimer were characterized. *EIF2S1* transcripts, encoding the α subunit, are overexpressed in HNSCC (n=520) in comparison to the normal tissue (n=44) (p-value= 1.62^{-12}) (Figure 5A). This subunit is responsible for Met-tRNAi binding and contains a phosphorylatable serine residue, rendering it a crucial regulator for the entire translation. The gene *EIF2S2* encodes the subunit β, which forms the nucleotide-binding pocket, while *EIF2S3*, encoding the subunit γ, forms the GTPase catalytic site and contributes to the binding of Met-tRNAi. Transcripts of both genes are highly expressed in HNSCC ($p<1^{-12}$ and $p=3.69^{-14}$, respectively) (Figures 5A and 6A-D). The role of eIF2 in translation depends on its interaction with eIF2B, a stoichiometrically less abundant, multi-subunit protein complex acting as a GTP-exchange factor. eIF2B comprises 5 subunits: α, β, γ, δ and ε encoded by *EIF2B1- 5*. eIF2B carries out its function as a dimer of pentamers: the subunits α, β and γ constitute the hexameric core, which binds eIF2α, while the laterally positioned δ/ε heterodimers have a catalytic function (Gordiyenko et al., 2019). All components, except the *EIF2B4*, are also overexpressed in HNSCC (Figures 5A, 7, 8 and 9). The *EIF2S1* transcript expression is elevated in cancers of all stages and progresses with cancer grade (Figure 5B and 5C). Similarly, *EIF2S2* and *EIF2S3* are overexpressed at all stages and in cancers of all grades. The median transcript expression gradually increases between these categories. This trend is also observed for most eIF2B subunits, suggesting that the deregulation of its components is an early event in cancer formation and continues with the proceeding malignant process (Figures 7, 8 and 9). Of note, the diagrams include the eukaryotic initiation factor 2A gene (*EIF2A*), which participates in a similar biological process to EIF2 yet is not a functional homolog of *EIF2S1* as it functions in a codon- rather than GTP-dependent manner. The role of *EIF2A* in translation is limited to specific contexts, such as re-initiation, internal and non-AUG initiation (Komar & Merrick, 2020).

(A)

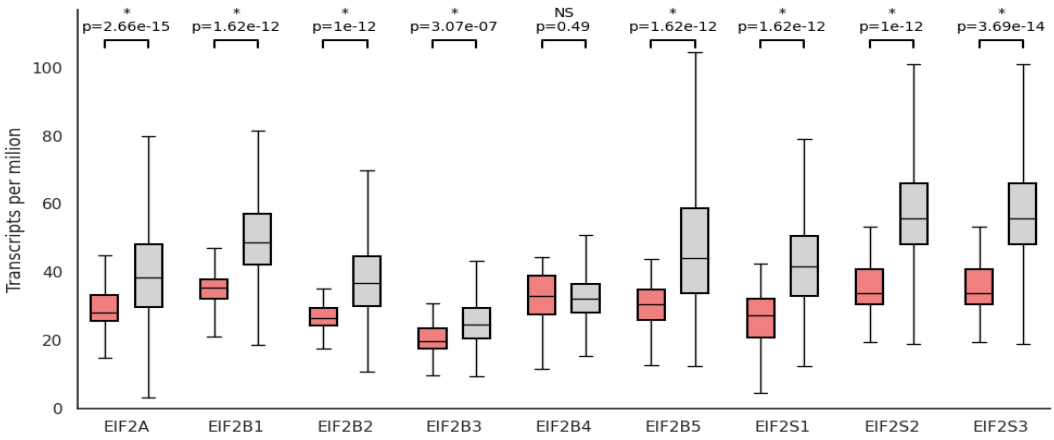

(B)

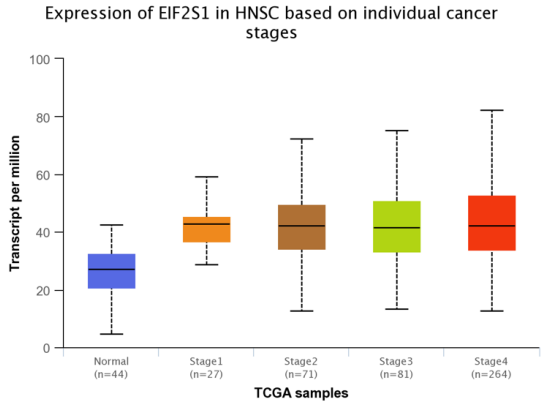

Comparison	Statistical significance
Normal-vs-Stage1	3.15E-07
Normal-vs-Stage2	1.46E-08
Normal-vs-Stage3	2.67E-12
Normal-vs-Stage4	1.62E-12
Stage1-vs-Stage2	4.31E-01
Stage1-vs-Stage3	6.20E-01
Stage1-vs-Stage4	9.74E-01
Stage2-vs-Stage3	1.77E-01
Stage2-vs-Stage4	3.14E-01
Stage3-vs-Stage4	4.47E-01

(C)

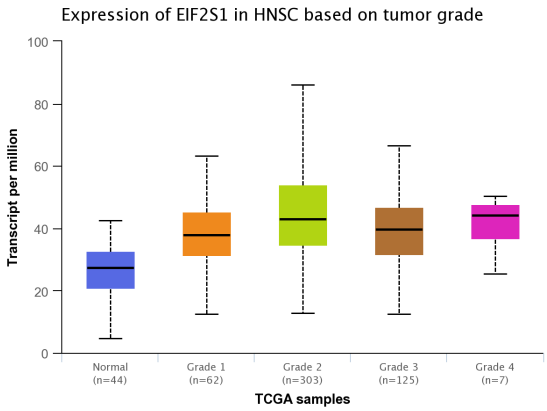

Comparison	Statistical significance
Normal-vs-Grade 1	9.04E-10
Normal-vs-Grade 2	1.62E-12
Normal-vs-Grade 3	1.20E-13
Normal-vs-Grade 4	9.77E-05
Grade 1-vs-Grade 2	1.26E-03
Grade 1-vs-Grade 3	7.24E-01
Grade 1-vs-Grade 4	9.12E-01
Grade 2-vs-Grade 3	6.25E-04
Grade 2-vs-Grade 4	1.34E-01
Grade 3-vs-Grade 4	9.72E-01

Figure 5. Genes encoding eIF2 complex members are overexpressed in head and neck squamous cell carcinoma (HNSCC). (A) *EIF2S1* transcript expression is significantly higher in HNSCC, represented in grey (n= 520) than in normal epithelium as shown in red (n=44) (p-value= 1.62^{-12}). (B, C) *EIF2S1* is elevated in HNSCC at all stages and all histological grades compared to normal epithelium. In all box-and-whisker diagrams, the horizontal line within the box corresponds to the median, box boundaries to lower and upper quartiles and vertical lines stretch from minimum to maximum values. Statistical analysis was performed by comparing the interquartile range of each group by the Welch's t-test, significance level $p<0.05$.

(A)

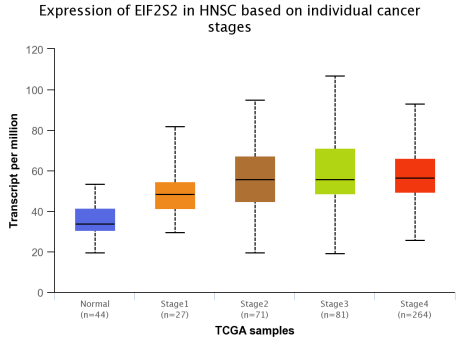

Comparison	Statistical significance
Normal-vs-Stage1	4.96E-03
Normal-vs-Stage2	2.44E-08
Normal-vs-Stage3	8.52E-10
Normal-vs-Stage4	1.62E-12
Stage1-vs-Stage2	7.87E-01
Stage1-vs-Stage3	3.31E-01
Stage1-vs-Stage4	7.27E-01
Stage2-vs-Stage3	2.82E-01
Stage2-vs-Stage4	9.04E-01
Stage3-vs-Stage4	1.98E-01

(C)

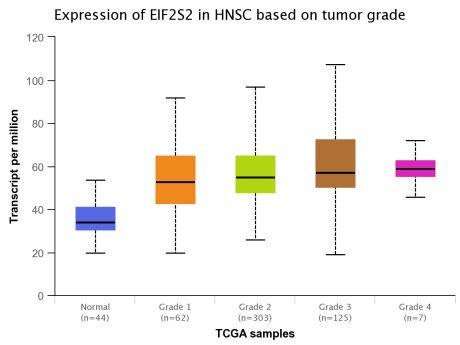

Comparison	Statistical significance
Normal-vs-Grade 1	8.70E-08
Normal-vs-Grade 2	1.62E-12
Normal-vs-Grade 3	<1E-12
Normal-vs-Grade 4	2.68E-09
Grade 1-vs-Grade 2	3.87E-01
Grade 1-vs-Grade 3	5.33E-02
Grade 1-vs-Grade 4	8.72E-01
Grade 2-vs-Grade 3	6.40E-02
Grade 2-vs-Grade 4	4.65E-01
Grade 3-vs-Grade 4	4.76E-02

(B)

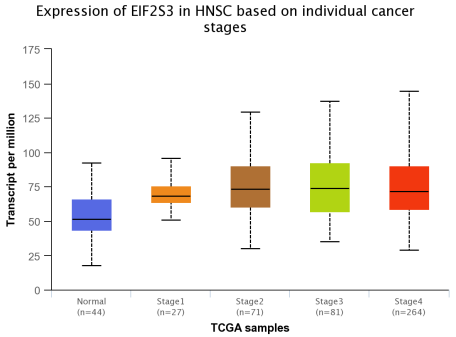

Comparison	Statistical significance
Normal-vs-Stage1	1.91E-02
Normal-vs-Stage2	5.55E-09
Normal-vs-Stage3	9.03E-08
Normal-vs-Stage4	8.46E-13
Stage1-vs-Stage2	7.76E-01
Stage1-vs-Stage3	7.77E-01
Stage1-vs-Stage4	8.25E-01
Stage2-vs-Stage3	9.95E-01
Stage2-vs-Stage4	8.41E-01
Stage3-vs-Stage4	8.35E-01

(D)

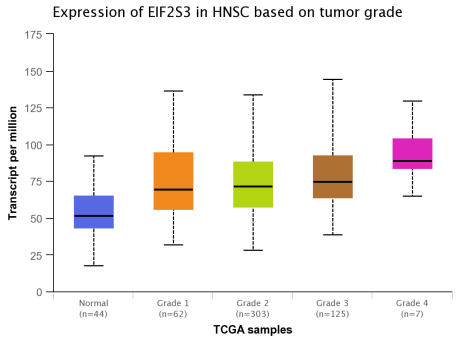

Comparison	Statistical significance
Normal-vs-Grade 1	1.63E-05
Normal-vs-Grade 2	2.42E-12
Normal-vs-Grade 3	6.66E-12
Normal-vs-Grade 4	2.13E-02
Grade 1-vs-Grade 2	2.86E-01
Grade 1-vs-Grade 3	1.96E-02
Grade 1-vs-Grade 4	9.53E-02
Grade 2-vs-Grade 3	8.20E-02
Grade 2-vs-Grade 4	1.37E-02
Grade 3-vs-Grade 4	1.13E-01

Figure 6. *EIF2S2* and *EIF2S3* genes are overexpressed in head and neck squamous cell carcinoma (HNSCC). (A, B) *EIF2S2* and *EIF2S3* transcript expression is elevated in HNSCC of all stages; the increase becomes more pronounced with cancer progression. (C, D) *EIF2S2* and *EIF2S3* are elevated in HNSCC across all histological grades. The transcript expression increases with cancer grade. In all box-and-whisker diagrams, the horizontal line within the box corresponds to the median, box boundaries to lower and upper quartiles and vertical lines stretch from minimum to maximum values. Statistical analysis was performed by comparing the interquartile range of each group by the Welch's t-test, significance level $p<0.05$.

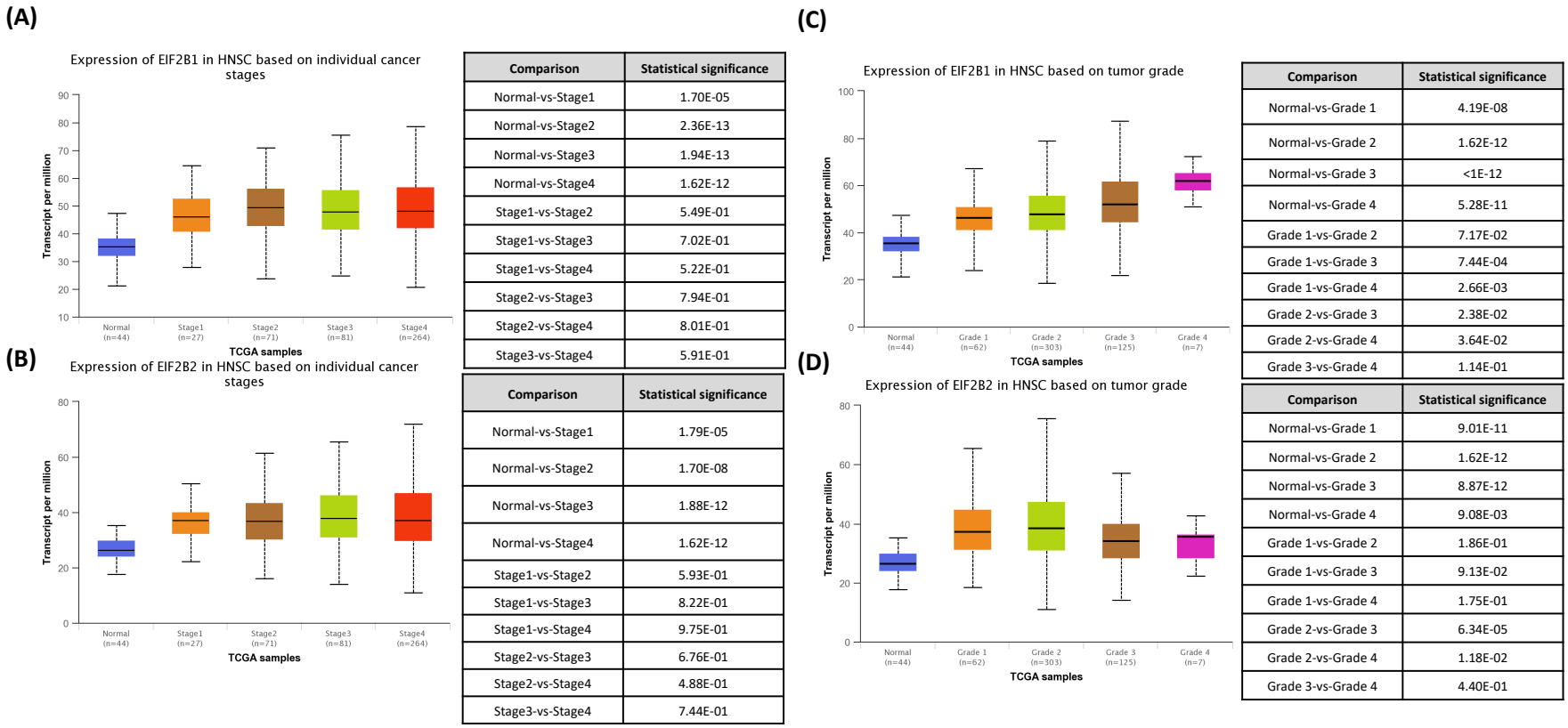

Comparison	Statistical significance
Normal-vs-Stage1	1.70E-05
Normal-vs-Stage2	2.36E-13
Normal-vs-Stage3	1.94E-13
Normal-vs-Stage4	1.62E-12
Stage1-vs-Stage2	5.49E-01
Stage1-vs-Stage3	7.02E-01
Stage1-vs-Stage4	5.22E-01
Stage2-vs-Stage3	7.94E-01
Stage2-vs-Stage4	8.01E-01
Stage3-vs-Stage4	5.91E-01

Comparison	Statistical significance
Normal-vs-Stage1	1.79E-05
Normal-vs-Stage2	1.70E-08
Normal-vs-Stage3	1.88E-12
Normal-vs-Stage4	1.62E-12
Stage1-vs-Stage2	5.93E-01
Stage1-vs-Stage3	8.22E-01
Stage1-vs-Stage4	9.75E-01
Stage2-vs-Stage3	6.76E-01
Stage2-vs-Stage4	4.88E-01
Stage3-vs-Stage4	7.44E-01

Comparison	Statistical significance
Normal-vs-Grade 1	4.19E-08
Normal-vs-Grade 2	1.62E-12
Normal-vs-Grade 3	<1E-12
Normal-vs-Grade 4	5.28E-11
Grade 1-vs-Grade 2	7.17E-02
Grade 1-vs-Grade 3	7.44E-04
Grade 1-vs-Grade 4	2.66E-03
Grade 2-vs-Grade 3	2.38E-02
Grade 2-vs-Grade 4	3.64E-02
Grade 3-vs-Grade 4	1.14E-01

Comparison	Statistical significance
Normal-vs-Grade 1	9.01E-11
Normal-vs-Grade 2	1.62E-12
Normal-vs-Grade 3	8.87E-12
Normal-vs-Grade 4	9.08E-03
Grade 1-vs-Grade 2	1.86E-01
Grade 1-vs-Grade 3	9.13E-02
Grade 1-vs-Grade 4	1.75E-01
Grade 2-vs-Grade 3	6.34E-05
Grade 2-vs-Grade 4	1.18E-02
Grade 3-vs-Grade 4	4.40E-01

Figure 7. *EIF2B1* and *EIF2B2* genes are overexpressed in head and neck squamous cell carcinoma (HNSCC). (A, B) *EIF2B1* and *EIF2B2* transcript expression is elevated in HNSCC of all stages; the increase becomes more pronounced with cancer progression. (C, D) *EIF2B1* and *EIF2B2* are elevated in HNSCC across all histological grades. *EIF2B1* transcript expression increases with increasing cancer grade, whereas *EIF2B2* is highest in grade 2 tumors. In all box-and-whisker diagrams, the horizontal line within the box corresponds to the median, box boundaries to lower and upper quartiles and vertical continuous lines stretch from minimum to maximum values. Statistical analysis was performed by comparing the interquartile range of each group by the Welch's t-test, significance level $p<0.05$.

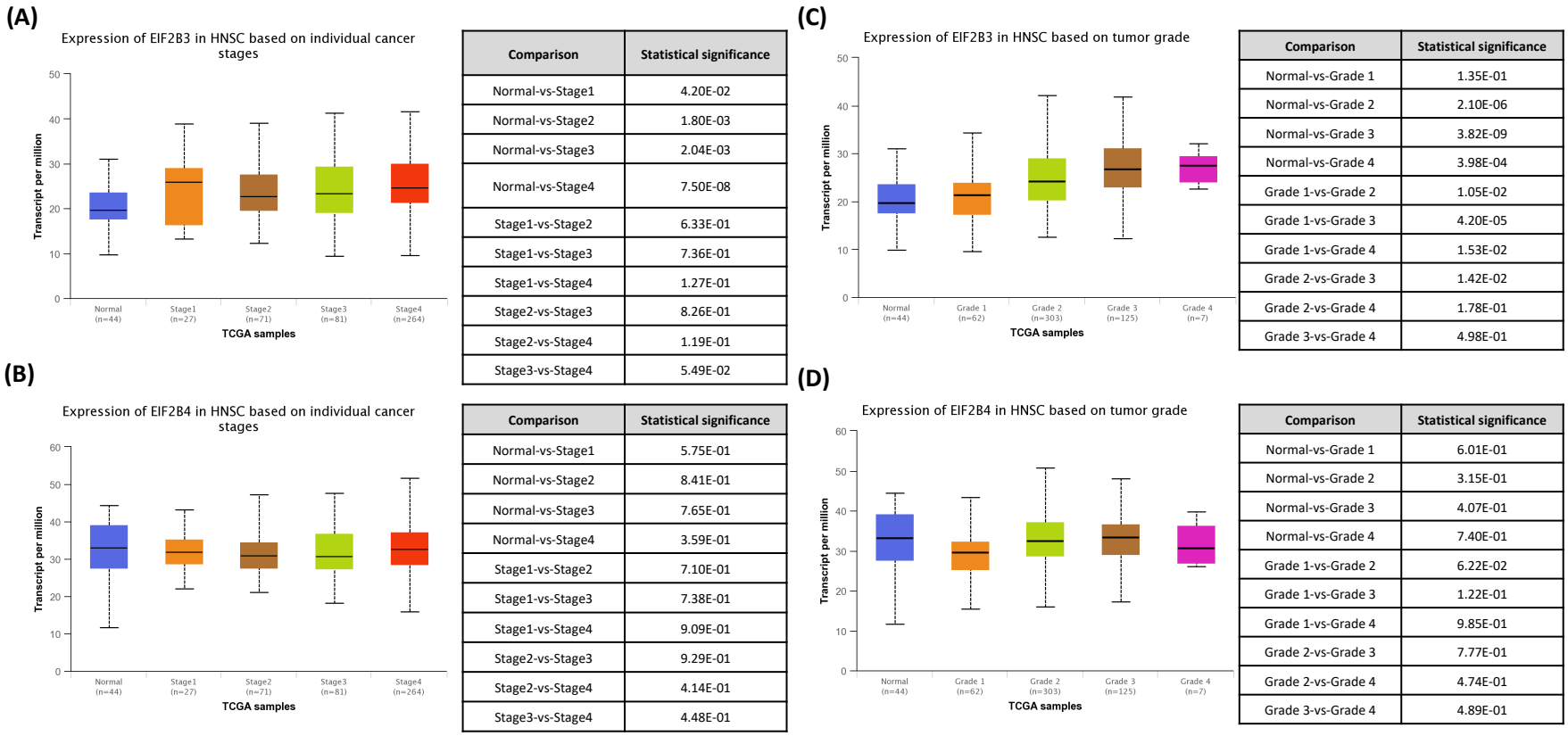

Comparison	Statistical significance
Normal-vs-Stage1	4.20E-02
Normal-vs-Stage2	1.80E-03
Normal-vs-Stage3	2.04E-03
Normal-vs-Stage4	7.50E-08
Stage1-vs-Stage2	6.33E-01
Stage1-vs-Stage3	7.36E-01
Stage1-vs-Stage4	1.27E-01
Stage2-vs-Stage3	8.26E-01
Stage2-vs-Stage4	1.19E-01
Stage3-vs-Stage4	5.49E-02

Comparison	Statistical significance
Normal-vs-Stage1	5.75E-01
Normal-vs-Stage2	8.41E-01
Normal-vs-Stage3	7.65E-01
Normal-vs-Stage4	3.59E-01
Stage1-vs-Stage2	7.10E-01
Stage1-vs-Stage3	7.38E-01
Stage1-vs-Stage4	9.09E-01
Stage2-vs-Stage3	9.29E-01
Stage2-vs-Stage4	4.14E-01
Stage3-vs-Stage4	4.48E-01

Comparison	Statistical significance
Normal-vs-Grade 1	1.35E-01
Normal-vs-Grade 2	2.10E-06
Normal-vs-Grade 3	3.82E-09
Normal-vs-Grade 4	3.98E-04
Grade 1-vs-Grade 2	1.05E-02
Grade 1-vs-Grade 3	4.20E-05
Grade 1-vs-Grade 4	1.53E-02
Grade 2-vs-Grade 3	1.42E-02
Grade 2-vs-Grade 4	1.78E-01
Grade 3-vs-Grade 4	4.98E-01

Comparison	Statistical significance
Normal-vs-Grade 1	6.01E-01
Normal-vs-Grade 2	3.15E-01
Normal-vs-Grade 3	4.07E-01
Normal-vs-Grade 4	7.40E-01
Grade 1-vs-Grade 2	6.22E-02
Grade 1-vs-Grade 3	1.22E-01
Grade 1-vs-Grade 4	9.85E-01
Grade 2-vs-Grade 3	7.77E-01
Grade 2-vs-Grade 4	4.74E-01
Grade 3-vs-Grade 4	4.89E-01

Figure 8. *EIF2B3* gene is overexpressed in head and neck squamous cell carcinoma (HNSCC). (A, B) *EIF2B3* transcript expression is elevated in HNSCC of all stages; the increase becomes more pronounced with cancer progression. *EIF2B4* transcript levels are not altered in HNSCC. (C, D) *EIF2B3* is elevated in HNSCC grade 2, 3 and 4, while *EIF2B4* transcript levels are unchanged across tumor grades. In all box-and-whisker diagrams, the horizontal line within the box corresponds to the median, box boundaries to lower and upper quartiles and vertical lines stretch from minimum to maximum values. Statistical analysis was performed by comparing the interquartile range of each group by the Welch's t-test, significance level $p<0.05$.

(A)

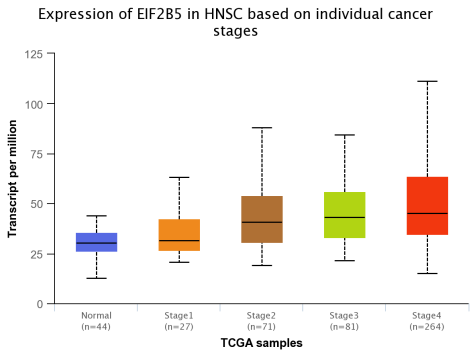

Comparison	Statistical significance
Normal-vs-Stage1	5.66E-02
Normal-vs-Stage2	2.16E-08
Normal-vs-Stage3	3.93E-11
Normal-vs-Stage4	1.62E-12
Stage1-vs-Stage2	2.52E-01
Stage1-vs-Stage3	3.60E-01
Stage1-vs-Stage4	4.67E-02
Stage2-vs-Stage3	7.66E-01
Stage2-vs-Stage4	4.10E-02
Stage3-vs-Stage4	6.34E-03

(B)

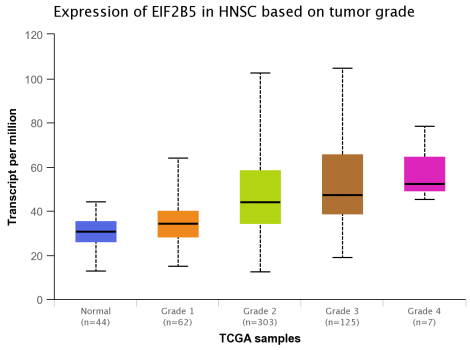

Comparison	Statistical significance
Normal-vs-Grade 1	1.66E-03
Normal-vs-Grade 2	1.62E-12
Normal-vs-Grade 3	1.62E-12
Normal-vs-Grade 4	7.64E-03
Grade 1-vs-Grade 2	9.37E-02
Grade 1-vs-Grade 3	6.20E-02
Grade 1-vs-Grade 4	1.46E-01
Grade 2-vs-Grade 3	5.69E-01
Grade 2-vs-Grade 4	3.23E-01
Grade 3-vs-Grade 4	2.72E-01

Figure 9. *EIF2B5* gene is overexpressed in head and neck squamous cell carcinoma (HNSCC). (A) *EIF2B5* transcript expression is elevated in HNSCC at stages 2, 3 and 4; the increase becomes more pronounced with cancer progression. (B) *EIF2B5* is elevated in HNSCC across all histological grades; the median number of transcripts increases gradually from grade 1 to 4. In all box-and-whisker diagrams, the horizontal line within the box corresponds to the median, box boundaries to lower and upper quartiles and continuous lines stretch from minimum to maximum values. Statistical analysis was performed by comparing the interquartile range of each group by the Welch's t-test, significance level $p<0.05$.

3.2 Elevated *EIF2S1* Gene Expression is Associated with Shorter OS and DFS Survival in HNSCC

The *EIF2S1* expression correlates negatively with OS (log-rank test; p=0.00016) and DFS (log-rank test; p=0.044) (Figure 10A and B). High expression of other members of the eIF2 complex is often associated with shorter OS but does not reach the level of statistical significance with a cut-off point set at the median. Figure 11 provides a global overview of the relationship between the eIFs and survival across 33 cancer types. The expression patterns and their relation to OS differ for each disease entity, reflecting diverse cancer biology. For this analysis, a more stringent statistical test was used- the survival of patients with high and low eIF expression was compared by the log-rank test, followed by the false detection rate (FDR) adjustment. Nevertheless, *EIF2S1* remains the only prognostically significant factor in HNSCC.

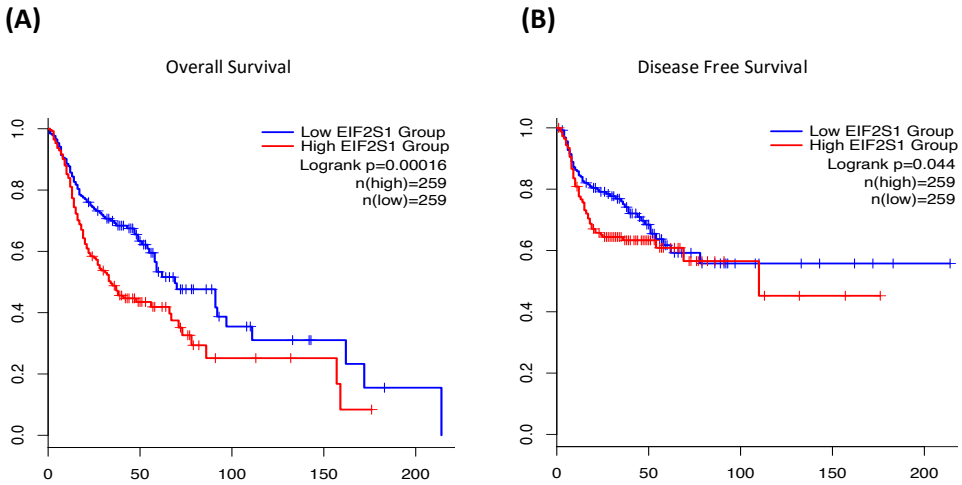

Figure 10. High transcript expression of *EIF2S1* is associated with significantly shorter overall survival (OS) (p=0.00016) and disease-free survival (DFS) (p=0.044) in head and neck squamous cell carcinoma (HNSCC). Patients (n=519) were divided into groups with low and high *EIF2S1* transcript expression with a cut-off point at the median. OS and DFS in months were compared between the two groups. Significance level: $p<0.05$, log-rank test.

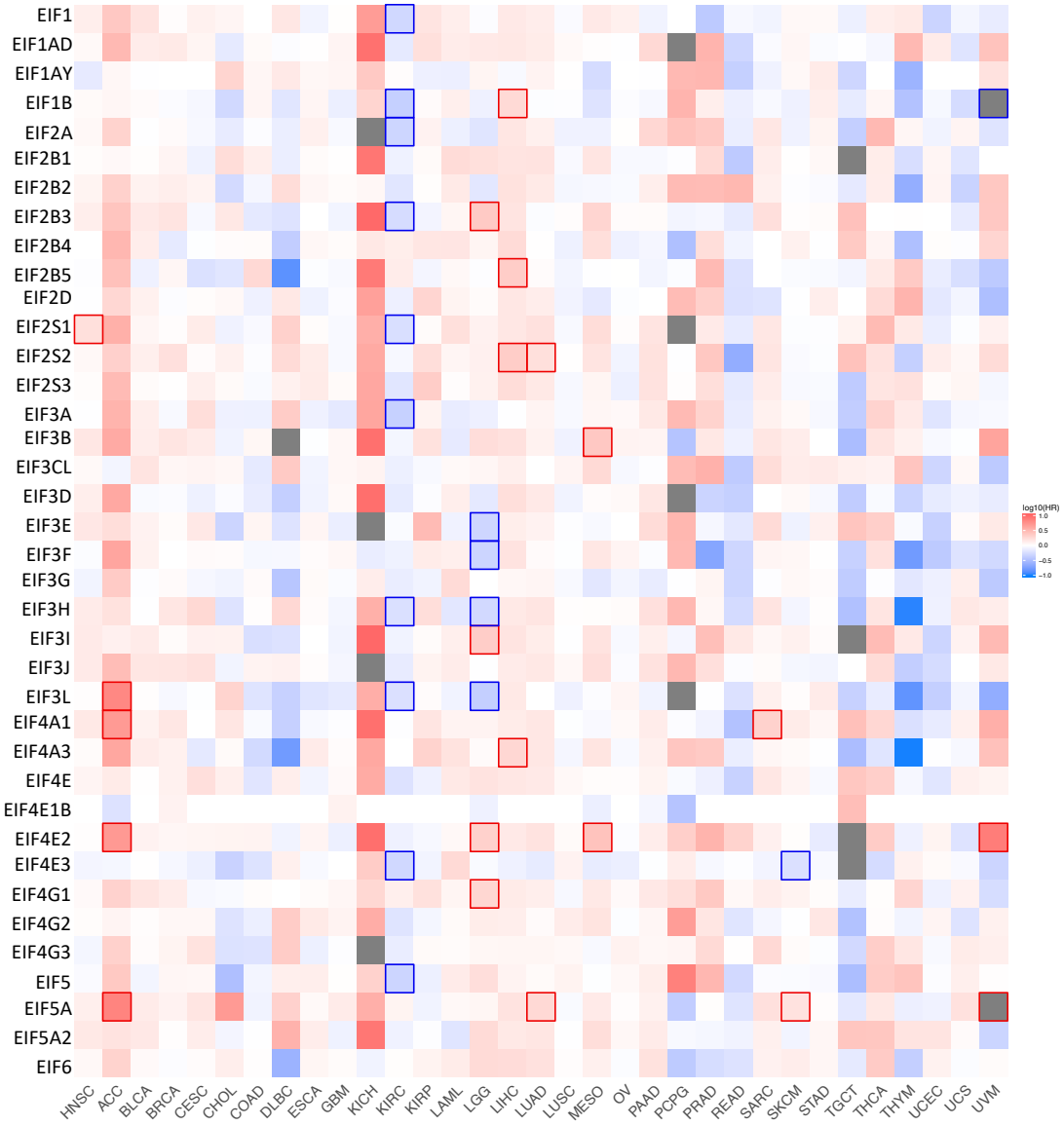

Figure 11. The eukaryotic initiation factor (eIF) gene expression across 33 types of human cancers. The heatmap illustrates the relationship between eIF gene expression in transcripts per million bases (TPM) and the overall patient survival (OS) in months. Red cells correspond to shorter OS (higher hazard ratio), blue cells correspond to longer OS (lower hazard ratio). Thick cell borders mark statistically significant relationships. A detailed description of the figure and explanation of abbreviations are provided on the following page.

Figure 11. The eukaryotic initiation factor (eIF) gene expression across 33 types of human cancers (continued from the previous page). Patients were divided into groups with high and low mRNA expression in TPM with a cut-off point at the median. Each heatmap cell corresponds to a $\log_{10}$HR (hazard ratio) for a given cancer type. Cells marked with shades of red represent shorter OS ($\log_{10}$HR>0); cells marked with shades of blue represent longer OS ($\log_{10}$HR<0) (See legend on the right side of the heatmap). Statistically significant relationships are marked with blue and red cell borders. Grey squares denote missing data. Significance level: $p<0.05$, log-rank test followed by false-discovery rate adjustment. **Abbreviations**: HNSC head and neck squamous cell cancer; ACC adrenocortical carcinoma; BLCA bladder urothelial carcinoma; BRCA breast invasive carcinoma; CESC cervical squamous cell carcinoma and endocervical adenocarcinoma; CHOL cholangiocarcinoma; COAD colon adenocarcinoma; DLBC diffuse large B-cell lymphoma; ESCA esophageal carcinoma; GBM glioblastoma; KICH kidney chromophobe carcinoma; KIRC kidney clear cell carcinoma; KIRP kidney papillary carcinoma; LAML acute myeloid leukemia; LGG low grade glioma; LIHC hepatocellular carcinoma; LUAD lung adenocarcinoma; LUSC lung squamous cell carcinoma; MESO mesothelioma; OV ovarian serous cystadenocarcinoma; PAAD pancreatic adenocarcinoma; PCPG pheochromocytoma and paraganglioma; PRAD prostate adenocarcinoma; READ rectal adenocarcinoma; SARC sarcoma; SKCM cutaneous melanoma; STAD stomach adenocarcinoma; TGCT testicular germ cell tumors; THCA thyroid carcinoma; THYM thymoma; UCEC Endometrial carcinoma; UCS uterine carcinosarcoma; UVM uveal melanoma.

3.3 Elevated *EIF2S1* Expression in HNSCC is Associated with Clinicopathological Features Indicating Disease Aggressiveness and Severity

EIF2S1 transcript expression was analyzed in relation to clinicopathological features. In the TCGA cohort, patients with elevated levels of *EIF2S1* significantly more frequently presented with extracapsular spread in metastatic lymph nodes (p=0.04), perineural invasion (p=0.02), as well as more frequently required postoperative adjuvant systemic therapy ($p=3.72^{-3}$) and developed secondary tumors ($p=8.36^{-3}$) (Figure 12A-D). These features are indicative of disease aggressiveness and severity and have been shown to correlate with poor patient outcomes (Budach & Tinhofer, 2019).

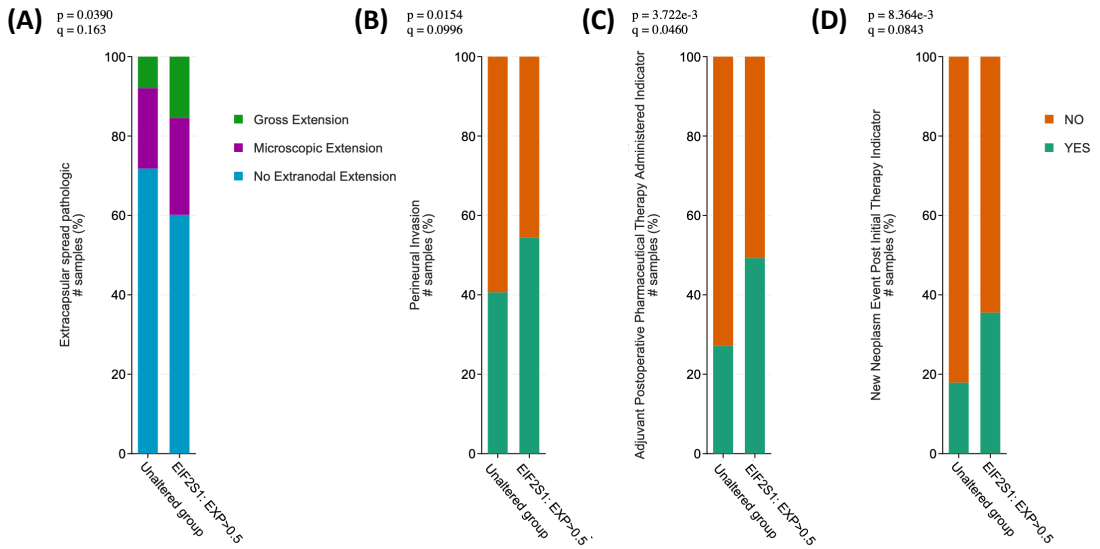

Figure 12. Elevated *EIF2S1* expression is associated with clinicopathological parameters indicating disease severity and aggressiveness in patients with head and neck squamous cell carcinoma (n=522, HNSCC). (A) Patients with high mRNA expression of *EIF2S1* more frequently develop nodal metastasis with extracapsular spread (p=0.04); (B) tumors with perineural invasion (p=0.02); (C) require postoperative adjuvant systemic therapy ($p=3.72^{-3}$); and (D) develop secondary tumors ($p=8.36^{-3}$). Transcript expression was normalized to diploid samples, statistical significance ($p<0.05$) was determined with the X^2 test.

3.4 eIF2S1 Expression in HPV-Positive and -Negative HNSCC

Persistent high-risk HPV infection is a known driver of carcinogenesis, especially in the oropharynx and oral cavity. This subgroup of tumors is characterized by a distinct biology and a markedly better prognosis. The viral proteins E6 and E7 mediate the degradation of key regulatory proteins, including TP53 and RB, and promote cell cycle re-entry by the host cell, allowing further amplification of the viral genome (Sabatini & Chiocca, 2020). In a model of HPV infection, eIF2α was shown to control E6 transcription and vice versa. Accordingly, eIF2α phosphorylation by PKR represses E6 and induces apoptosis, yet the remaining pool of E6 associate with the GADD34/PP1c phosphatase complex and partially rescue *their own* translation by dephosphorylating eIF2α (Kazemi et al., 2004). The results of the current study show that *EIF2S1* is elevated in both HPV-positive and -negative HNSCC, yet the expression is higher in HPV- (n=434) than in HPV+ (n=80) cancers ($p=1.36^{-3}$) (Figure 13A). This phenomenon is evident irrespective of the method of HPV detection (Supplement S5) (Campbell et al., 2018). Further, an increased expression of EIF2S1 is seen in HNSCC with mutated *TP53* (Figure 13B). In contrast, the overwhelming majority of HPV-related tumors maintain an intact *TP53* gene, the product of which is directed for degradation by viral proteins, leading merely to a 'functional' impairment of its tumor suppressor activity. In agreement with this, Figure 14A illustrates the *EIF2S1* expression in relation to P16 status and *TP53* mutations. Almost all HPV-related tumors feature functional *TP53*, while *TP53* driver mutations are associated with elevated *EIF2S1* expression, irrespective of their molecular architecture. The corresponding Figure 14B shows the relationship between *EIF2S1* expression in *TP53* wild-type and mutant samples while distinguishing between P16-positive and negative samples.

(A)

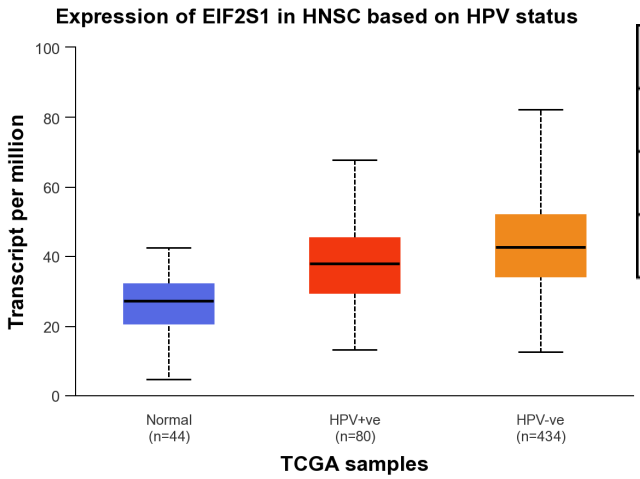

Comparison	Statistical significance
Normal-vs-HPV+ve	2.53E-09
Normal-vs-HPV-ve	<1E-12
HPV+ve-vs-HPV-ve	1.36E-03

(B)

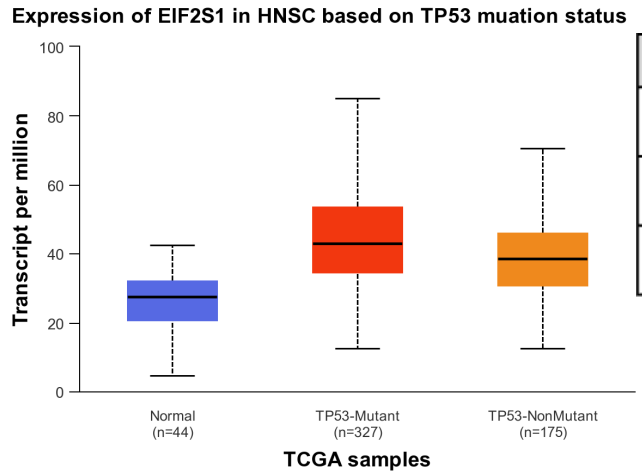

Comparison	Statistical significance
Normal-vs-TP53-Mutant	1.62E-12
Normal-vs-TP53-NonMutant	1.69E-12
TP53-Mutant-vs-TP53-NonMutant	5.39E-04

Figure 13. *EIF2S1* expression differs with human papillomavirus (HPV) and *TP53* mutation status in head and neck carcinoma (HNSCC). (A) *EIF2S1* transcript expression is highest in HPV- tumors. In HPV+ HNSCC, *EIF2S1* is also increased compared to the normal control. For this analysis, HPV positivity was determined based on HPV read count. (B) Tumors with mutated *TP53* feature the highest *EIF2S1* expression; *TP53* non-mutant tumors also express *EIF2S1* mRNA at higher levels than normal tissue. Statistical significance was determined with the student t-test, significance level $p<0.05$.

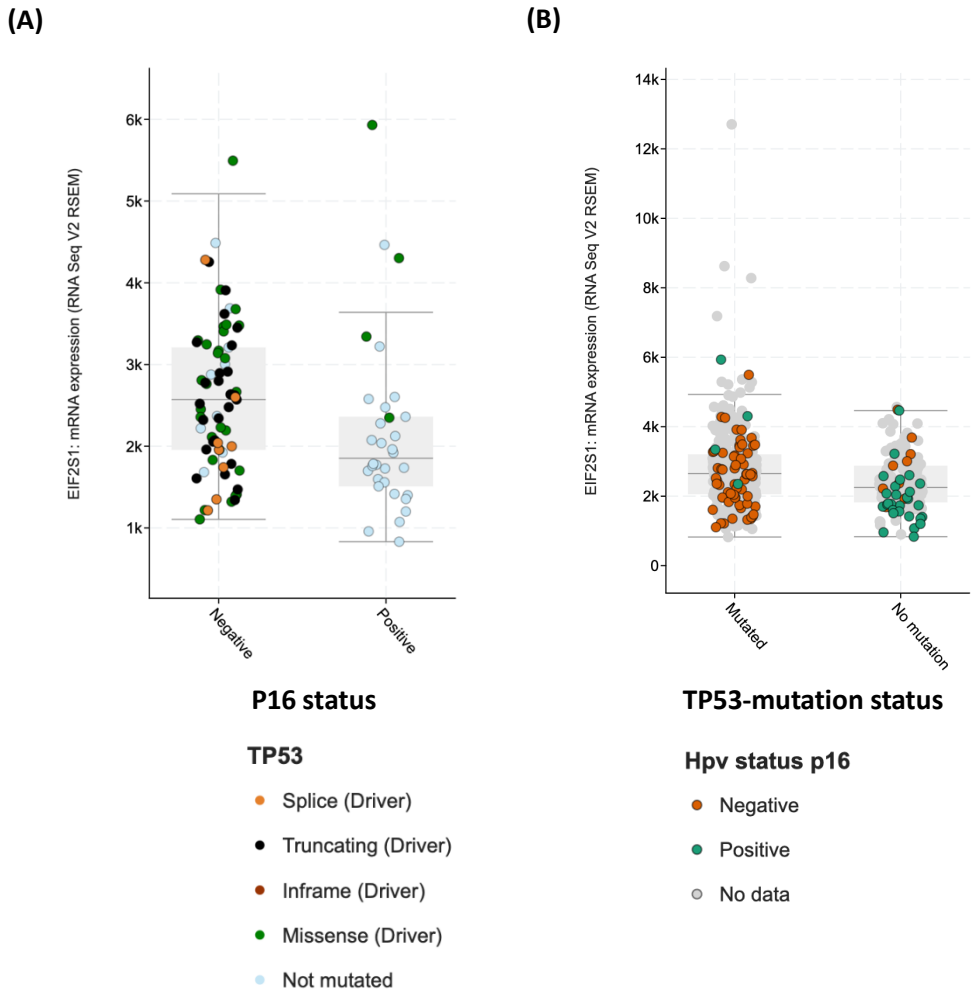

Figure 14. *EIF2S1* expression differs with human papillomavirus (HPV) and *TP53* mutation status in head and neck carcinoma (HNSCC). (A) *EIF2S1* transcript expression is higher in HPV- tumors. The diagram shows the relationship between *EIF2S1* transcript expression and HPV status determined by P16 detection. The samples (n=522) are grouped by *TP53* mutation types (see legend). (B) The diagram shows the relationship between the *EIF2S1* expression and *TP53* status (mutated or wild type). P16+ samples are represented in green and are predominantly present in the *TP53* wild-type group. In contrast, P16- tumors overwhelmingly feature mutations in the tumor suppressor. Transcript expression was normalized to diploid samples.

3.5 Drivers of *EIF2S1* Overexpression in HNSCC

3.5.1 Structural Gene Alterations

Potential drivers of EIF2 complex members overexpression in HNSCC were investigated. Generally, the EIF2 factors are infrequently mutated. Gene copy amplifications are an important cause of *EIF2A* and *EIF2B5* deregulation. The remaining genes, including *EIF2S1*, are highly transcribed irrespective of mutations and copy-number alterations (Figure 15). Although a detailed analysis of these relationships exceeds the scope of this work, it is interesting to note that several of the eIFs are localized to previously described cancer susceptibility loci. For example, the segment 3q26-29 harboring *EIF2B5* and *EIF5A2* is estimated to be amplified in approximately 20% of human malignancies (Fields et al., 2016).

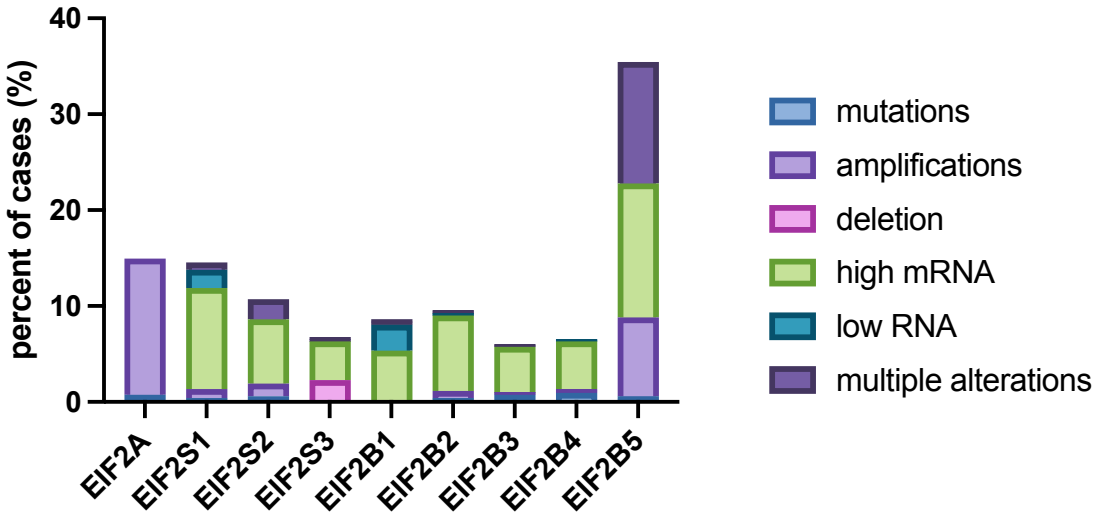

Figure 15. Genetic drivers of eukaryotic initiation factor 2 (eIF2) complex expression. Genes encoding eIF2 complex members are seldom mutated; the most frequent genetic alterations are copy-number amplifications. Transcript expression in transcripts per million bases (TPM) was normalized to diploid samples (n=522).

3.5.2 Chromosomal Co-localization Determines EIF Cluster Expression in HNSCC

Next, a correlation analysis of eIF mRNA expression was carried out. As expected, the transcript expression of functionally related factors and those situated on neighboring chromosomal loci frequently co-occur. A strong co-expression of *EIF2S1* and *EIF2B2* is observed ($p<0.001$; $q<0.001$). The genes are situated close to one another, on the long arm of chromosome 14, as well as encode subunits that come into direct interaction during translation initiation. However, *EIF2S2* and *EIF2S3* are also co-expressed, although located on distant chromosomal loci, likely due to their functional closeness. Table 8 lists co-transcribed factors with their respective chromosomal loci and the statistical significance of their co-occurrence. The heatmap shown in Figure 16 correlates the mRNA expression levels of all eIFs and groups them into regulatory clusters according to the Euclidian distance between the Spearman's rho values. Shades of red represent positive correlations, shades of blue negative. Based on this analysis, three main clusters can be seen: (1) in the top left corner of the heatmap with the majority of genes situated at the long arm of chromosome 14; (2) bottom right corner of the heatmap with genes situated at the long arm of chromosome 3; and the largest and most diverse (3) cluster in the central part of the heatmap, where factors located on the short arm of chromosome 1, as well as the long arms of chromosomes 20 and 8 are frequently co-expressed. Negative correlations are rare and are observed for *EIF3A*, *EIF4G1* and to a lesser degree *EIF2B5*.

Gene name Gene locus		Log_2 Odds Ratio	p-value	q-value	Tendency
EIF2A 3q25.1	*EIF2B5* 3q27.1	>3	<0.001	<0.001	Co-occurrence
EIF2S1 14q.23.3	*EIF2B2* 14q24.3	>3	<0.001	<0.001	Co-occurrence
EIF2S2 20q11.22	*EIF2B3* 1p34.1	>3	<0.001	<0.001	Co-occurrence
EIF2B3 1p34.1	*EIF2B4* 2p23.3	>3	<0.001	<0.001	Co-occurrence
EIF2S2 20q11.22	*EIF2B4* 2p23.3	>3	<0.001	<0.001	Co-occurrence
EIF2B2 14q24.3	*EIF2B3* 1p34.1	2.304	<0.001	0.005	Co-occurrence
EIF2S2 20q11.22	*EIF2S3* Xp22.11	1.848	0.004	0.023	Co-occurrence
EIF2B2 14q24.3	*EIF2B4* 2p23.3	1.699	0.011	0.049	Co-occurrence

Table 8. Transcription of EIF2 complex members co-occurs. The table shows the relationships between the mRNA expression of individual factors, the odds ratio of their co-transcription and statistical significance of the relationship. Elevated expression of factors co-localized on neighboring chromosomal loci and functionally related factors frequently co-occur. mRNA expression in transcripts per million bases (TPM) was normalized to diploid samples, statistical significance was determined with the Fisher's exact test, followed by the false-detection rate (FDR) adjustment and q-value generation.

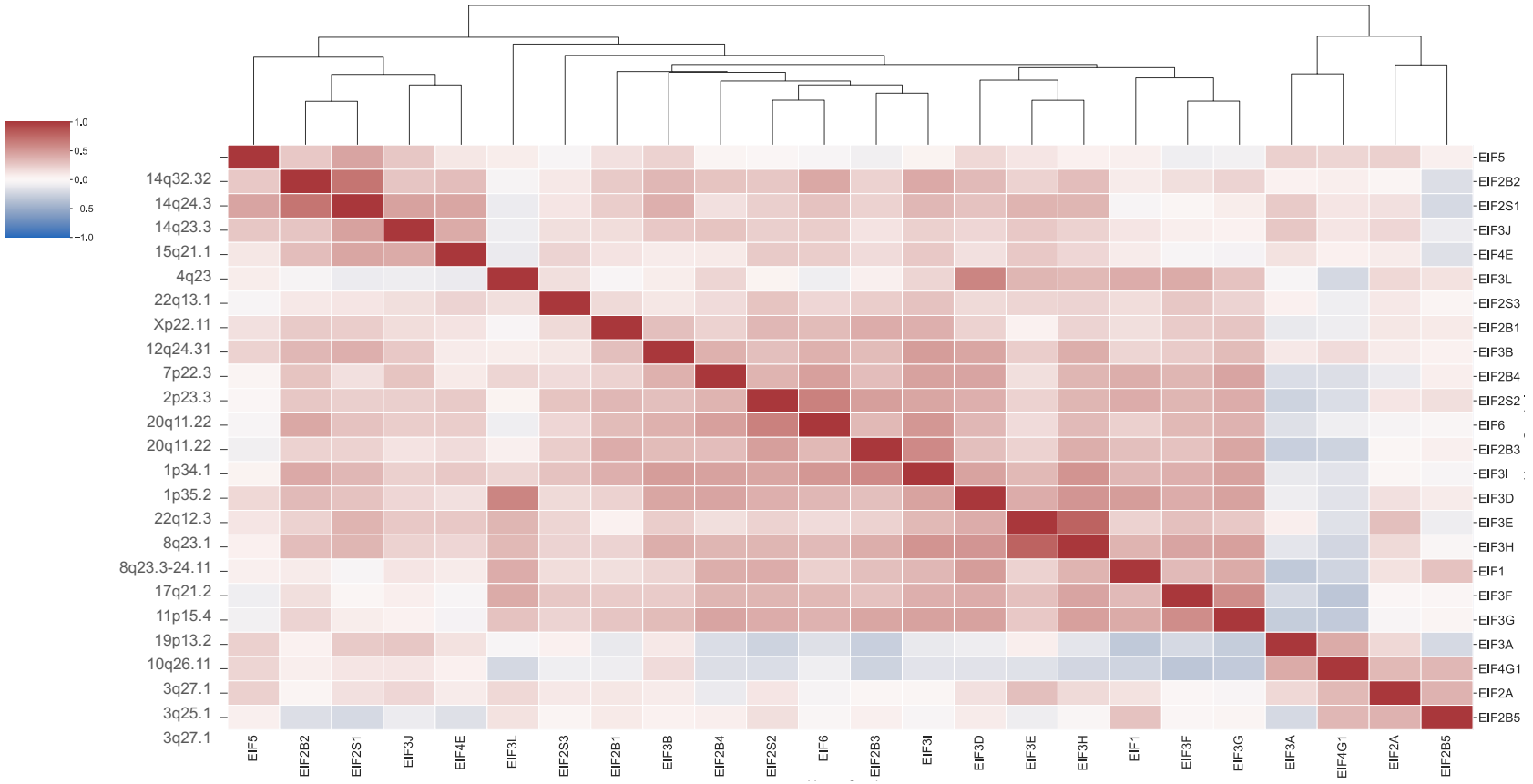

Figure 16. Heatmap representing regulatory clusters of eukaryotic initiation factors (eIFs) mRNA transcript expression in head and neck squamous cell carcinoma (HNSCC). Three main clusters are distinguished. eIFs are commonly co-expressed according to the gene locus. The legend in the top left corner assigns colors to Spearman's rho values. The dendrogram at the top shows three regulatory clusters and is based on the Euclidian distance between Spearman's rho values correlating mRNA expression values of individual eIFs.

3.5.3 DNA Methylation

DNA methylation involves the addition of a -CH_3 residue to a 5-carbon atom of cytosine within a DNA strand. It is mediated by specialized enzymes- the DNA methyltransferases (DNMT). Like other epigenetic modifications, it is reversible, heritable and determines gene expression without changes to the DNA base sequence (Curradi et al., 2002). Gene promoter methylation precludes the binding of transcription factors and silences the gene, while removal of the methyl residue has the opposite effect. Aberrant promoter methylation patterns are common in cancers and may contribute to carcinogenesis (Nishiyama & Nakanishi, 2021). Environmental factors, such as toxins (tobacco smoke, alcohol) and viral infections, are known methylation modulators. Global hypomethylation is a common epigenetic alteration linked to the activation of oncogenes and increased genomic instability. In this analysis, the degree of promoter methylation is expressed as the Beta-value, ranging from 0 – unmethylated to 1- methylated, obtained by dividing the methylated probe intensity by the total probe intensity (methylated and unmethylated) (Men et al., 2017; Shinawi et al., 2013).

Promoter methylation levels of several EIF2 members- *EIF2S3*, *EIF2B1*, *EIF2B4* and *EIF2B5*- were significantly decreased (p-values: 1.44^{-2}, 3.98^{-2}, 1.67^{-4} and 1.84^{-3}, in respective order). *EIF2S1* promoter methylation decreases with cancer stage, mirroring the increasing transcript expression discussed above (Figure 17A). Decreased promoter methylation is also seen in samples with mutated *TP53* ($p=6.25^{-5}$) (Figure 17B) and HPV-HNSCC ($p=2.69^{-4}$). The relative differences in methylation levels are statistically significant, though the Beta-values do not meet the criteria for hyper- and hypomethylation referenced in the literature (Men et al., 2017; Shinawi et al., 2013). HPV infection is also associated with aberrant methylation, usually elevated. Two mechanisms involving viral early antigens have been described. In the first, E7 forms complexes with DNMT1 and stabilizes it. In the second one, despite the inhibition of DNMT1 by wild-type *TP53*, E6-mediated degradation of the tumor suppressor recapitulates the enzyme activity, again leading to increased methylation (Nakagawa et al., 2021). Taken together, the results indicate that epigenetic regulation plays a role in EIF2 member upregulation in HNSCC.

(A)

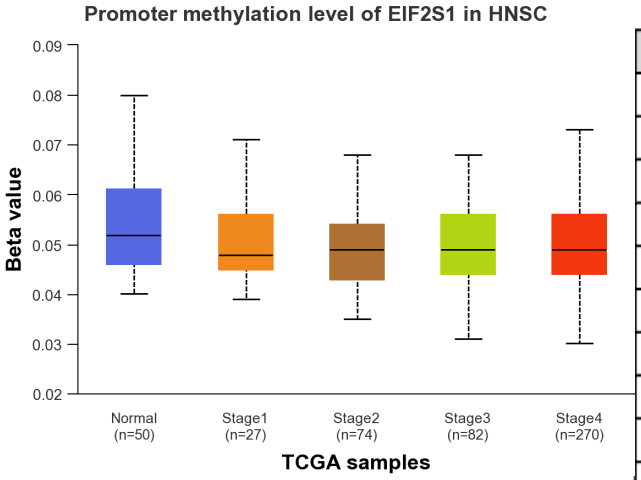

Comparison	Statistical significance
Normal-vs-Stage1	6.15E-01
Normal-vs-Stage2	**1.16E-02**
Normal-vs-Stage3	**4.24E-02**
Normal-vs-Stage4	**3.00E-02**
Stage1-vs-Stage2	2.20E-01
Stage1-vs-Stage3	2.91E-01
Stage1-vs-Stage4	3.23E-01
Stage2-vs-Stage3	7.39E-01
Stage2-vs-Stage4	3.76E-01
Stage3-vs-Stage4	6.412E-01

(B)

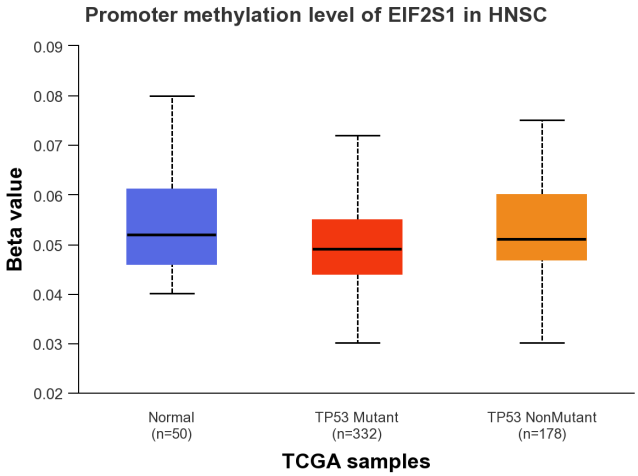

Comparison	Statistical significance
Normal-vs-TP53 Mutant	**7.24E-03**
Normal-vs-TP53 NonMutant	8.78E-01
TP53 Mutant-vs-TP53 NonMutant	**6.25E-05**

Figure 17. *EIF2S1* promoter methylation levels are decreased in head and neck carcinoma (HNSCC). Beta-values indicate the degree of promoter methylation ranging from 0 – unmethylated to 1- methylated. Beta-values are obtained by dividing the methylated probe intensity by the total probe intensity (methylated and unmethylated). (A) HNSCC show a lower degree of *EIF2S1* promoter methylation than normal samples. (B) Tumors with mutated *TP53* have lower promoter methylation than *TP53* wild-type tumors and normal samples. Statistical significance was determined with the Student t-test, significance level $p<0.05$.

3.6 Protein Levels of EIF2 Complex Members are Elevated in HNSCC

In the next step, data from a mass spectrometry-based proteomics assay provided by the CPTAC was used to characterize the eIF2 complex protein abundance. In a dataset including 108 HNSCC samples and 71 non-tumorous controls, EIF2α is significantly overexpressed in cancer (p-value= 7.56^{-16}) (Figure 18A). eIF2α abundance is highest in stage 2 and grade 1 tumors, followed by grade 2. Though the average protein expression in grade 3 tumors was higher than in controls, the difference was not significant, likely due to the low number of undifferentiated tumors in the dataset (Figure 18B and C). Similarly, EIF2β and EIF2γ are overexpressed in HNSCC ($p=1.59^{-18}$ and 3.29^{-31}, respectively). In contrast to the mRNA expression pattern, protein levels are highest in grade 1 and stage 3 HNSCC (Figure 19A-D).

Upon binding to eIF2B, eIF2 comes into contact with the regulatory core, in particular the subunits eIF2Bα and EIF2β, and the catalytic subunit eIF2Bδ (Gordiyenko et al., 2019). These subunits are indeed overexpressed in HNSCC (1.91^{-7}; 3.5^{-9} and 1.24^{-3} in respective order), (Figures 18A, 20A-D, 21B, D). eIF2 is capable of binding eIF2B in both phosphorylated and unphosphorylated form, however, the presence of a phosphate residue at serine 51 greatly enhances the binding affinity through interaction with eIF2Bα (directly) and eIF2Bδ (indirectly). eIF2 interacts more loosely with eIF2Bγ and eIF2Bε (Adomavicius et al., 2019). In contrast to RNA, these two subunits are not overexpressed on a protein level (Figure 18A, 21A, C, 22A-B). Together they form the nucleotide-exchange terminus. Interestingly, mechanistic studies have shown that eIF2B is an unusual nucleotide-exchange factor and is primarily regulated by the interaction with eIF2 and not nucleotide availability (Adomavicius et al., 2019). Changes observed in protein abundance do not exactly match transcript levels, indicating the importance of RNA processing.

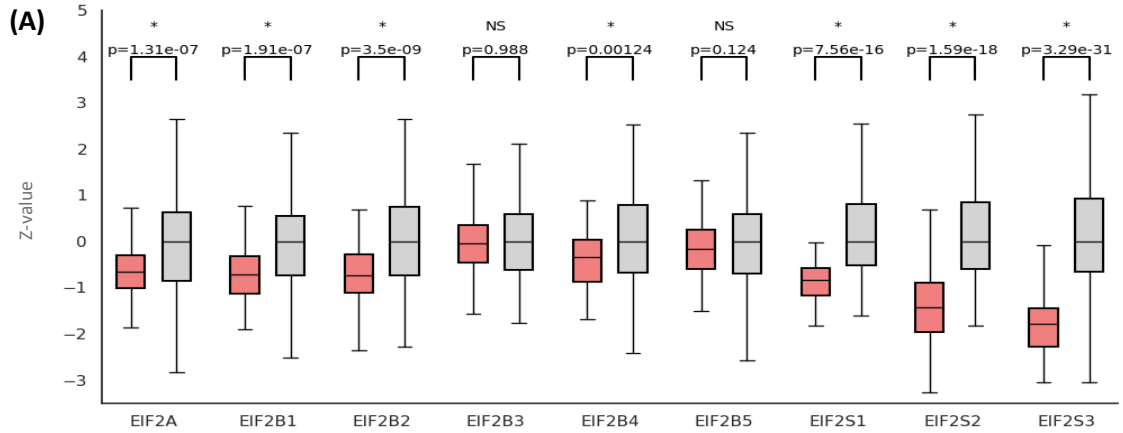

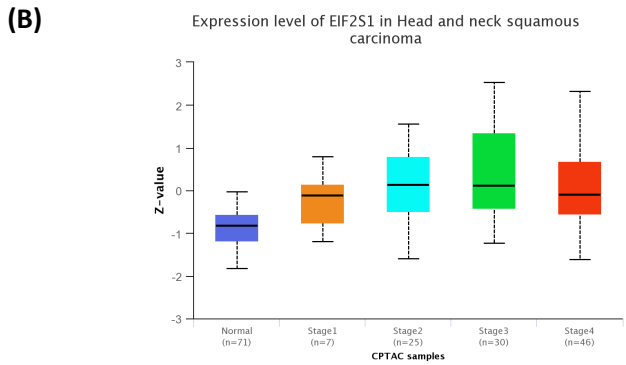

Comparison	Statistical significance
Normal-vs-Stage1	6.93E-02
Normal-vs-Stage2	8.85E-05
Normal-vs-Stage3	1.29E-06
Normal-vs-Stage4	9.25E-08
Stage1-vs-Stage2	3.05E-01
Stage1-vs-Stage3	5.02E-02
Stage1-vs-Stage4	3.45E-01
Stage2-vs-Stage3	2.06E-01
Stage2-vs-Stage4	8.14E-01
Stage3-vs-Stage4	9.63E-02

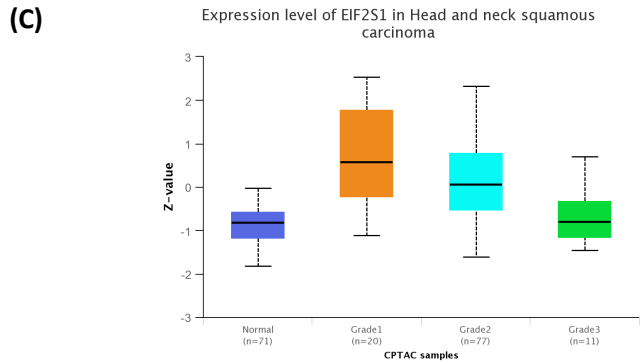

Comparison	Statistical significance
Normal-vs-Grade1	6.00E-06
Normal-vs-Grade2	3.66E-13
Normal-vs-Grade3	5.06E-01
Grade1-vs-Grade2	8.67E-05
Grade1-vs-Grade3	1.81E-03
Grade2-vs-Grade3	<1E-12

Figure 18. EIF2α is overexpressed in head and neck squamous cell carcinoma (HNSCC). (A) EIF2α protein abundance is significantly higher in HNSCC, represented in grey (n= 108) than in normal epithelium, as shown in red (n=71) (p-value= 1.62^{-12}). (B) EIF2α increases with the HNSCC stage. (C) EIF2α is elevated in histological grade 1 and 2 HNSCC. In all box-and-whisker diagrams, the horizontal line within the box corresponds to the median, box boundaries to lower and upper quartiles and vertical continuous lines stretch from minimum to maximum values. Statistical analysis was performed by comparing the interquartile range of each group by the Welch's t-test, significance level $p<0.05$.

(A)

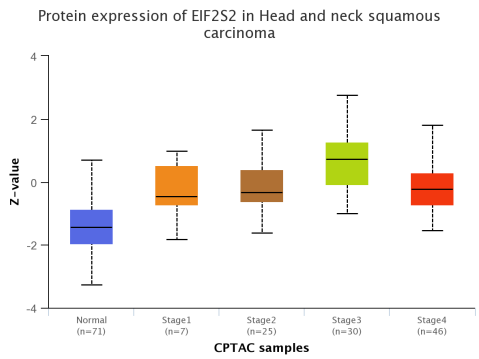

Comparison	Statistical significance
Normal-vs-Stage1	3.14E-02
Normal-vs-Stage2	1.12E-06
Normal-vs-Stage3	3.07E-12
Normal-vs-Stage4	4.03E-10
Stage1-vs-Stage2	6.34E-01
Stage1-vs-Stage3	5.85E-02
Stage1-vs-Stage4	5.64E-01
Stage2-vs-Stage3	1.13E-02
Stage2-vs-Stage4	8.83E-01
Stage3-vs-Stage4	6.99E-03

(C)

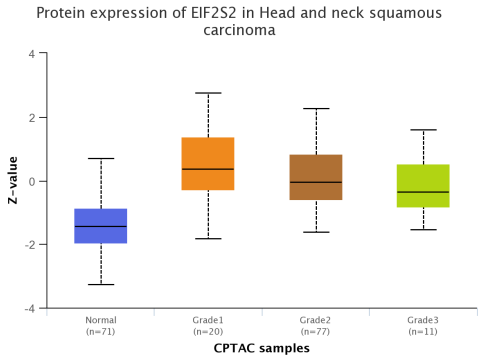

Comparison	Statistical significance
Normal-vs-Grade1	2.88E-06
Normal-vs-Grade2	3.96E-16
Normal-vs-Grade3	3.61E-03
Grade1-vs-Grade2	8.77E-02
Grade1-vs-Grade3	3.75E-01
Grade2-vs-Grade3	<1E-12

(B)

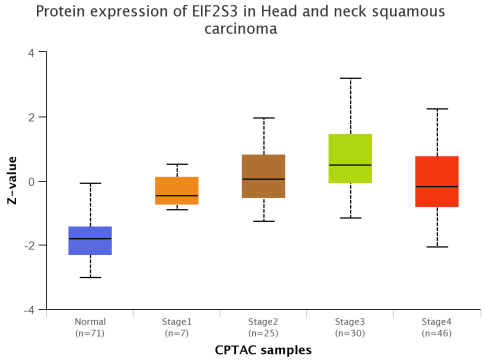

Comparison	Statistical significance
Normal-vs-Stage1	1.49E-04
Normal-vs-Stage2	1.25E-11
Normal-vs-Stage3	3.07E-14
Normal-vs-Stage4	2.72E-16
Stage1-vs-Stage2	1.36E-01
Stage1-vs-Stage3	4.96E-03
Stage1-vs-Stage4	3.62E-01
Stage2-vs-Stage3	7.24E-02
Stage2-vs-Stage4	3.10E-01
Stage3-vs-Stage4	6.70E-03

(D)

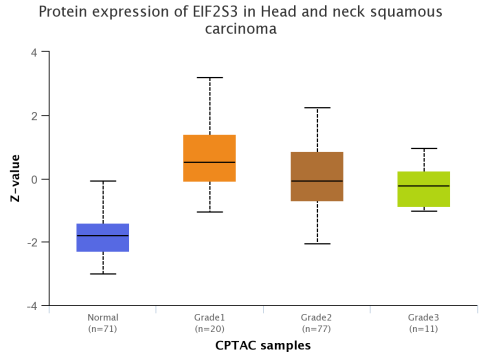

Comparison	Statistical significance
Normal-vs-Grade1	1.14E-09
Normal-vs-Grade2	4.07E-26
Normal-vs-Grade3	4.97E-06
Grade1-vs-Grade2	7.44E-03
Grade1-vs-Grade3	2.09E-01
Grade2-vs-Grade3	<1E-12

Figure 19. EIF2β and EIF2γ, encoded by *EIF2S2* and *EIF2S3,* are overexpressed in head and neck squamous cell carcinoma (HNSCC). (A, B) EIF2β and EIF2γ protein abundance levels are elevated in HNSCC of all stages; the increase becomes more pronounced with cancer progression and is highest at stage 3. (C, D) EIF2β and EIF2γ are elevated in HNSCC in all histological grades and highest in grade 1. In all box-and-whisker diagrams, the horizontal line within the box corresponds to the median, box boundaries to lower and upper quartiles and vertical continuous lines stretch from minimum to maximum values. Statistical analysis was performed by comparing the interquartile range of each group by the Welch's t-test, significance level $p<0.05$.

(A)

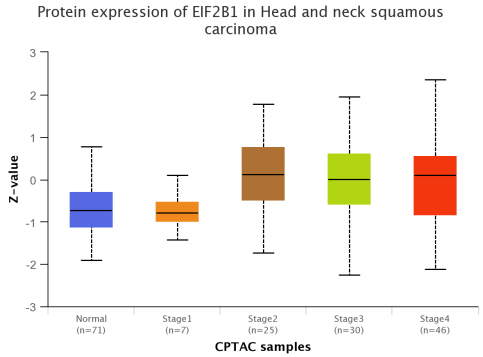

Comparison	Statistical significance
Normal-vs-Stage1	8.90E-01
Normal-vs-Stage2	1.76E-04
Normal-vs-Stage3	4.68E-03
Normal-vs-Stage4	2.05E-04
Stage1-vs-Stage2	3.70E-03
Stage1-vs-Stage3	2.23E-02
Stage1-vs-Stage4	1.21E-02
Stage2-vs-Stage3	4.94E-01
Stage2-vs-Stage4	4.32E-01
Stage3-vs-Stage4	9.96E-01

(B)

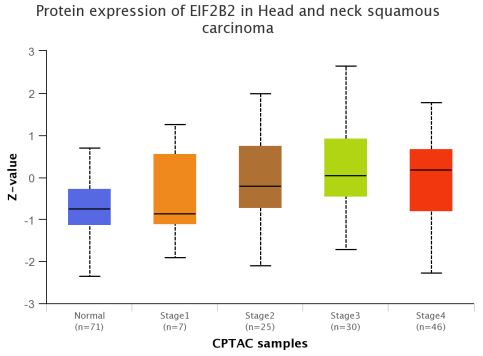

Comparison	Statistical significance
Normal-vs-Stage1	3.82E-01
Normal-vs-Stage2	9.48E-04
Normal-vs-Stage3	1.80E-05
Normal-vs-Stage4	3.40E-05
Stage1-vs-Stage2	4.13E-01
Stage1-vs-Stage3	2.62E-01
Stage1-vs-Stage4	5.27E-01
Stage2-vs-Stage3	5.89E-01
Stage2-vs-Stage4	6.61E-01
Stage3-vs-Stage4	2.57E-01

(C)

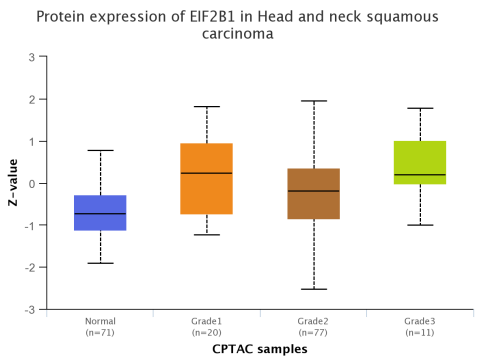

Comparison	Statistical significance
Normal-vs-Grade1	7.67E-04
Normal-vs-Grade2	1.79E-04
Normal-vs-Grade3	1.67E-03
Grade1-vs-Grade2	6.46E-01
Grade1-vs-Grade3	6.76E-02
Grade2-vs-Grade3	<1E-12

(D)

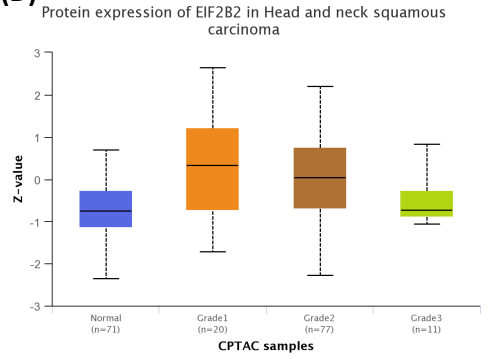

Comparison	Statistical significance
Normal-vs-Grade1	9.66E-04
Normal-vs-Grade2	9.90E-08
Normal-vs-Grade3	9.36E-02
Grade1-vs-Grade2	8.53E-02
Grade1-vs-Grade3	1.60E-01
Grade2-vs-Grade3	<1E-12

Figure 20. Subunits EIF2Bα and EIF2Bβ, encoded by *EIF2B1* and *EIF2B2,* are overexpressed in head and neck squamous cell carcinoma (HNSCC). (A, B) EIF2Bα and EIF2Bβ protein abundance is elevated in HNSCC at stages 2, 3 and 4. (C, D) EIF2Bα protein abundance increases with increasing cancer grade, whereas EIF2Bβ is most abundant in grade 2 tumors. In all box-and-whisker diagrams, the horizontal line within the box corresponds to the median, box boundaries to lower and upper quartiles and vertical continuous lines stretch from minimum to maximum values. Statistical analysis was performed by comparing the interquartile range of each group by the Welch's t-test, significance level $p<0.05$.

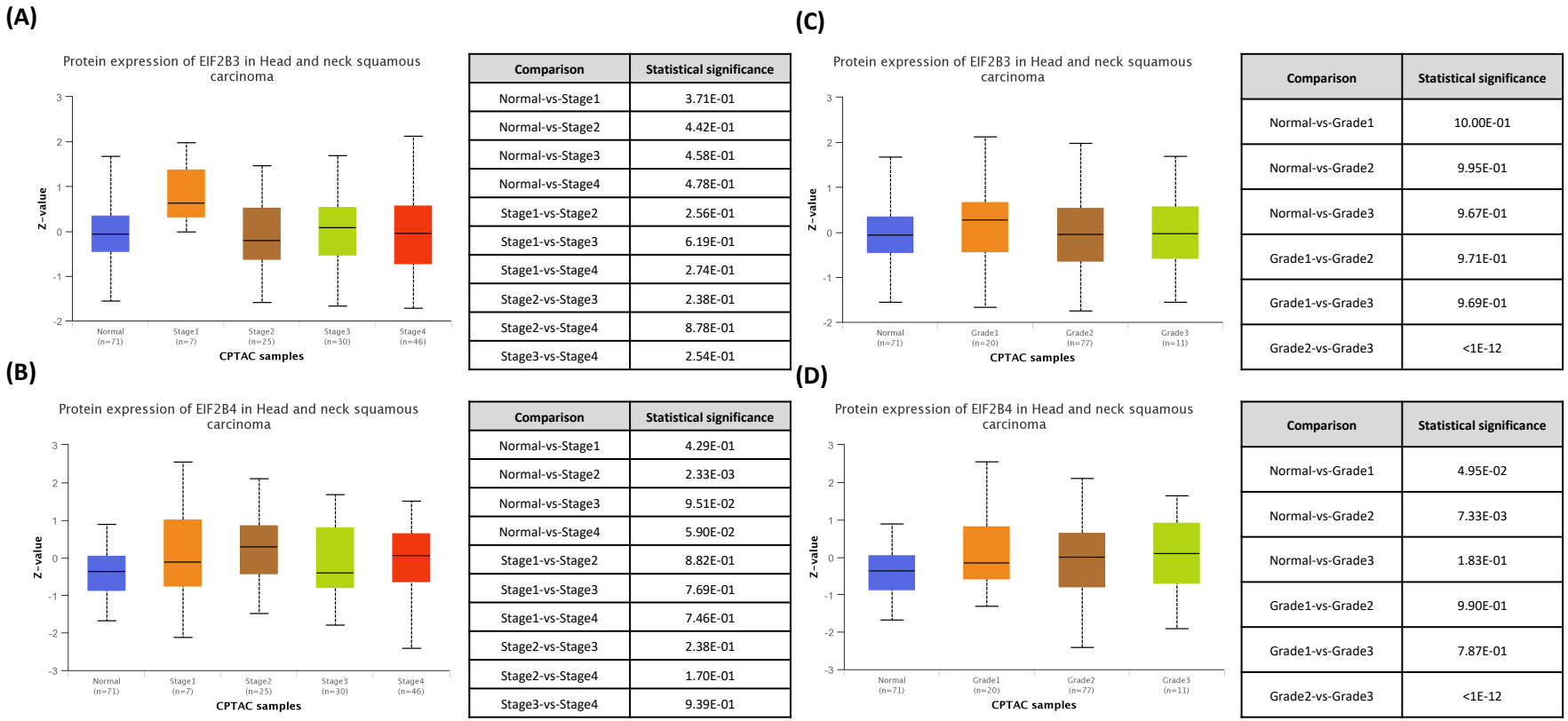

Comparison	Statistical significance
Normal-vs-Stage1	3.71E-01
Normal-vs-Stage2	4.42E-01
Normal-vs-Stage3	4.58E-01
Normal-vs-Stage4	4.78E-01
Stage1-vs-Stage2	2.56E-01
Stage1-vs-Stage3	6.19E-01
Stage1-vs-Stage4	2.74E-01
Stage2-vs-Stage3	2.38E-01
Stage2-vs-Stage4	8.78E-01
Stage3-vs-Stage4	2.54E-01

Comparison	Statistical significance
Normal-vs-Grade1	10.00E-01
Normal-vs-Grade2	9.95E-01
Normal-vs-Grade3	9.67E-01
Grade1-vs-Grade2	9.71E-01
Grade1-vs-Grade3	9.69E-01
Grade2-vs-Grade3	<1E-12

Comparison	Statistical significance
Normal-vs-Stage1	4.29E-01
Normal-vs-Stage2	2.33E-03
Normal-vs-Stage3	9.51E-02
Normal-vs-Stage4	5.90E-02
Stage1-vs-Stage2	8.82E-01
Stage1-vs-Stage3	7.69E-01
Stage1-vs-Stage4	7.46E-01
Stage2-vs-Stage3	2.38E-01
Stage2-vs-Stage4	1.70E-01
Stage3-vs-Stage4	9.39E-01

Comparison	Statistical significance
Normal-vs-Grade1	4.95E-02
Normal-vs-Grade2	7.33E-03
Normal-vs-Grade3	1.83E-01
Grade1-vs-Grade2	9.90E-01
Grade1-vs-Grade3	7.87E-01
Grade2-vs-Grade3	<1E-12

Figure 21. *EIF2B4* gene product (EIF2Bδ), but not *EIF2B3* (EIF2Bγ) is overexpressed in head and neck squamous cell carcinoma (HNSCC). (A, B) EIF2Bδ is elevated in HNSCC across all stages, while EIF2Bγ abundance is unaltered in HNSCC. (C, D) EIF2Bγ does not change with cancer grade. EIF2Bδ is significantly elevated in grade 2 cancers. In all box-and-whisker diagrams, the horizontal line within the box corresponds to the median, box boundaries to lower and upper quartiles and vertical continuous lines stretch from minimum to maximum values. Statistical analysis was performed by comparing the interquartile range of each group by the Welch's t-test, significance level $p<0.05$.

(A)

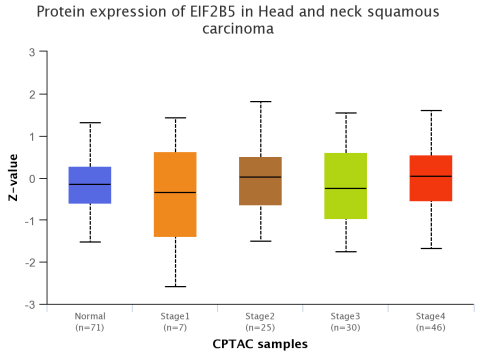

Comparison	Statistical significance
Normal-vs-Stage1	7.11E-01
Normal-vs-Stage2	9.09E-02
Normal-vs-Stage3	6.85E-01
Normal-vs-Stage4	1.54E-01
Stage1-vs-Stage2	3.22E-01
Stage1-vs-Stage3	6.22E-01
Stage1-vs-Stage4	4.56E-01
Stage2-vs-Stage3	2.52E-01
Stage2-vs-Stage4	4.96E-01
Stage3-vs-Stage4	5.05E-01

(B)

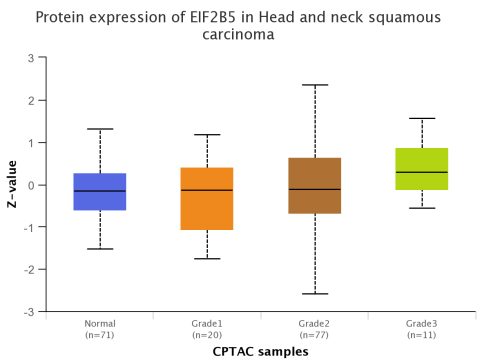

Comparison	Statistical significance
Normal-vs-Grade1	7.078E-01
Normal-vs-Grade2	8.91E-02
Normal-vs-Grade3	2.53E-01
Grade1-vs-Grade2	2.21E-01
Grade1-vs-Grade3	6.61E-01
Grade2-vs-Grade3	<1E-12

Figure 22. *EIF2B5* gene product- EIF2Bε is not overexpressed in head and neck squamous cell carcinoma (HNSCC). (A, B) EIF2Bε is not elevated in HNSCC, irrespective of cancer grade and stage. In all box-and-whisker diagrams, the horizontal line within the box corresponds to the median, box boundaries to lower and upper quartiles and vertical continuous lines stretch from minimum to maximum values. Statistical analysis was performed by comparing the interquartile range of each group by the Welch's t-test, significance level $p<0.05$.

3.7 eIF2α Protein Abundance is Elevated in Immunohistochemically Stained HNSCC Tissue Samples

To validate the results on an independent cohort, tissue samples from 83 patients with HNSCC originating from the larynx, epipharynx, hypopharynx, oropharynx, and oral cavity were stained with immunohistochemistry and evaluated for eIF2α expression. Table 9 shows the characteristics of the group studied. The neighboring non-neoplastic epithelium was used as a control (n=55). eIF2α is present predominantly in the cytoplasm. Staining intensity is significantly stronger in cancer than controls ($p<0.0001$). Similarly, the total immunostaining score (TIS), which represents the proportion and intensity of stained cells, is significantly higher in tumors than in controls ($p<0.0001$), with the median TIS value in cancer being twice that of control (Figure 23A-C).

Number of patients (%)	Total	83 (100%)
	Male	73 (88%)
	Female	10 (12%)
Localization	Larynx	57 (69.7%)
	Pharynx	13 (15.7%)
	Tongue/ base of tongue	6 (7.2%)
	Tonsil	2 (2.4%)
	Other	5 (6%)
Metastasis	Localized disease	47 (56.6%)
	Nodal metastasis	16 (19.3%)
	Distant metastasis	15 (18.1%)
	N/D	5 (6.0%)
HPV status	Positive	11 (13.2%)
	Negative	66 (79.5%)
	N/D	6 (7.2%)
P16 status	Positive	20 (24.1%)
	Negative	56 (67.5%)
	N/D	7 (8.4%)

Table 9. The characteristics of the patient cohort used for immunohistochemical (IHC) assessment of eukaryotic initiation factor α (eIF2α) protein expression in head and neck squamous cell carcinoma (HNSCC).

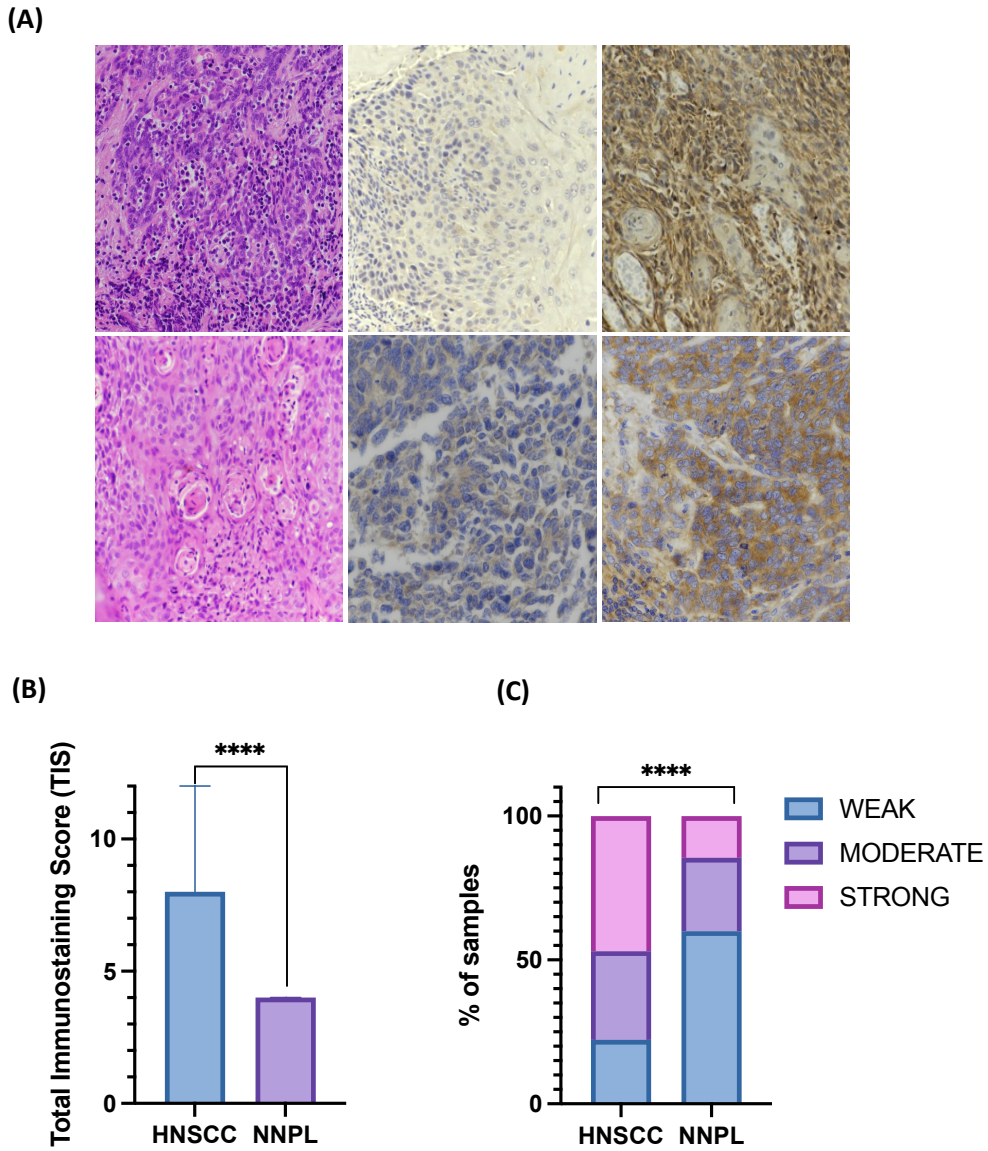

Figure 23. eIF2α is overexpressed in head and neck squamous cell carcinoma (HNSCC). (A) Representative photomicrographs of HNSCC slides showing hematoxylin/eosin (H&E) and immunohistochemical staining. Top row (20x) in respective order: H&E, low eIF2α expression with total immunostaining score (TIS= 2) and high eIF2α expression (TIS=12). Bottom row (40x): H&E, low and high eIF2α expression. (B) TIS is significantly higher HNSCC than in adjacent non-neoplastic tissue (NNPL), (Mann-Whitney U test; $p<0.0001$). (C) eIF2α staining intensity is significantly stronger in HNSCC than in adjacent NNPL (X^2 test; $p<0.0001$).

3.8 eIF2α Protein Expression in Relation to HPV Infection

To assess the eIF2α expression in relation to the HPV status, IHC for E6 (HPV 16/18) and P16 was performed. P16 positivity is reported when tissue samples feature at least 75% cytoplasmic and nuclear expression with moderate to strong intensity (Hayes et al., 2015). Irrespective of the detection method, there are no statistically significant differences in the eIF2α expression between HPV+ and – HNSCC in this cohort (Figure 24A-D). However, a trend for a higher eIF2α staining intensity in HPV- HNSCC was seen; 63% of E6-expressing samples featured moderate or strong eIF2α IS, while in the E6-negative group, this proportion rises to 80% (Figure 24A, C).

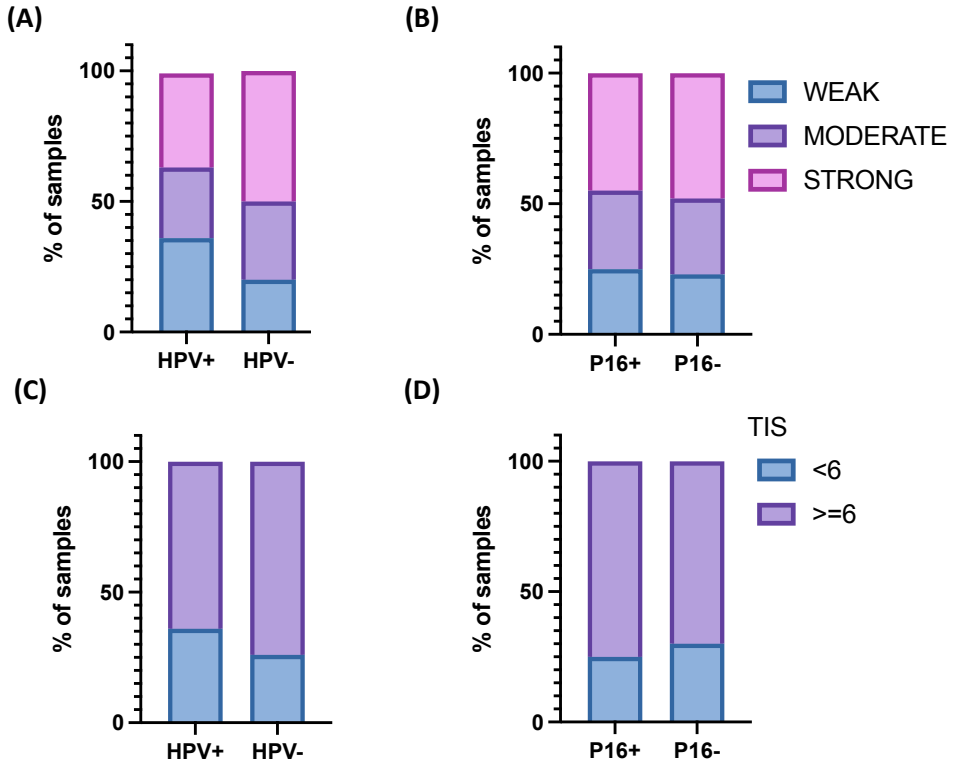

Figure 24. eIF2α expression in relation to the HPV status in head and neck squamous cell carcinoma (HNSCC). The presented bar graphs show eIF2α staining intensity in relation to the HPV status determined by (A) E6 (HPV16/18) immunohistochemistry (IHC); (B) HPV status determined by P16 IHC. In graphs C and D samples were divided into groups with high and low total immunostaining scores (TIS) with a cut-off point at the median. eIF2α expression is shown in relation to HPV status defined by E6 (HPV16/18) and P16, respectively. No statistically significant differences in eIF2α protein abundance were observed between HPV+ and – HNSCC. However, a trend for a stronger staining intensity in HPV- HNSCC was observed. Statistical analysis: X^2 test; p-value: ns.

3.9 eIF2α Abundance Increases with Malignant Progression

The pathogenesis of HNSCC involves a gradual progression from dysplastic epithelium to invasive cancer, triggered and accompanied by alterations in different signaling pathways. To further characterize the eIF2α expression at different stages of HNSCC development, the cohort was narrowed down to samples where carcinoma (n=40), as well as intermediate stadia of HNSCC development (i.e., dysplasia and carcinoma *in situ* and metastasis), could be delineated. Detailed characteristics of the patient subgroup are provided in Table 10. Strikingly, the progression of the disease is mirrored by the increase in EIF2α staining intensity and TIS. The TIS score is highest in cancer metastasis (median TIS=9), followed by invasive cancer (TIS=8), carcinoma *in situ* (TIS=7), dysplasia (TIS=6), and lowest in neighboring normal tissue (TIS=4) ($p<0.0001$) (Figure 25A). Similar to the above analysis of mRNA transcript and mass spectrometry-based proteomics data, samples in this cohort were divided into high- and low-eIF2α abundance, using the median TIS as a cut-off value. Almost 90% of normal samples featured low eIF2α expression. In dysplasia and carcinoma *in situ*, there was an approximately equal distribution of samples exhibiting high and low expression levels, while in carcinoma and metastatic cancer high-eIF2α expression was seen in most samples (Figure 25B). The assessment of staining intensity showed that over a third of cancer samples are strongly stained for eIF2α, while none in the control group. Conversely, weak signal intensity is seen in over 80% of control and only 26% of cancers. Dysplasia and carcinoma *in situ* show intermediate staining intensity with around 40% of samples with moderate IS (Figure 25C). Detailed information on the statistical significance levels of differences in TIS and IS observed between these histological lesions are provided in Figures 26A and B.

Number of patients (%)	Total	40 (100%)
	Male	34 (85%)
	Female	6 (15%)
Tumor localization	Larynx	35 (87.5%)
	Pharynx	0 (0%)
	Tongue/ base of tongue	2 (5%)
	Tonsil	0 (0%)
	Other	3 (7.5%)
Histological grade	G1	4 (10%)
	G2	19 (47.5%)
	G3	13 (32.5%)
	GX	4 (10%)
Tumor stage	T1	7 (17.5%)
	T2	6 (15%)
	T3	13 (32.5%)
	T4	9 (22.5%)
	TX	5 (12.5%)
Nodal stage	N0	19 (47.5%)
	N1	3 (7.5%)
	N2	11 (27.5%)
	N3	1 (2.5%)
	N4	1 (2.5%)
	NX	5 (12.5%)
Metastasis	M0	25 (62.5%)
	M1	5 (12.5)
	Mx	9 (25%)
HPV status	Positive	4 (10%)
	Negative	30 (75%)
	N/D	6 (15%)
P16 status	Positive	10 (25%)
	Negative	23 (57.5%)
	N/D	7 (17.5%)

Table 10. The characteristics of the patient subgroup used for immunohistochemical (IHC) assessment of eukaryotic initiation factor alfa (eIF2α) protein expression across different stages of head and neck squamous cell carcinoma (HNSCC) development, including dysplasia, carcinoma *in situ*, invasive cancer and metastasis.

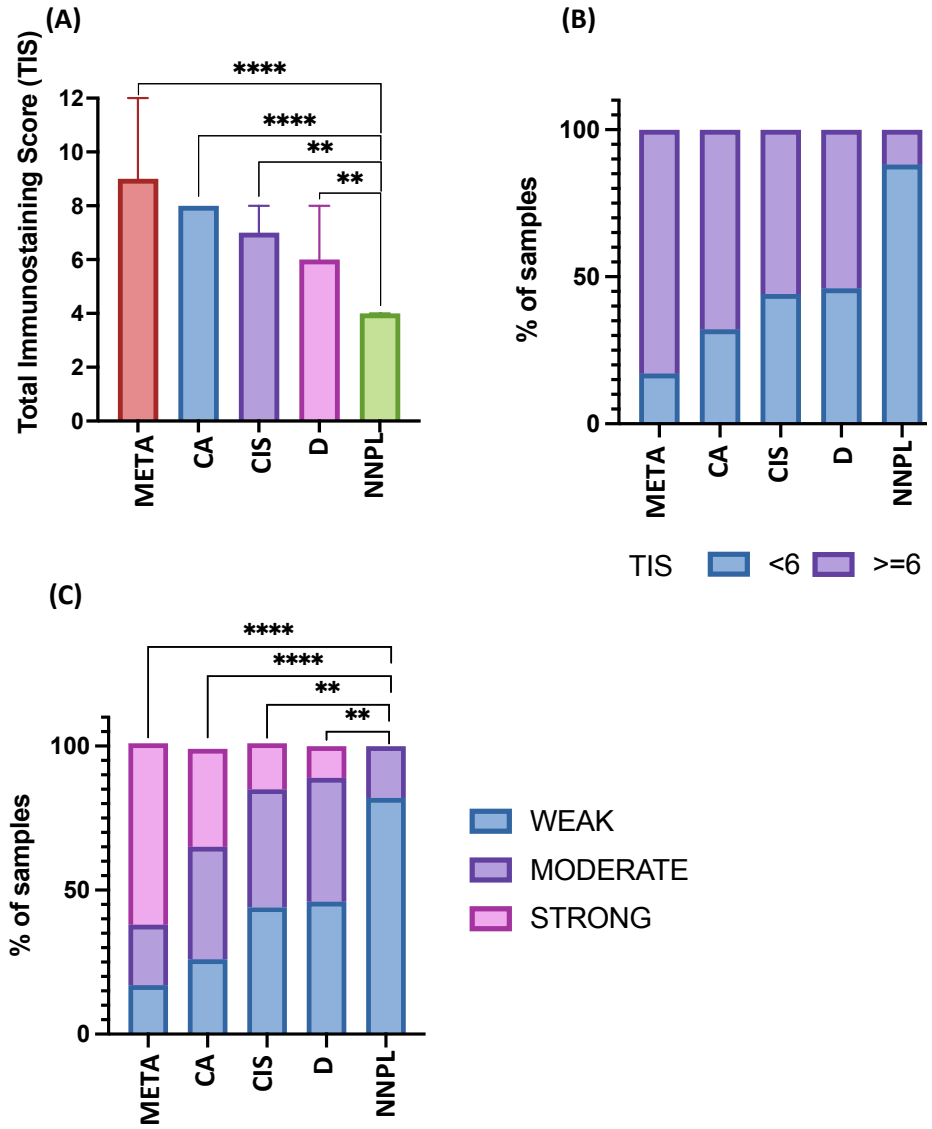

Figure 25. eIF2α abundance in mucosal epithelium increases with progression to malignancy. (A) eIF2α total immunostaining score (TIS) is highest in metastatic tissue, followed by HNSCC primum and precancerous lesions (X^2 test; *p<0.05; **p<0.01; p<0.001***; p<0.0001****). (B) The proportion of samples overexpressing eIF2α increases gradually, in parallel with progression to malignancy. Samples were divided into groups with high and low expression with a cut-off point at the median (TIS≥6). (C) eIF2α staining intensity differs across stages of HNSCC development, with the highest IS observed in cancer metastasis and the lowest in tumor-adjacent non-neoplastic tissue (X^2 test; p<0.0001).

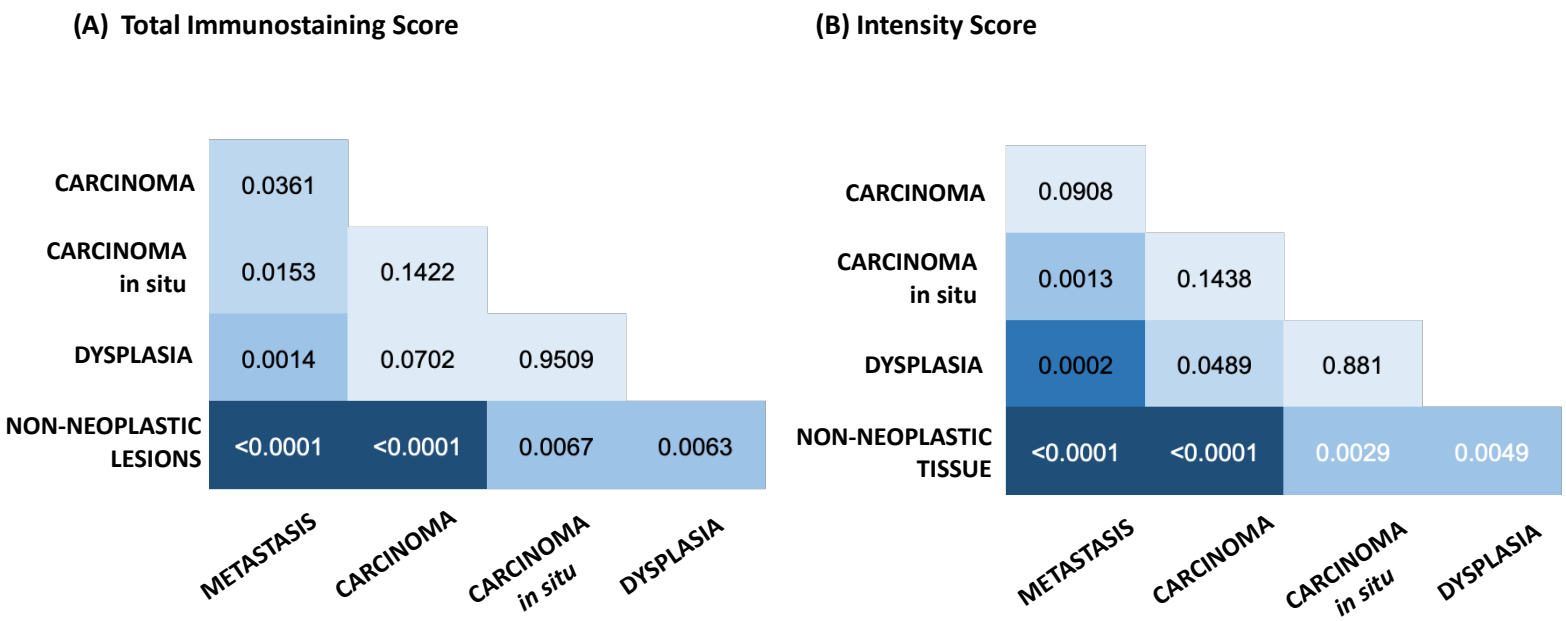

Figure 26. eIF2α expression increases with malignant progression in head and neck squamous cell carcinoma (HNSCC). The heatmaps show statistical significance levels (p-values; X^2 test) between (A) the total immunostaining score (TIS); and (B) the intensity score (IS) across different histological entities: metastasis, invasive carcinoma, carcinoma *in situ*, dysplasia and the adjacent non-neoplastic tissue used as control.

3.10 eIF2α Abundance and Phosphorylation in Freshly Frozen Intraoperative Patient Samples

Phosphorylation of the α subunit of eIF2 at serine 51 by stress-responsive kinases is a key mechanism for driving down the translation. Phosphorylated eIF2α remains bound to eIF2B, unable to form the ternary complex (Gordiyenko et al., 2019). The results described to this point show that cancer cells synthesize high levels of the regulatory subunit eIF2α. Given that cells in solid tumors are permanently subjected to stress resulting from hypoxia, nutrient depletion and genomic instability, the arising question is whether tumor cells also have higher steady-state eIF2α phosphorylation in comparison to normal epithelial cells.

Western blot analysis of freshly frozen intraoperative tissue samples (n=16) once again confirmed a higher expression of eIF2α in tumor than in adjacent normal epithelium ($p=0.0021$) (Figure 27A and B). The abundance of phosphorylated eIF2α was also significantly elevated in cancer ($p= 0.0125$) (Figure 27A and C), consistent with the concept that cancers initially benefit from the cytoprotective aspect of increased basal eIF2α phosphorylation. The ratio of phosphorylated and unphosphorylated eIF2α was higher in HNSCC but not significantly ($p=0.0583$) (Figure 27D).

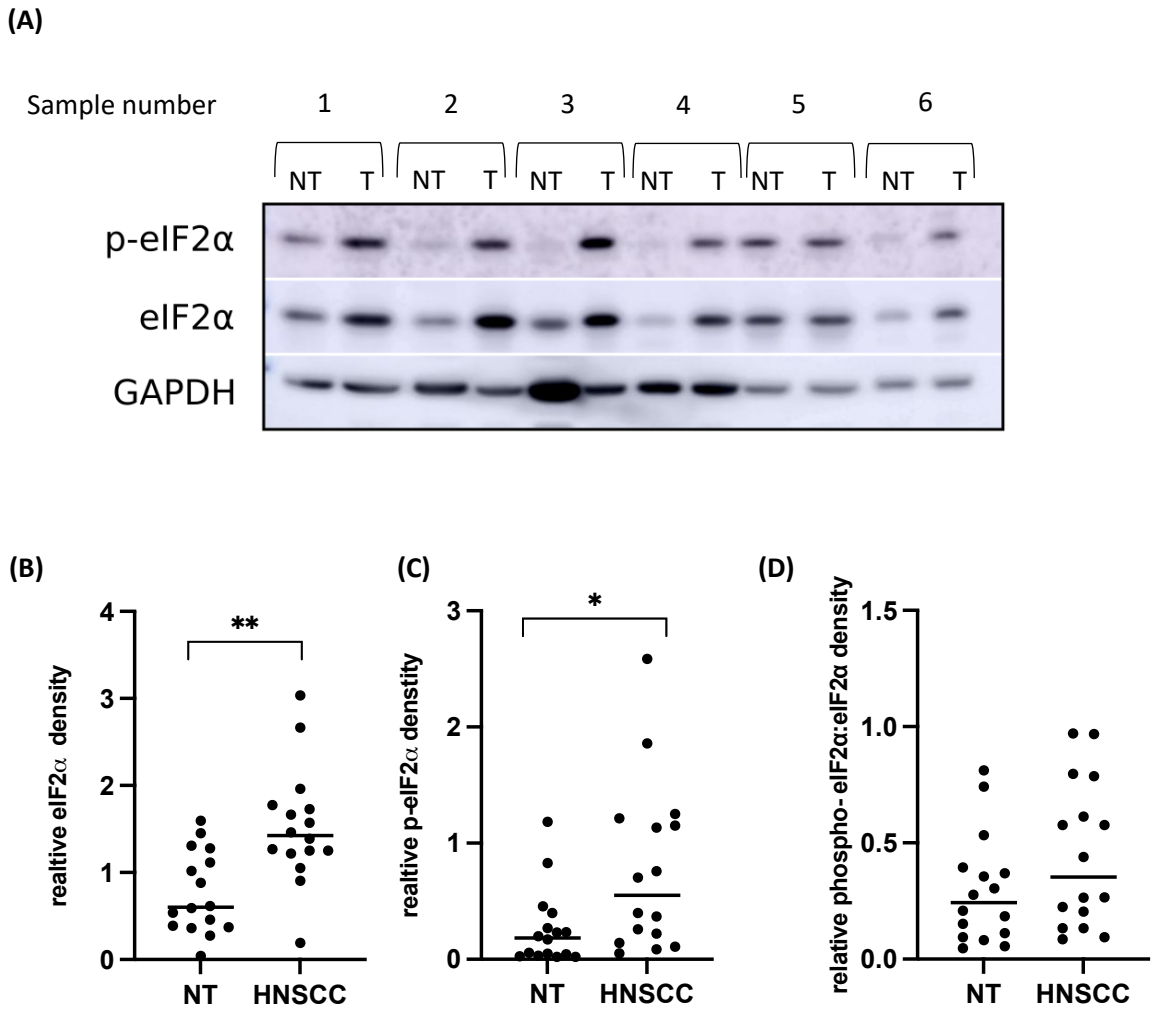

Figure 27. eIF2α abundance and phosphorylation are significantly increased in head and neck squamous cell carcinoma (HNSCC) in comparison to adjacent normal epithelium. (A) Examples of western blots from intraoperative freshly frozen tissue samples from six patients with HNSCC. From each patient, 2 samples were collected: tumor (T) and adjacent normal tissue (NT). GAPDH was used as a loading control. (B, C) Densitometric analyses of eIF2α and p-eIF2α protein expression show higher protein abundance in HNSCC (n=16; p=0.0021 and p=0.0125, respectively; Wilcoxon test). The intensity of the signal was normalized to GAPDH. (D) The ratio of phosphorylated-eIF2α to *un*phosphorylated-eIF2α is higher in HNSCC than in NT but not significantly (p=0.0583; Wilcoxon test).

3.11 EIF2 Complex Members are Essential for HNSCC Survival *in vitro*

To further elucidate the function of EIF2, data from CRISPR-Cas9 knockdown experiments on 81 HNSCC cell lines were analyzed bioinformatically. The list of cell lines used is provided in Supplement S6. The depletion effects of eIF2 complex genes, eIF2 kinases and phosphatases are expressed as the dependency score, corresponding to the degree to which a given gene is essential for cell survival and proliferation. A dependency score of 0 indicates that a gene is not essential; a score of 1 corresponds to the median of all pan-essential genes. *EIF2S1* is a common essential gene in HNSCC, as are other members of the EIIF2 complex. *EIF2S1* ablation results in the most prominent perturbations. This is in agreement with the unpublished experimental observations made during the preparation of this work, whereby a transient knockdown with siRNA was detrimental to HNSCC cell survival. In congruence with previous reports, suggesting a degree of functional redundancy between the phosphorylating kinases- *EIF2AK1-4* - are not essential to HNSCC survival (Donnelly et al., 2013). The regulatory subunit of protein phosphatase 1- GADD34 (encoded by *PPP1R15A*), reversing stress-induced phosphorylation of eIF2α is also not an essential gene, while the susceptibility to depletion of the constitutively active CREP (*PPP1R15B*) varies between cell lines (Figure 28).

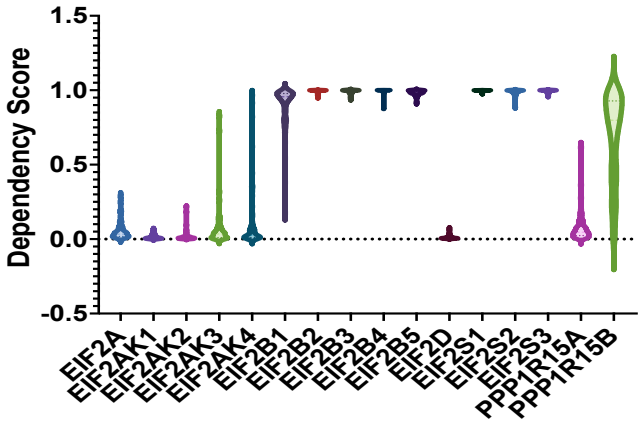

Figure 28. EIF2 factors are essential for head and neck squamous cell carcinoma (HNSCC) cell survival. The violin plot shows the effects of CRISPR-Cas9 knockdown of eIF2 complex members, eIF2 kinases (*EIF2AK1-4*) and phosphatase regulatory subunits GADD34 and CREP (*PPP1R15A* and *PPP1R15B*) across 81 HNSCC cell lines expressed as dependency scores (0= non-essential; 1=essential). Abbreviations of kinase encoding gene names: *EIF2AK1*(HRI), *EIF2AK2* (PKR), *EIF2AK3* (PERK), *EIF2AK4* (GCN2).

3.12 Treatment with an eIF2α Phosphorylation Inhibitor Decreases Cell Viability and Clonogenic Survival *in vitro* by Disrupting Cell Cycle Progression

A small molecule compound- salubrinal (Sal003, S4451)- inhibits dephosphorylation of eIF2α by GADD34/PP1 and CREP/PP1 complexes in a dose-dependent manner. Proteomics studies report no global changes in protein phosphorylation levels following treatment with salubrinal, and thus, a remarkable substrate specificity (Boyce et al., 2005). Prolonged incubation of human hypopharyngeal (FaDu) and oral (SCC4) cells with the drug resulted in a sustained phosphorylation of eIF2α, which could be confirmed by western blot (Figure 29). Original uncropped western blots and complete densitometric raw data are provided in Supplement S7.

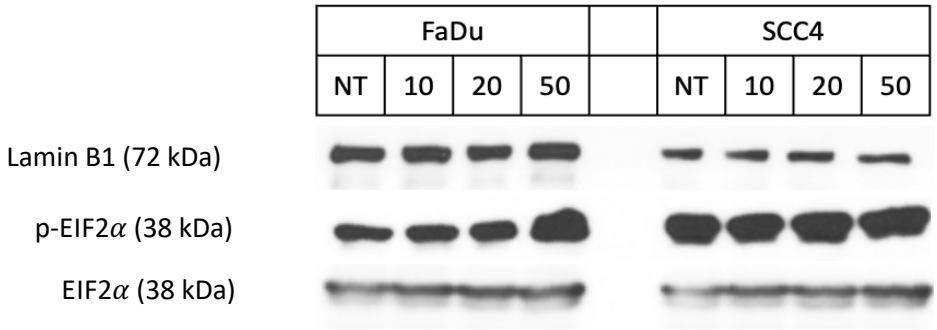

Densitometric analysis		phospho-eIF2a:eIF2a
FaDu	NT	1
	10	1.19584212
	20	1.279310135
	50	1.85494508
SCC4	NT	1
	10	1.208618336
	20	1.213790672
	50	1.129933483

Figure 29. Prolonged treatment with salubrinal results in sustained phosphorylation of EIF2α in head and neck squamous cell carcinoma (HNSCC) cells. Western blots and densitometric analysis of EIF2α and p-EIF2α abundance after 12h treatment with salubrinal (non-treated, 10, 20 and 50 μM) in human hypopharyngeal (FaDu) and oral (SCC4) cells.

The cells were incubated with increasing doses of salubrinal for 24, 48, and 72h, followed by an MTT-based viability assay. A significant decrease in cell viability was seen in both cell lines starting at 24h, which became more pronounced after 48 and 72h of treatment (Figure 30A and B). Treatment with salubrinal also drastically impaired the colony-forming ability of the cells (Figure 31A-D). The decreased cell viability following treatment with salubrinal was not associated with caspase and PARP cleavage (negative data not shown). To determine whether a persistent eIF2α phosphorylation could disrupt the cell cycle progression, cells were incubated with increasing doses of salubrinal for 36h and stained with propidium iodide (PI) in the presence of RNAse. Cell cycle analysis with flow cytometry showed a significantly higher percentage of cells in G_0/G_1 in samples treated with salubrinal and fewer cells entering S and G_2/M phases (multiple t-tests; $p<0.05$) (Figure 32A-C).

Cell cycle progression requires a coordinated interaction of cyclins and cyclin-dependent kinases. At the entry point, D-type cyclins complexed with CDK4/6 phosphorylate RB1, releasing E2F1 (Matthews et al., 2022). The activated transcription factor targets multiple genes, including cyclins A and E, driving the passage from the G_1 to the S phase. Western blot analysis of cell cycle components revealed a decrease in cyclin D1, whose abundance is highly dependent on translation rate and is rate-limiting in cells with intact RB signaling (Brewer et al., 1999). Treatment with salubrinal also decreased phosphorylation levels of RB1 and depleted E2F1 and cyclin A. Lastly, P21, the CDK-inhibitor, restricting S-phase entry, normally degraded at the end of G_1 (Fitzgerald et al., 2015), is induced by the treatment. The induction becomes more pronounced over time (Figure 33; original uncropped western blot images are provided in Supplement S8). Taken together, the data suggest an impairment of G_1/S transition caused by salubrinal treatment.

(A)

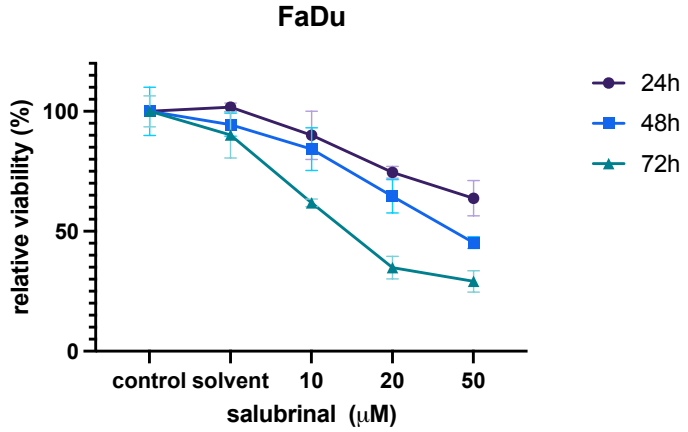

%	control	solvent	10	20	50
24h	100	101.7	90.0	74.5	63.8
48h	100	94.5	84.2	64.6	45.3
72h	100	90.1	61.8	34.9	29.1

(B)

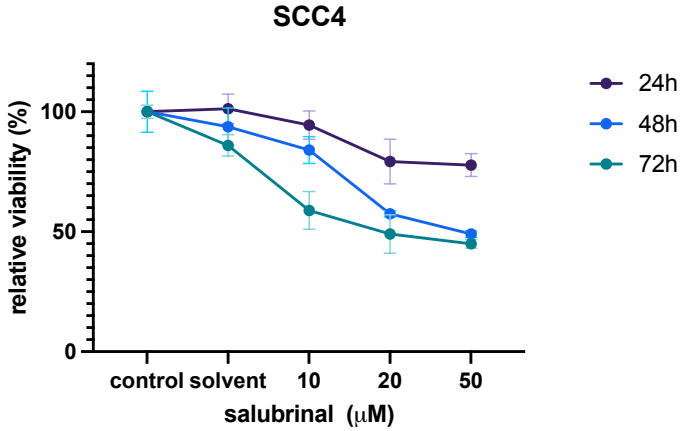

%	control	solvent	10	20	50
24h	100	101.2	94.5	79.3	77.8
48h	100	93.8	84.0	57.5	49.0
72h	100	86.0	58.9	49.1	45.0

Figure 30. Treatment with the eIF2α dephosphorylation inhibitor salubrinal decreases head and neck squamous cell carcinoma (HNSCC) cell viability. (A) FaDu and (B) SCC4 cells were treated with increasing concentrations of salubrinal (10, 20 and 50μ). Cell viability was measured after 24h, 48h and 72h of incubation with an MTT assay.

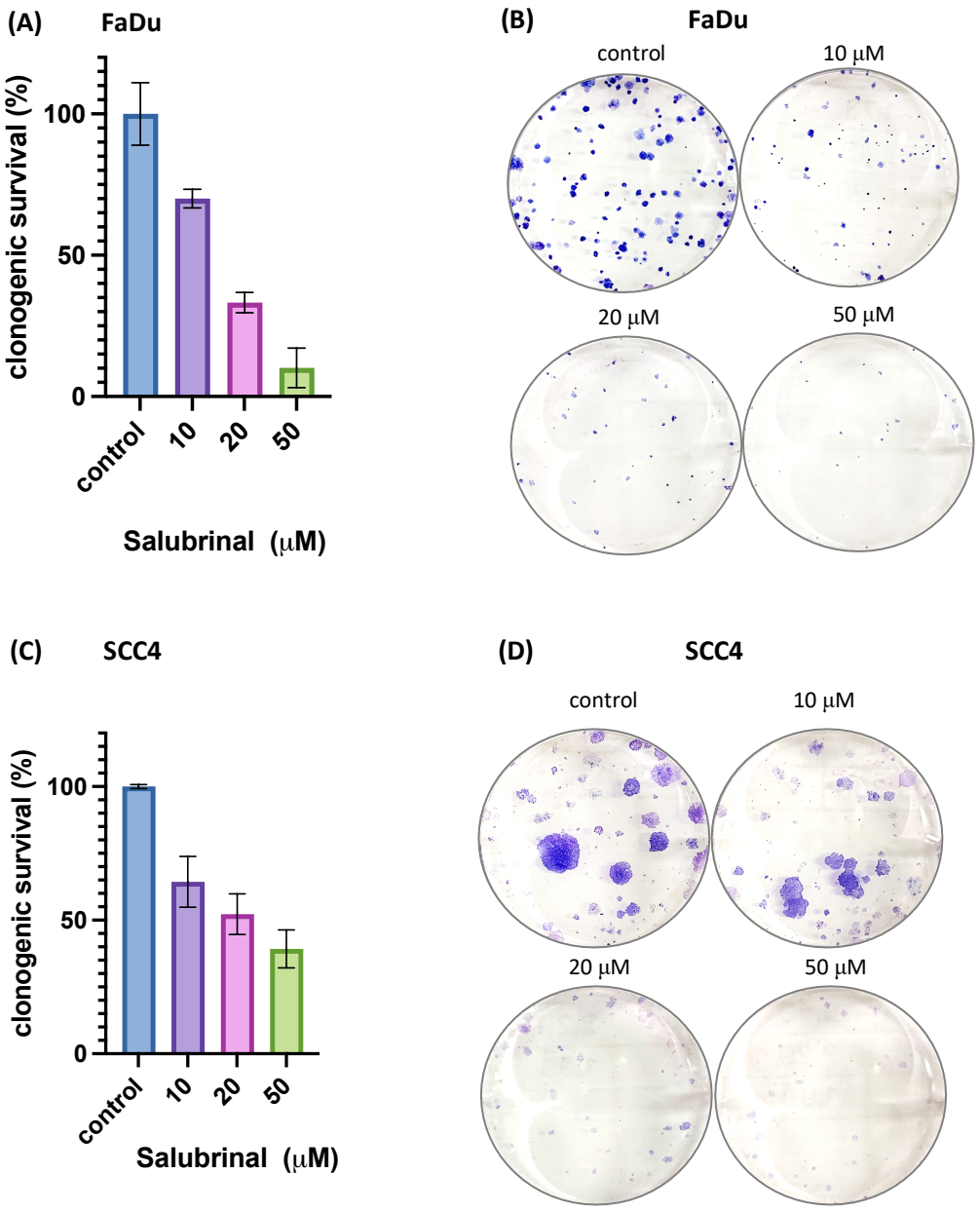

Figure 31. Treatment with the eIF2α dephosphorylation inhibitor salubrinal decreases clonogenic survival of head and neck squamous cell carcinoma cells (HNSCC). Increasing concentrations of salubrinal (10, 20 and 50 μM) were added to cell cultures and incubated for 10 days, followed by fixation, staining and manual counting of colonies. Salubrinal markedly decreased clonogenic survival in (A, B) FaDu and (C, D) SCC4 cells.

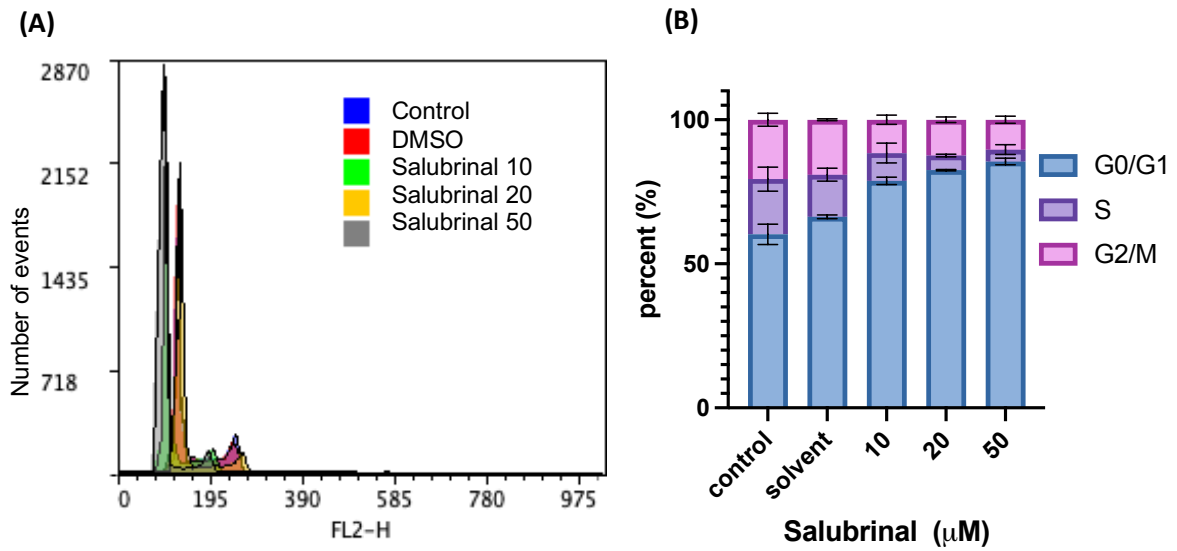

(C)

%	control	solvent	sal 10μ	sal 20μ	sal 50μ
G_0/G_1	60.03	66.08 (ns)	78.46 (0.02)	82.22 (0.01)	85.07 (0.01)
S	19.07	14.54 (ns)	9.66 (0.13)	5.05 (0.04)	4.10 (0.04)
G_2/M	20.54	18.99 (ns)	11.51 (0.04)	12.35 (0.04)	10.31 (0.03)

Figure 32. Treatment with the eIF2α dephosphorylation inhibitor salubrinal (sal) impairs the cell cycle progression in head and neck squamous cell carcinoma (HNSCC). FaDu cells were treated with increasing concentrations of salubrinal (10, 20 and 50μ) and the relative DNA content was measured with flow cytometry. (A) Histogram overlay showing cell cycle distribution across samples treated with different inhibitor concentrations. (B and C) The treatment resulted in changes in cell cycle distribution with an increasing number of cells arrested in G_0/G_1 and fewer cells entering the S and G_2/M phases (t-test, $p<0.05$). The table and bar graph depict percentages of live cells in G_0/G_1, S, G_2/M phases and statistical significance of differences in comparison to untreated control (p-value; t-test).

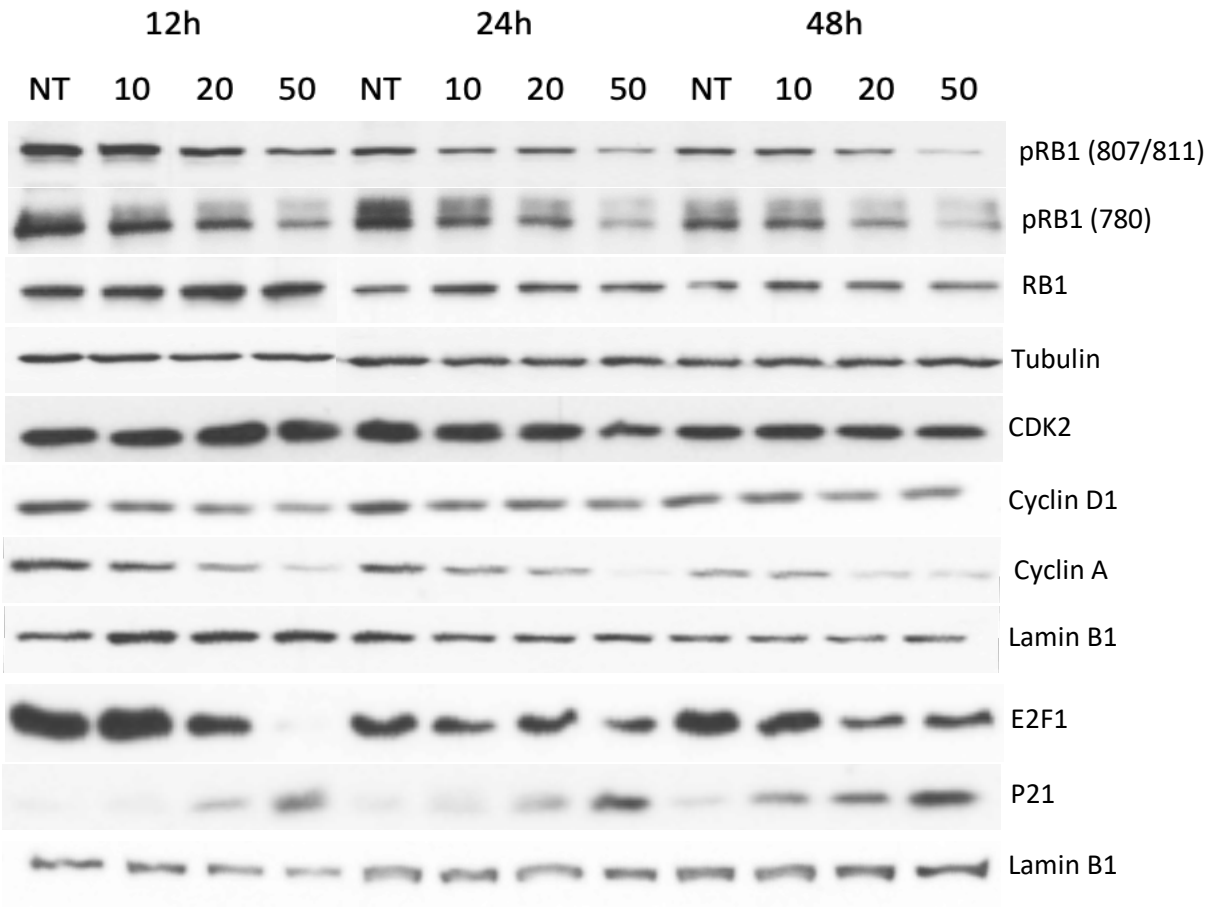

Figure 33. Salubrinal disrupts the cell cycle progression in head and neck squamous cell carcinoma (HNSCC). Treatment of FaDu cells with salubrinal for 24, 48 and 72h leads to a decrease in RB1 phosphorylation, cyclin D1, cyclin A and E2F1 depletion, with simultaneous induction of P21.

3.13 Salubrinal Decreases the Viability of Patient-Derived 3D Tumor Spheroids (PD3DS) and Enhances the Cytotoxicity of Selected Chemotherapeutics

Patient-derived spheroids were expanded and used for chemosensitivity testing. The luminescence signal in samples treated with increasing doses of salubrinal was compared to the vehicle (DMSO), and dose-response curves were generated using a non-linear regression model. Salubrinal decreased HNSCC spheroid viability with an IC_{50} range from 15.63 to 73.55 µM (Figure 34). Interestingly, the lowest dose of salubrinal was non-toxic and slightly increased PD3DS viability, in keeping with its ability to alleviate ER stress (Boyce et al., 2005).

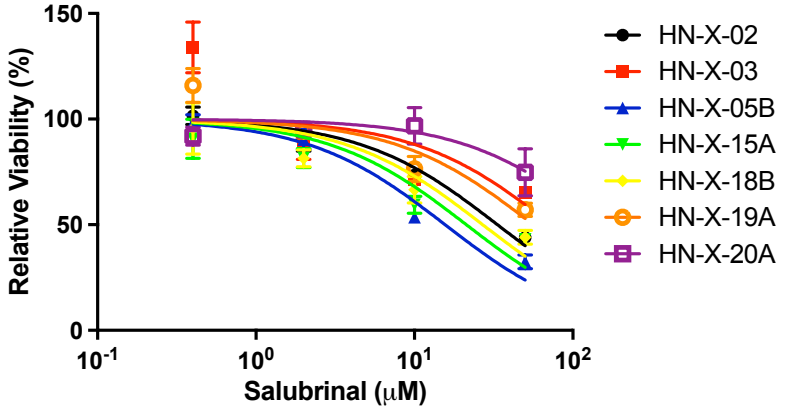

	HN-X-02	HN-X-03	HN-X-05B	HN-X-15A	HN-X-18B	HN-X-19A	HN-X-20A
$LogIC_{50}$	1.524	1.867	1.194	1.328	1.431	1.750	2.183
95% CI ($LogIC_{50}$)	1.414 - 1.635	1.414 - 2.319	1.066 - 1.321	1.115 - 1.540	1.197 - 1.666	1.520 - 1.980	1.842 - 2.525
IC_{50}	33.45	73.55	15.63	21.27	27.00	56.20	152.5
95% CI (IC_{50})	25.92 - 43.16	25.95 - 208.4	11.65 - 20.96	13.04 - 34.70	15.74 - 46.34	33.09 - 95.44	69.51 - 334.8

Figure 34. Salubrinal decreases the viability of patient-derived 3D tumor spheroids (PD3DS). PD3DS were cultured on 384-well plates in a mixture of Matrigel and medium, in the presence of increasing salubrinal concentrations (0.4, 2, 10 and 50 µM) for 4 days followed by an ATP-based viability assay. Dose-response curves were obtained from 4 biological replicates, using non-linear regression. The table represents IC_{50} and $LogIC_{50}$ for each sample with 95% confidence intervals (CI).

The mainstay of therapy for inoperable HNSCC is platin-based chemotherapy combined with irradiation. The widely used chemotherapeutic TPF regimen comprises a taxane drug, a platinum compound, and 5-fluorouracil (5FU) (Q. Li et al., 2023). Accordingly, we looked at FaDu viability after 48 h of co-treatment with salubrinal and paclitaxel, cisplatin or 5FU. The obtained synergy scores represent the average excess response to a given drug combination compared to the expected response assuming no interaction. Scores above 10 indicate a synergistic interaction of the two agents; below -10 indicate an antagonistic interaction; and between -10 and +10 an additive effect (Ianevski et al., 2022). We observed a strong synergy between salubrinal and cisplatin (synergy score 35.02). Adding a minimally toxic dose of salubrinal (10 μM) caused a synergistic potency shift across all doses of cisplatin. The cisplatin efficacy shift is most pronounced at low doses, with a relative viability inhibition increasing from 33.96% to 89.43%. Similarly, 5FU works synergistically with salubrinal - synergy score 13.77 (Figures 35 and 36). The effect of paclitaxel and salubrinal is likely additive (synergy score 10.21) (Figure 37).

Proteasome inhibitors (PI) cause cancer cell death by disrupting proteasome homeostasis. The combination of salubrinal and bortezomib is highly effective in multiple myeloma and eradicates PI-resistant cells (Drexler, 2009; Schewe & Aguirre-Ghiso, 2009). We observed a synergy between salubrinal and bortezomib (score 13.13), yet the synergy score was nearly twice higher (25.07) when salubrinal was combined with MG-132. The latter is a PI, used for research purposes only, known to have a more pleiotropic mode of action. At 0.2 μM MG-132, salubrinal induced a potency shift from 6.6% inhibition to 44.1% and 52.6% when adding 10 and 50 μM, respectively (Figures 38 and 39).

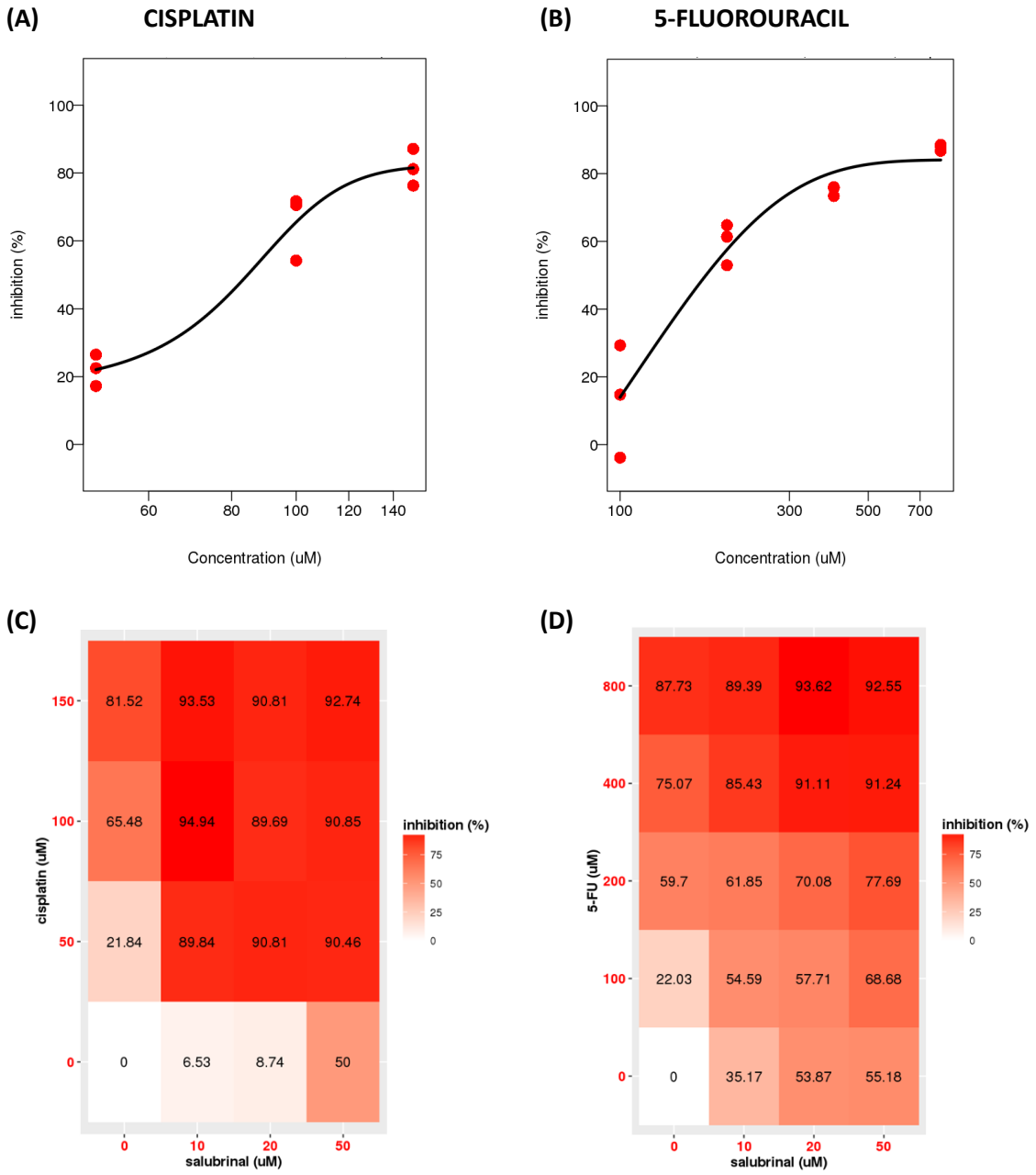

Figure 35. Salubrinal synergizes with cisplatin and 5-fluorouracil (5FU), inhibiting head and neck carcinoma (HNSCC) cell growth. FaDu cells were treated continuously for 48h with increasing concentrations of the respective drugs, followed by an MTT assay performed in triplicates. The graphs represent the dose-response curves for (A) cisplatin and (B) 5FU. Percentages indicate cell viability inhibition. (C, D) Dose-response matrices representing percentage cell viability inhibition for the co-treatments. The graphs were generated using the MuSyC consensus framework and LL4 curve fitting, available via the SynergyFinder web platform (Ianevski et al., 2022).

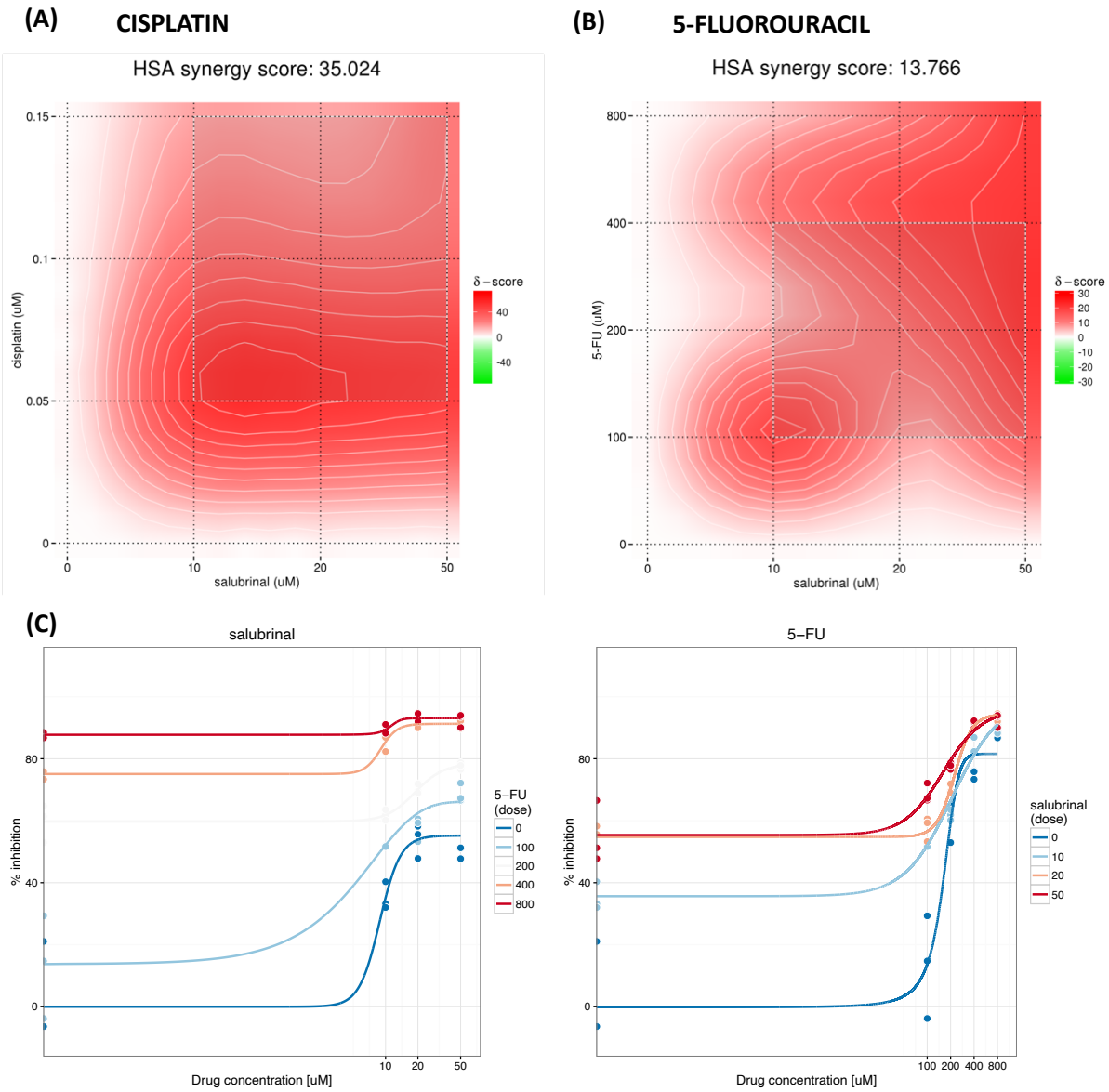

Figure 36. Salubrinal synergizes with cisplatin and 5-fluorouracil (5FU), inhibiting head and neck carcinoma (HNSCC) cell growth. FaDu cells were treated continuously for 48h with increasing concentrations of the respective drugs, followed by an MTT assay performed in triplicates. The heatmaps represent synergy scores for salubrinal co-treatments with (A) cisplatin and (B) 5FU. (C) Graphic analysis of the synergistic interaction between salubrinal and 5FU. The combination increases the maximal effect of 5FU by 16%. The heatmaps and graph were generated using the MuSyC consensus framework and the highest-single agent (HSA) reference model to represent synergy metrics. The analysis was performed via the SynergyFinder web platform (Ianevski et al., 2022).

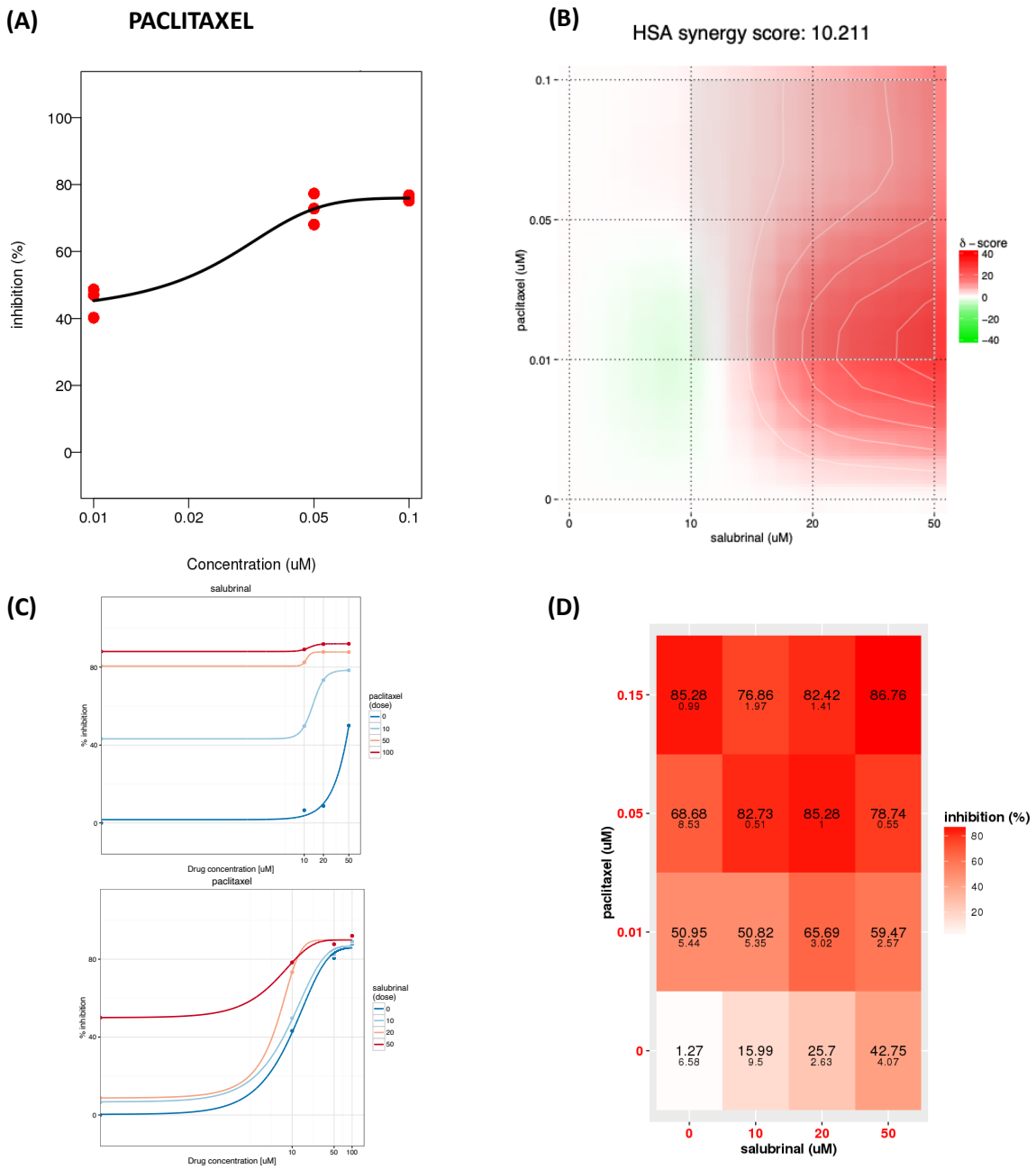

Figure 37. Salubrinal has an additive effect with paclitaxel in inhibiting head and neck carcinoma (HNSCC) cell growth. FaDu cells were treated continuously for 48h with increasing concentrations of paclitaxel and salubrinal, followed by an MTT assay performed in triplicates. (A) The graph represents the dose-response curve for paclitaxel. Percentages indicate cell viability inhibition. (B, C) Heatmap and efficiency curves for the co-treatment with salubrinal and paclitaxel, showing no synergistic effect. (D) The dose-response matrix for paclitaxel and salubrinal co-treatment. The efficacy curves and heatmaps were generated using MuSyC consensus framework and LL4 curve fitting, via the SynergyFinder web platform (Ianevski et al., 2022).

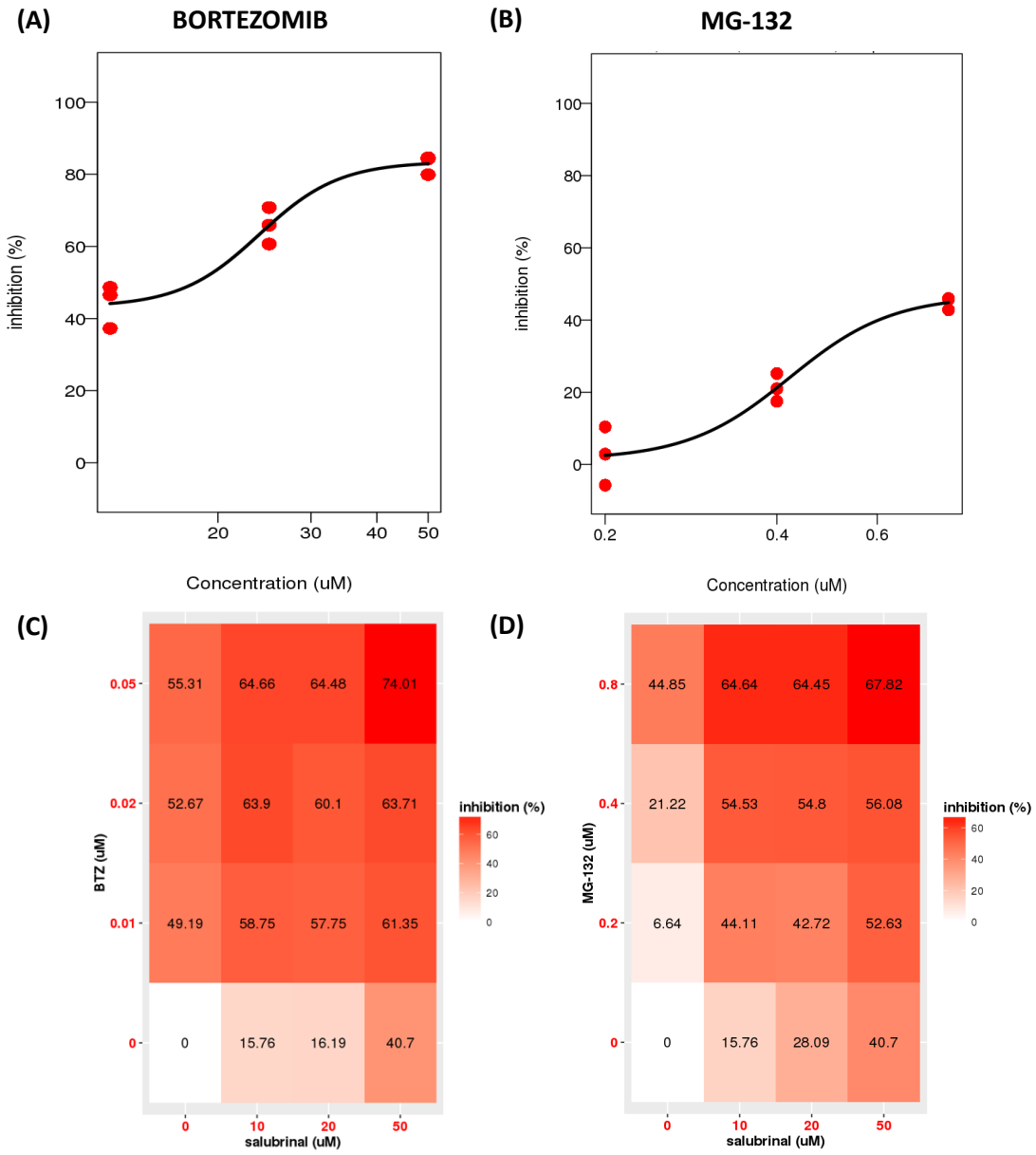

Figure 38. Salubrinal and proteasome inhibitors (PI) bortezomib and MG-132 synergistically inhibit head and neck carcinoma (HNSCC) cell growth. FaDu cells were treated continuously for 48h with increasing concentrations of the respective drugs, followed by an MTT assay performed in triplicates. The graphs represent the dose- response curves for (A) bortezomib and (B) MG-132. Percentages indicate cell viability inhibition. (C, D) Dose-response matrices representing percentage cell viability inhibition for the co-treatments with salubrinal and PI. The graphs were generated using the MuSyC consensus framework and LL4 curve fitting, available via the SynergyFinder web platform (Ianevski et al., 2022)

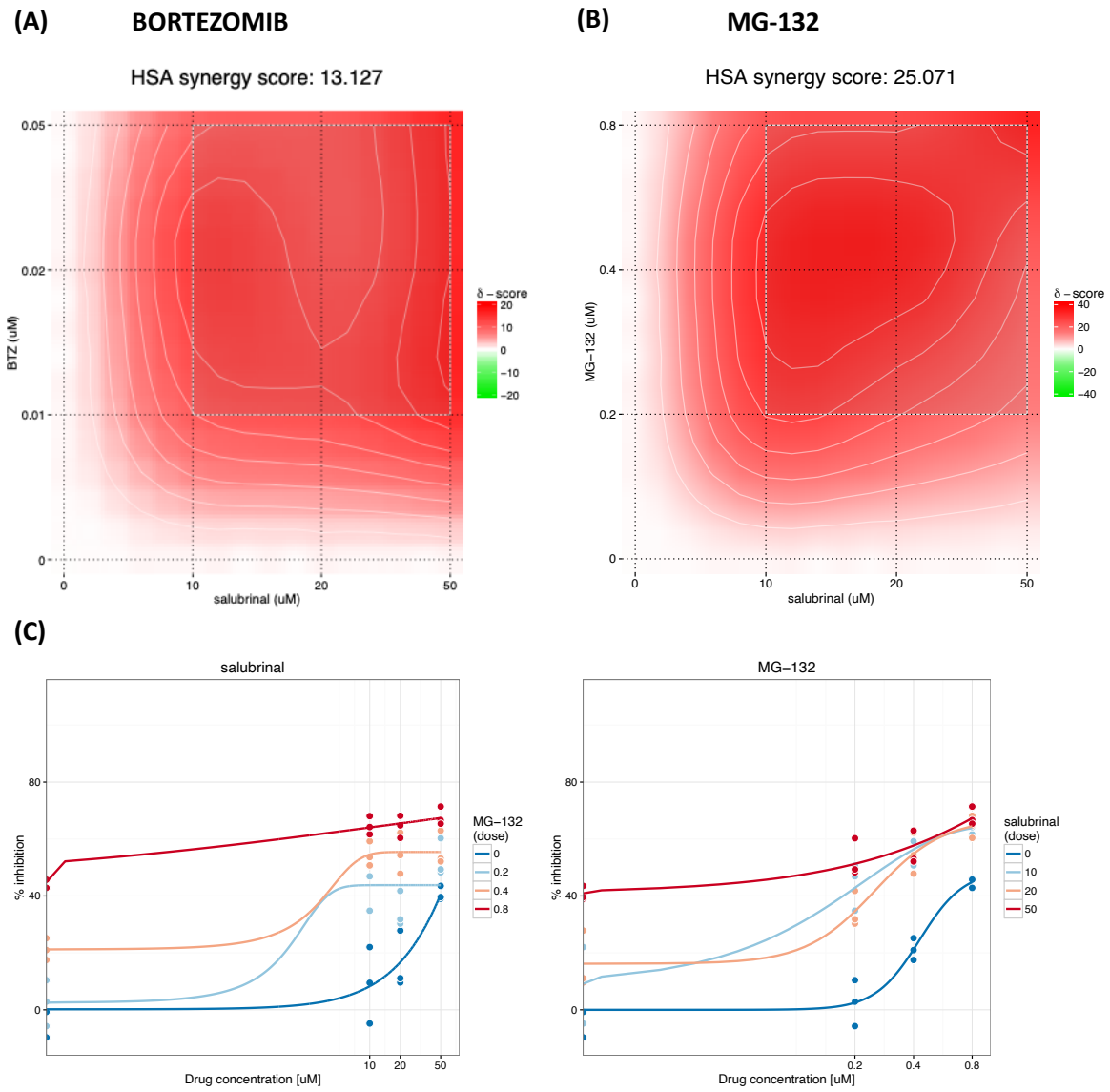

Figure 39 . Salubrinal and proteasome inhibitors (PI) bortezomib and MG-132 synergistically inhibit head and neck carcinoma (HNSCC) cell growth. FaDu cells were treated continuously for 48h with increasing concentrations of the respective drugs, followed by an MTT assay performed in triplicates. The heatmaps represent synergy scores for the salubrinal co-treatments with (A) bortezomib and (B) MG-132. (C) Graphic analysis of the synergistic action of salubrinal and MG-132. Salubrinal induces a synergistic potency shift when combined with MG-132 with a fold change of 120.76. The heatmaps and graphs were generated using MuSyC consensus framework and highest-single agent (HSA) reference model to represent synergy metrics. The analysis was performed via the SynergyFinder web platform (Ianevski et al., 2022).

4.0 Discussion

4.1 Characterization of *EIF2S1* Gene and Protein Expression

eIF2α is an integrator of environmental signals implicated in tumorigenesis. It is upregulated in many cancer types, precipitating diverse effects. A high abundance of phosphorylated eIF2α is associated with a favorable prognosis in gastrointestinal carcinoma (Lobo et al., 2000), breast cancer (Guo et al., 2017) and non-small-cell lung cancer (Hao et al., 2020b). On the other hand, in pancreatic cancer (Wang et al., 2019) and PTEN null prostate carcinoma (Nguyen et al., 2018), high expression of p-eIF2α is associated with disease recurrence.

In this study, the *EIF2S1* gene and its encoded protein were overexpressed in HNSCC. *EIF2S1* is associated with shorter OS, DFS and clinicopathological features indicating disease aggressiveness and severity, such as perineural invasion and extracapsular spread in metastatic lymph nodes. Patients with elevated *EIF2S1* more frequently required postoperative adjuvant systemic therapy and developed secondary tumors. Phosphorylated eIF2α was overexpressed in intraoperative samples, and a trend for a higher proportion of phosphorylation in HNSCC was seen.

EIF2S1 transcript levels are more highly expressed in HPV-, than in HPV+ HNSCC, and in both groups are significantly elevated in comparison to normal epithelium. While HPV- HNSCC frequently feature *TP53* mutations, elevated pRB1, and low P16 expression; HPV+ cancers exhibit low TP53 and pRB1 levels due to proteasomal degradation, and elevated P16 (Economopoulou et al., 2020). The underlying mechanism involves PKR sensing dsRNA and reducing global translation via eIF2α to curb viral replication. eIF2α phosphorylation depletes E6, but the remaining pool of the protein associates with GADD34/PP1 and promotes eIF2α dephosphorylation, partly restoring its own transcription. This allows HPV-infected cells to avoid apoptosis (Kazemi et al., 2004). Whether pharmacologically induced phosphorylation of eIF2α can be a preventive strategy in high-risk HNSCC patients with HPV is an interesting research question for future studies. *EIF2S1* is also highly expressed in HNSCC with *TP53* mutations. In contrast, P16 positive (HPV16/18 positive) HNSCC with intact *TP53* express comparatively lower levels of *EIF2S1*. Collectively, the results suggest that *EIF2S1* overexpression is linked to HNSCC arising on the background of genotoxic insults.

4.2 Drivers of *EIF2S1* Expression

The eIF2 complex genes are infrequently mutated and their deregulation in HNSCC is unrelated to structural gene alterations. Two exceptions are *EIF2A* and *EIF2B5*, both situated on the long arm of chromosome 3, the most frequently amplified genome segment in HNSCC. The region 3q26.3- 3q27 contains several oncogenes, among others *MAPK13*, *CCNK* and *PIK3CA*, whose activation and downstream effects on the PTEN-AKT pathway are crucial for squamous carcinogenesis (Szyfter et

al., 2016). EIF2B5 makes up the guanine nucleotide exchange domain and may be subject to posttranslational modifications by phosphorylation. It requires the presence of other subunits, especially *EIF2B3*, to unfold its activity fully. (Hao et al., 2020a). *EIF2A*, on the other hand, participates in similar biological processes as EIF2, yet it is not a functional homolog of EIF2α, as it functions in a codon- rather than a GTP-dependent manner. The role of EIF2A in translation is limited to specific contexts, such as re-initiation, internal and non-AUG initiation (Komar & Merrick, 2020). While *EIF2S1*- alongside other *EIF2* genes- is an essential gene in the CRISPR-Cas9 knockdown screen on 81 HNSCC cell lines, *EIF2A* is not. The low dependency score for this gene obtained in this study is consistent with its lesser role in translation.

Because *EIF2S1* is highly transcribed in the absence of structural gene alterations, promoter methylation was examined. Methylation of 5' cytosines in gene promoters by DNA methyltransferases prevents the binding of transcription factors and is similar in its repressive effect to point mutations (Worsham et al., 2014). In normal cells, single Cytosine-phosphate-Guanine (CpG) sites are strongly methylated, while CpG islands, present in about 50% of gene promoters, are not. Cancers are characterized by aberrant methylation patterns. The frequently described global hypomethylation contributes to oncogene activation and genomic instability. At the same time, hypermethylation of CpG islands drives down the expression of tumor suppressors (Gaździcka et al., 2020). *DAPK*, *MGMT*, *CDH1* and *CDKN2A* are among the commonly hypermethylated tumor suppressors in HNSCC. Such modifications were shown to be associated with smoking and tobacco use (Hier et al., 2021). HPV infection is associated with a decreased methylation of *CDKN2A* and *RPA2* (involved in DNA repair) against the backdrop of high global methylation (Degli Esposti et al., 2017). Worsham *et al.* (Worsham et al., 2014) have postulated an epigenetic continuum of abnormally methylated genes from benign lesions to invasive HNSCC. Accordingly, *CDKN2A/B*, *APC* and *BRCA* are already subject to methylation in benign lesions (papillomata), while *CDH13*, *CCNA1*, *RB1* and *GADD45* in malignant and metastatic tumors. The current study found a significant hypomethylation of *EIF2S1* promoter in stage 2, 3 and 4 HNSCC, which could be at least in part responsible for the elevated transcript and protein expression. More studies linking changes in methylation to proliferation, invasion and differentiation potential, as well as defining different methylation sub-patterns are still emerging (Nakagawa et al., 2021; C. Zhou et al., 2018). Given the limited experimental evidence in the existing literature, the observations presented here serve as an initial exploration, rather than conclusive evidence, prompting further investigation.

4.3 The effects of eIF2α expression and phosphorylation on carcinogenesis

The observation that eIF2α abundance increases as epithelial lesions progress from dysplasia to invasive cancer holds potential clinical significance. Exposure to carcinogens, such as tobacco smoke,

and chronic inflammation leads to changes in the mucosa, known as field cancerization. Diverse degrees and types of genetic and epigenetic alterations render exposed mucosal areas susceptible to cancerization. As a result, multiple primary tumors are exceptionally prevalent in HNSCC, and individual cancerous lesions are frequently surrounded by macroscopically normal but dysplastic epithelium (Sabharwal et al., 2014). Identifying markers allowing the delineation of malignant and pre-malignant lesions would limit surgical interventions to areas where they are necessary. Also, defining targets for preventive measures in high-risk groups of patients is of utmost interest.

It is well-documented that eIF2α phosphorylation has 3 possible outcomes: cytoprotection, growth arrest and apoptosis (Walczak et al., 2019). Expression of an unphosphorylatable, mutated eIF2α (in cells with low basal phosphorylation of eIF2α) triggered a malignant transformation of murine and human fibroblasts. In contrast, a phosphomimetic mutant induced apoptosis (Donzé et al., 1995). A similar observation was made by Ranganathan *et al.* (Ranganathan et al., 2008), in squamous carcinoma cells with low basal PERK-eIF2α signaling. Reinforcing this axis resulted in G_0/G_1 arrest but not apoptosis. Kinases phosphorylating eIF2α have been studied extensively; both inactivation and stimulation of their activity were considered strategies for anticancer therapies. Though the phosphorylation occurs at the same serine residue, the consequences are often diverse as each enzyme modifies also other targets (Koromilas, 2015).

Basal levels of p-eIF2α mediate adaptive responses to background stress. In normal conditions, eIF2α phosphorylation is counteracted by CREP (*PPP1R15B*), a constitutively active subunit of the PP1 phosphatase complex (Jousse et al., 2003). GADD34, on the other hand, is stress-inducible and specifically dephosphorylates eIF2α, allowing translation of a subset of mRNA involved in cytoprotective stress response programs. In severe stress, cells with defective GADD34 accumulate high levels of p-eIF2α and are unable to induce gene expression programs facilitating survival and recovery (Novoa et al., 2003). GADD34-mediated de-repression of translation determines the availability of both long-term adaptors to stress, as well as intermediate factors required to invoke stress-response gene expression programs (Kojima et al., 2003; Novoa et al., 2003).

4.4 Pharmacological Modification of EIF2α Phosphorylation

The key finding of this work is that salubrinal decreases the viability of HNSCC cell lines and PD3DS. Salubrinal is mechanistically different from kinases as it directly counters phosphatase activity. Physiologically, EIF2B is less abundant than EIF2α. Therefore, even subtle changes in the phosphorylation of eIF2α are impactful. The exact mechanism of action of salubrinal is not known, but it most likely affects both GADD34 and CREP (Boyce et al., 2005). By abrogating phosphatase

activity, salubrinal disrupts the negative feedback loop, tipping the scales between survival and cell death during stress and recovery.

An alternative experimental approach involves genetic knockdown of the respective phosphatase subunits. According to existing reports, GADD34-null mice are viable and largely unaffected (Kojima et al., 2003), while CREP-null mice are smaller than their wild-type littermates and do not thrive (Harding et al., 2009). This is in agreement with the gene dependency analysis described in Section 3.11, which shows that- unlike *EIF2S1*- *GADD34* and *CREP* are not common essential genes in HNSCC. At the same time, a simultaneous knockdown of both genes leads to embryonic lethality (Harding et al., 2009). As the focus of the present work was to establish the clinical potential of targeting EIF2α in HNSCC, salubrinal was used to 'mimic' the effects of such pharmacologic intervention.

The concept of eIF2α hyperphosphorylation triggering cell death is well illustrated in a study on glioblastoma, in which irradiation activated PERK and triggered a cytoprotective cascade. However, irradiation combined with salubrinal enhanced cytotoxicity (Dadey et al., 2018). Other studies have also shown a moderate efficacy of salubrinal *in vitro* and *in vivo*, and an enhanced efficacy in combination with other therapeutic agents. In ER+ breast cancer, phosphorylation of eIF2α by salubrinal induced ATF4 and C/EBP, triggering apoptosis, which was further potentiated by 4-hydroxytamoxifen (Sengupta et al., 2019). In triple-negative breast cancer salubrinal and (similar in its mode of action) guanabenz (Tsaytler et al., 2011) reduced the proliferation, invasion, and motility of cancer cells. Salubrinal also reduced tumor size when injected into murine tumors (Hamamura et al., 2014). Salubrinal reduces the proliferation of chondrosarcoma and sensitizes it to irradiation. The drug was more effective in chondrosarcoma cells than in normal chondrocytes (Koizumi et al., 2012). Finally, combining salubrinal with established therapeutic agents, such as proteasome inhibitors (Drexler, 2009; Schewe & Aguirre-Ghiso, 2009), and doxorubicin (Jeon et al., 2016) improves drug efficacy.

4.5 The Effects of eIF2α Hyperphosphorylation on Cell Cycle

Cell cycle control is frequently altered in HNSCC. Loss-of-function mutations of key tumor suppressors *TP53* and *P16* are prevalent in HNSCC and allow cells to bypass the G_1/S checkpoint (de Bakker et al., 2022). P16 interrupts the formation of cyclin D-CDK complexes. Its frequent inactivation coupled with cyclin D1 gene (CCND1) amplifications (present in up to 28% of HNSCC) facilitate the S phase entry and replication. Moreover, the inhibitory effect of TP53 on the cell cycle resulting from P21 activation is often abolished (Leemans et al., 2018). The current report used human hypopharyngeal squamous cell carcinoma cells (FaDu) with mutated *P16* and *TP53*. Prolonged treatment with salubrinal induced G_1/S arrest. According to the literature, ER stress is associated with

cell cycle arrest either at G_1/S or G2/M checkpoints. G_2/M arrest can be attributed to the depletion of cyclin B1, which was not confirmed in this study. Instead, eIF2α phosphorylation downregulated the synthesis of cyclins D1, A, and E. Cyclin D1 is an unstable protein; its abundance directly depends on translation rate (Brewer et al., 1999).

Our observations also agree with previous studies showing an induction of P21- a CDK inhibitor, and tumor suppressor, via an eIF2α-dependent mechanism (Ding et al., 2016). Recently, Darini *et al*. (Darini et al., 2019) demonstrated that salubrinal potentiates the antitumor activity of trastuzumab in HER2+ cancer xenografts by increasing P21 and JNK1/2 activity, thus providing a strong experimental rationale for the therapeutic use of salubrinal in breast and gastric cancers.

A novel aspect of this study is the depletion of E2F1 following eIF2α phosphorylation. E2F1, though a tumor suppressor in normal cells; in HNSCC, promotes proliferation and invasion while suppressing squamous differentiation and inhibiting apoptosis (Berton et al., 2005). E2F1 is elevated in aggressive and metastatic cancers and is a marker of poor prognosis (Wong et al., 2003). CDK inhibitors (palbociclib, ribociclib) indirectly target E2F1. Results of clinical trials in HNSCC are still emerging but appear promising in combination with cisplatin, 5-FU and docetaxel (Q. Li et al., 2023). It would be interesting to test whether additional pharmacological phosphorylation of eIF2α with salubrinal is beneficial. Lastly, E2F1 is implicated in therapy resistance to many genotoxic agents such as cisplatin, doxorubicin, and etoposide by, among other mechanisms, inducing efflux transporters (Rosenfeldt et al., 2014; Yan et al., 2014).

4.6 Salubrinal Synergizes with Genotoxic Drugs in HNSCC

Intrinsic and acquired drug resistance is a major obstacle in HNSCC therapy. The response rates for cisplatin, taxanes, and 5FU range between 13 and 40%. At the same time, these drugs have a significant systemic toxicity (Wen & Grandis, 2015). This study employed a concentration-weighted analysis to assess drug efficacy, focusing on identifying synergies at low doses with the aim of minimizing off-target toxicity. The results show a strong synergy between salubrinal and two genotoxic agents- cisplatin and 5FU. There are several possible mechanisms contributing to this effect. During apoptosis- the dominant cytotoxic mechanism of anticancer drugs- caspases cleave eIF2α. (1) As the ternary complex becomes less abundant the pharmacological interventions on a smaller pool of the regulatory subunit become more effective (Clemens et al., 2000). (2) PKR senses DNA damage caused by genotoxic agents and *pre*-phosphorylates eIF2α. (3) It is also conceivable that salubrinal affects the cellular metabolism of other chemicals.

Salubrinal induces translocation of calreticulin to the cell surface, which stimulates the antitumor immune response in the presence of genotoxic agents (Kepp et al., 2015). Treatment with salubrinal

combined with mitomycin or etoposide causes tumor regression in immunocompetent mice but not in nude homozygotes (Nu/Nu) (Obeid et al., 2007). While cisplatin alone does not induce immunogenic cell death (ICD) (Bezu et al., 2015), it is conceivable that the addition of salubrinal would escalate the cytotoxic effect *in vivo* even more due to the immunogenic component. Anticancer therapy can induce clinically relevant immunogenic antitumor responses, and harnessing them with small-molecule ICD inducers, auxiliary to chemotherapy, is currently being explored (Fucikova et al., 2020). The first evidence suggests that combining ICD inducers with immune checkpoint inhibitors could elicit remarkable antitumor effects (Galluzzi et al., 2020; Qi et al., 2021).

The immunogenic properties of 5-FU are debated, but it likely modulates the tumor microenvironment rather than induces immunogenic cell death (Bezu et al., 2015). The main cytotoxic effects result from its pleiotropic genotoxicity, but 5FU also affects tumor cells by generating mitochondrial ROS, inhibiting angiogenesis, and influencing the cell cycle. Like salubrinal, 5FU was found to deplete cyclin D1, induce P21, and lead to G_1/S arrest (Li et al., 2004; Zhang et al., 2008).

Paclitaxel typically induces a strong ISR and was shown to phosphorylate eIF2α via PERK and GCN2 (Chen et al., 2019). Therefore, it was somewhat surprising that the combination of salubrinal and paclitaxel did not lead to a significant potency shift. However, paclitaxel also disrupts the microtubule (MT) cytoskeleton, which is critical for the ER distribution within the cell (Tikhomirova et al., 2022; Vajente et al., 2019). The functional relationships between eIF2α and MT cytoskeleton are complex. Compelling evidence shows that intact function of eIF2α is necessary for cells to recover from proteotoxic stress- first phosphorylation to gear translation towards the production of cytoskeletal components, then dephosphorylation to initiate MT organization and clear misfolded protein aggregates (Hurwitz et al., 2022). Chen *et al*. (Chen et al., 2019) have also shown that transcript-selective eIF2A is implicated in paclitaxel resistance.

We also observed a synergy between salubrinal and proteasome inhibitors. Their synergistic effect is well-documented in hematological malignancies (Drexler, 2009; Schewe & Aguirre-Ghiso, 2009). Bortezomib selectively inhibits the chymotrypsin-like activity of the 26S proteasome complex. It is approved for clinical use in multiple myeloma and mantle cell lymphoma, malignancies highly dependent on proteasomal degradation of toxic protein aggregates (Schewe & Aguirre-Ghiso, 2009). It was evaluated with standard-of-care therapy for HNSCC in phase II clinical trials but failed to improve OS and PFS significantly (Huang et al., 2014). MG-132 is less specific and has off-target effects on protein synthesis, cell cycle, and ubiquitination. The potency shift upon co-treatment with MG-132 and salubrinal is likely a result of less well-defined effects of the inhibitor.

4.7 Cytoprotective Properties of Salubrinal in Cisplatin-Induced Ototoxicity

Recently, a study evaluating salubrinal as a neuroprotective agent in the context of cisplatin-induced hearing loss was published (Lu et al., 2022). In the United States alone, around 500 000 patients are diagnosed with cancers requiring cisplatin. In this group of patients, 36% of adults and up to 60% of children suffer from a drug-induced hearing impairment (Chattaraj et al., 2023). Salubrinal was found to protect the cochlear hair cells from cisplatin-induced apoptosis via the PERK-eIF2α axis, owing to its ability to mitigate ER stress at low doses. Previous research implicated the aggregation of misfolded proteins in cisplatin-mediated ototoxicity and suggested that ER stress mitigation may be a protective strategy (Mandic et al., 2003). This is not surprising as a large body of work confirms the causative link between misfolded protein aggregation and neurodegeneration.

Salubrinal was extensively evaluated as a cytoprotective agent in the neuropathological context (Bond et al., 2020). In the article referenced above, cisplatin was shown to reduce the phosphorylation of eIF2α, which was countered by salubrinal. However, the results were obtained in immortalized murine cochlear cells (HEI-OC1), which have different biological properties than human epithelial cells used in the presented work. Moreover, due to the lack of studies evaluating salubrinal *in vivo*, the questions of drug delivery and bioavailability remain open. To date, salubrinal is not approved by the FDA and EMA for medicinal use. It would be of great interest to develop and assess compounds with comparable specificity and, preferably, improved solubility.

5.0 Conclusion

The expression of EIF2 complex members is elevated in HNSCC at both RNA and protein levels. *EIF2S1* is associated with shorter overall survival and clinicopathological features indicating disease severity and aggressiveness. The tissue abundance of EIF2α increases across premalignant and malignant lesions, mirroring the progression to malignancy. Consistent with its role in response to stress signals, the steady-state phosphorylation level in HNSCC is higher than in normal epithelium. EIF2α is also more abundant in non-viral HNSCC, associated with carcinogen exposure. Our data demonstrates that pharmacological hyperphosphorylation of EIF2α with the small-molecule inhibitor salubrinal decreases cell viability in adherent cell cultures, as well as in patient-derived 3D tumor spheroids. This effect was mediated by an impairment of cell cycle progression past the G_1/S checkpoint. Salubrinal also works synergistically with genotoxic drugs used in HNSCC management: cisplatin and 5-fluorouracil, and proteasome inhibitors. Future studies should evaluate salubrinal in combination with genotoxic agents in an *in vivo* model of HNSCC. Pharmacological hyperphosphorylation could also be a potential strategy for HNSCC prevention in selected high-risk patients.

Abstract

Study background: Drug resistance is a common cause of therapy failure in head and neck squamous cell carcinoma (HNSCC). One approach to tackle it is by targeting fundamental cellular processes, such as translation. The eukaryotic translation initiation factor 2 (EIF2) integrates diverse stress signals with key cellular processes. It consists of 3 subunits: α, β and γ. Phosphorylation of the α subunit is primarily a cytoprotective mechanism, curbing global protein synthesis in response to stress, however, prolonged phosphorylation is deleterious to cells.

Methods: Publicly available datasets were analyzed to determine the RNA and protein expression patterns of eIF2 complex factors in HNSCC, with focus on the regulatory subunit EIF2α, encoded by EIF2S1. Immunohistochemical staining (IHC) was used to determine EIF2α abundance in metastasis, carcinoma, premalignant lesions and adjacent non-neoplastic tissue. Intraoperative samples were used to evaluate steady-state phosphorylation levels in tumor and adjacent normal tissue. A small-molecule inhibitor of EIF2α dephosphorylation, salubrinal, was tested *in vitro,* followed by viability assays, flow cytometry, and immunoblot analyses. Patient-derived 3D tumor spheroids (PD3DS) were cultured with salubrinal, and their viability assessed. Lastly, salubrinal was evaluated in combination with standard-of-care chemotherapeutics.

Results: The analysis of RNA and proteomics data shows that many EIF2 complex factors are deregulated in HNSCC. EIF2S1 overexpression negatively impacts overall and disease-free survival and is associated with clinicopathological parameters indicating disease aggressiveness and severity. The elevation of EIF2S1 transcript and protein expression, though present irrespective of etiology, is significantly more pronounced in human papillomavirus (HPV) negative HNSCC. Mutations in the gene are infrequent, but its promoter methylation is decreased. Further, IHC staining reveals increasing EIF2α abundance from premalignant lesions to invasive and metastatic carcinoma. In immunoblots from intraoperative samples, EIF2α expression and steady-state phosphorylation are higher in HNSCC than in neighboring normal tissue. Inhibition of EIF2α dephosphorylation decreases HNSCC cell viability, clonogenic survival, and impairs G_1/S transition. Salubrinal also decreases the viability of PD3DS and acts synergistically with cisplatin, 5-fluorouracil, and proteasome inhibitors.

Conclusion: The results indicate that pharmacological inhibition of EIF2α dephosphorylation is a potential therapeutic and preventive strategy in HNSCC.

Zusammenfassung

Hintergrund: Arzneimittelresistenz ist eine häufige Ursache für das Versagen der Therapie bei Kopf- und Hals-Plattenepithelkarzinomen (HNSCC). Ein Ansatz ihr entgegenzuwirken, ist, grundlegende zelluläre Prozesse, wie die Translation, zu beeinflussen. Der eukaryotische Translationsinitiationsfaktor 2 (EIF2), mit den Untereinheiten α, β und γ, integriert verschiedene Stresssignale mit wichtigen zellulären Prozessen. Die Phosphorylierung der α-Untereinheit ist grundsätzlich eine zytoprotektive Reaktion auf Stress und hemmt die globale Proteinsynthese. Eine anhaltende Phosphorylierung ist jedoch schädlich für die Zellen.

Methoden: Öffentliche Datensätze wurden analysiert, um RNA- und Protein-Expressionsmuster der eIF2-Komplexfaktoren in HNSCC zu bestimmen, mit Schwerpunkt auf der regulatorischen Untereinheit EIF2α (durch EIF2S1 codiert). Mit der immunhistochemischen Färbung (IHC) wurde der Gehalt an EIF2α in Metastasen, Karzinomen, prämalignen Läsionen und angrenzendem, nicht-neoplastischem Gewebe bestimmt. Intraoperative Proben wurden verwendet, um die Phosphorylierungslevel im Tumor und im angrenzenden Normalgewebe zu bewerten. Ein Inhibitor der Dephosphorylierung von EIF2α, Salubrinal, wurde *in vitro* getestet, gefolgt von Viabilitätstestung, Durchflusszytometrie und Immunoblot-Analysen. Von Patienten stammende 3D-Tumorsphäroide (PD3DS) wurden mit Salubrinal kultiviert und ihre Viabilität bewertet. Schließlich wurde Salubrinal in Kombination mit Standardtherapeutika untersucht.

Ergebnisse: Die Analyse von RNA- und Proteomdaten zeigt, dass viele EIF2-Komplexfaktoren in HNSCC dereguliert sind. Die Überexpression von *EIF2S1* wirkt sich negativ auf das krankheitsfreie und Gesamtüberleben aus und ist mit klinisch-pathologischen Parametern der Aggressivität und Schwere der Krankheit verbunden. Der Anstieg von *EIF2S1* und EIF2α ist, unabhängig von der Ätiologie vorhanden, jedoch signifikant ausgeprägter bei HPV negativen HNSCC. Darüber hinaus zeigt die IHC eine zunehmende Anreicherung von EIF2α von prämalignen Läsionen bis hin zu invasivem und metastatischem Karzinom. In Immunoblots von intraoperativen Proben ist die Expression von EIF2α und die steady-state Phosphorylierung in HNSCC höher als im benachbarten normalen Gewebe. Die Hemmung der Dephosphorylierung von EIF2α verringert die Viabilität, die klonogene Überlebensfähigkeit und beeinträchtigt den Übergang von G_1/S in HNSCC Zellen. Salubrinal verringert auch die Viabilität von PD3DS und wirkt synergistisch mit Cisplatin, 5-Fluorouracil und Proteasom-Inhibitoren.

Schlussfolgerungen: Die pharmakologische Hemmung der Dephosphorylierung von EIF2α ist eine potenzielle therapeutische und präventive Strategie für HNSCC.

Graphical Abstract:

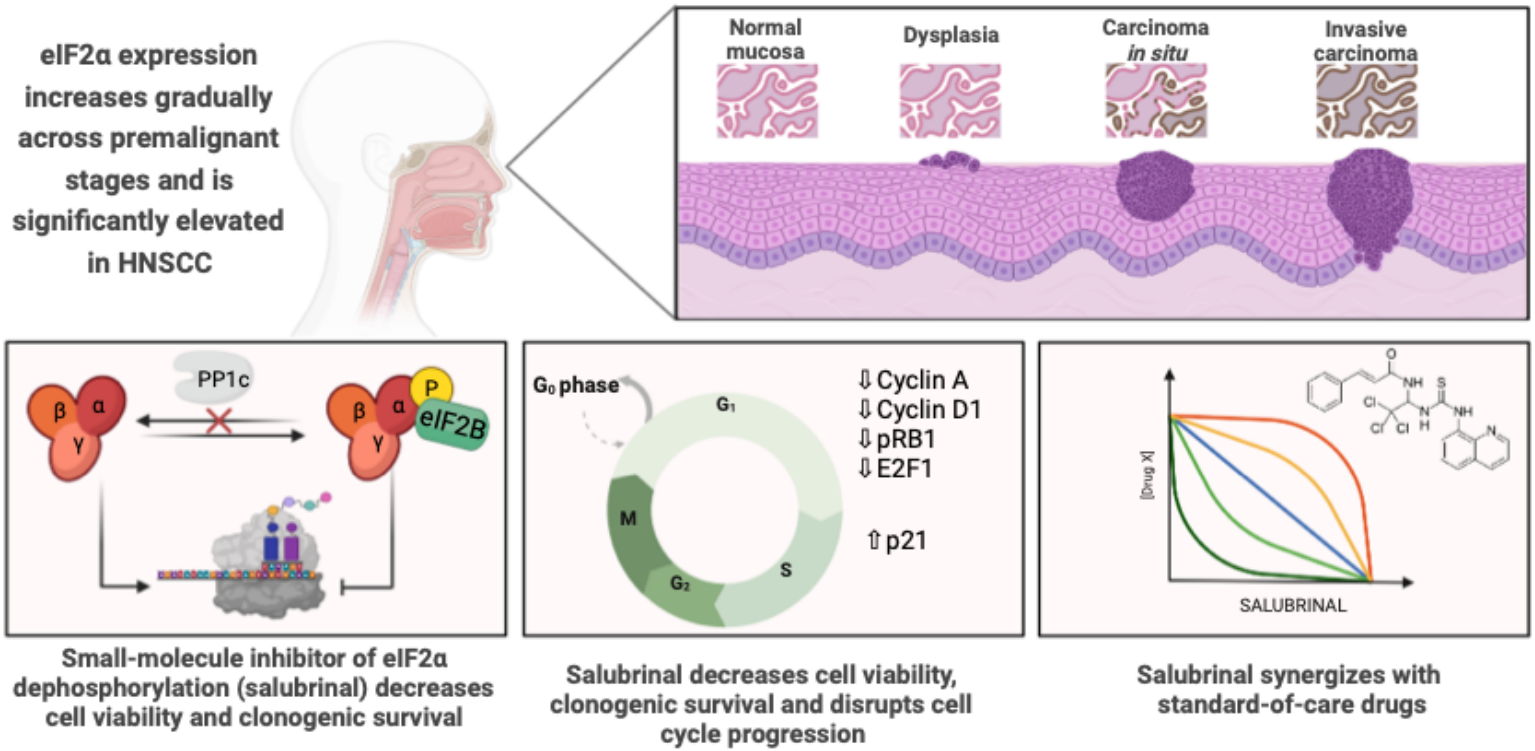

List of Tables

Table 1. Global incidence and mortality of HNSCC with subdivision into anatomic sites, excluding non-melanoma skin cancer. Data extracted from GLOBOCAN 2020 4
Table 2. Global incidence and mortality of HNSCC among men and women, with subdivision into individual anatomic sites, excluding non-melanoma skin cancer. Data extracted from GLOBOCAN 2020*. 4
Table 3. The characteristics of the patient cohort used for the RNA transcript analysis. 26
Table 4. The characteristics of the patient cohort used for the protein expression analysis. 28
Table 5. Antibodies used for immunohistochemical staining of tissue samples. 29
Table 6. Primary and secondary antibodies used for western blots. 31
Table 7. Cytotoxic agents used for co-treatment with salubrinal *in vitro*. Dimethyl sulfoxide (DMSO). 33
Table 8. Transcription of EIF2 complex members co-occurs. 51
Table 9. The characteristics of the patient cohort used for immunohistochemical (IHC) assessment of eukaryotic initiation factor α (eIF2α) protein expression in head and neck squamous cell carcinoma (HNSCC). 61
Table 10. The characteristics of the patient subgroup used for immunohistochemical (IHC) assessment of eukaryotic initiation factor alfa (eIF2α) protein expression across different stages of head and neck squamous cell carcinoma (HNSCC) development, including dysplasia, carcinoma *in situ*, invasive cancer and metastasis. 65

List of Figures

Figure 1. Schematic illustration of the anatomical sites of HNSCC development. The photomicrographs of H&E sections (20x and 40x magnification respectively) shown in the insets represent the typical histopathological features of HNSCC- nests of squamous cells with pink cytoplasm and keratinization set against fibrous stroma. 1
Figure 2. Projected increase in the incidence of HNSCC worldwide from 2020 to 2040. The estimated number of new cases is represented in thousands. Data extracted from GLOBOCAN 2020* 5
Figure 3. Projected increase in the incidence of HNSCC in selected European countries from 2020 to 2040. The estimated number of new cases is represented in thousands. Data extracted from GLOBOCAN 2020* 5
Figure 4. Schematic representation of translation regulation in the initiation phase by stress. 22
Figure 5. Genes encoding eIF2 complex members are overexpressed in head and neck squamous cell carcinoma (HNSCC). 37
Figure 6. *EIF2S2* and *EIF2S3* genes are overexpressed in head and neck squamous cell carcinoma (HNSCC) 38
Figure 7. *EIF2B1* and *EIF2B2* genes are overexpressed in head and neck squamous cell carcinoma (HNSCC) 39
Figure 8. *EIF2B3* gene is overexpressed in head and neck squamous cell carcinoma (HNSCC). 40
Figure 9. *EIF2B5* gene is overexpressed in head and neck squamous cell carcinoma (HNSCC). 41
Figure 10. High transcript expression of *EIF2S1* is associated with significantly shorter overall survival (OS) (p=0.00016) and disease-free survival (DFS) (p=0.044) in head and neck squamous cell carcinoma (HNSCC). 42
Figure 11. The eukaryotic initiation factor (eIF) gene expression across 33 types of human cancers. 43
Figure 12. Elevated *EIF2S1* expression is associated with clinicopathological parameters indicating disease severity and aggressiveness in patients with head and neck squamous cell carcinoma (n=522, HNSCC). 45

Figure 13. *EIF2S1* expression differs with human papillomavirus (HPV) and *TP53* mutation status in head and neck carcinoma (HNSCC). 47
Figure 14. *EIF2S1* expression differs with human papillomavirus (HPV) and *TP53* mutation status in head and neck carcinoma (HNSCC). 48
Figure 15. Genetic drivers of eukaryotic initiation factor 2 (eIF2) complex expression. 49
Figure 16. Heatmap representing regulatory clusters of eukaryotic initiation factors (eIFs) mRNA transcript expression in head and neck squamous cell carcinoma (HNSCC). 52
Figure 17. *EIF2S1* promoter methylation levels are decreased in head and neck carcinoma (HNSCC). 54
Figure 18. EIF2α is overexpressed in head and neck squamous cell carcinoma (HNSCC). 56
Figure 19. EIF2β and EIF2γ, encoded by *EIF2S2* and *EIF2S3,* are overexpressed in head and neck squamous cell carcinoma (HNSCC). 57
Figure 20. Subunits EIF2Bα and EIF2Bβ, encoded by *EIF2B1* and *EIF2B2,* are overexpressed in head and neck squamous cell carcinoma (HNSCC). 58
Figure 21. *EIF2B4* gene product (EIF2Bδ), but not *EIF2B3* (EIF2Bγ) is overexpressed in head and neck squamous cell carcinoma (HNSCC). 59
Figure 22. *EIF2B5* gene product- EIF2Bε is not overexpressed in head and neck squamous cell carcinoma (HNSCC). 60
Figure 23. eIF2α is overexpressed in head and neck squamous cell carcinoma (HNSCC). 62
Figure 24. eIF2α expression in relation to the HPV status in head and neck squamous cell carcinoma (HNSCC) 63
Figure 25. eIF2α abundance in mucosal epithelium increases with progression to malignancy. 66
Figure 26. eIF2α expression increases with malignant progression in head and neck squamous cell carcinoma (HNSCC). 67
Figure 27. eIF2α abundance and phosphorylation are significantly increased in head and neck squamous cell carcinoma (HNSCC) in comparison to adjacent normal epithelium. 69
Figure 28. EIF2 factors are essential for head and neck squamous cell carcinoma (HNSCC) cell survival 70
Figure 29. Prolonged treatment with salubrinal results in sustained phosphorylation of EIF2α in head and neck squamous cell carcinoma (HNSCC) cells. 71

Figure 30. Treatment with the eIF2α dephosphorylation inhibitor salubrinal decreases head and neck squamous cell carcinoma (HNSCC) cell viability. 73
Figure 31. Treatment with the eIF2α dephosphorylation inhibitor salubrinal decreases clonogenic survival of head and neck squamous cell carcinoma cells (HNSCC). 74
Figure 32. Treatment with the eIF2α dephosphorylation inhibitor salubrinal (sal) impairs the cell cycle progression in head and neck squamous cell carcinoma (HNSCC). 75
Figure 33. Salubrinal disrupts the cell cycle progression in head and neck squamous cell carcinoma (HNSCC). 76
Figure 34. Salubrinal decreases the viability of patient-derived 3D tumor spheroids (PD3DS). 77
Figure 35. Salubrinal synergizes with cisplatin and 5-fluorouracil (5FU), inhibiting head and neck carcinoma (HNSCC) cell growth. 79
Figure 36. Salubrinal synergizes with cisplatin and 5-fluorouracil (5FU), inhibiting head and neck carcinoma (HNSCC) cell growth. 80
Figure 37. Salubrinal has an additive effect with paclitaxel in inhibiting head and neck carcinoma (HNSCC) cell growth. 81
Figure 38. Salubrinal and proteasome inhibitors (PI) bortezomib and MG-132 synergistically inhibit head and neck carcinoma (HNSCC) cell growth. 82
Figure 39 . Salubrinal and proteasome inhibitors (PI) bortezomib and MG-132 synergistically inhibit head and neck carcinoma (HNSCC) cell growth. FaDu cells were treated continuously for 48h with increasing concentrations of the respective drugs, followed by an MTT assay performed in triplicates. 83

List of Abbreviations and Symbols:

5'UTR	5' Untranslated Region
5FU	5-Fluorouracil
AJCC	American Joint Committee on Cancer
AJUBA	Ajuba LIM Protein
AKT1	AKT Serine/Threonine Kinase 1, (PKB)
ALDH2	Aldehyde Dehydrogenase 2
APC	Adenomatous Polyposis Coli
APOBEC	Apolipoprotein B mRNA Editing Enzyme Catalytic Subunit
ASR	Adjusted Survival Rate
ATF	Activating Transcription Factor 1
ATM1	Serine-Protein Kinase Ataxia Telangiectasia Mutated
ATP	Adenosine Triphosphate
AUG	Start Codon Adenine-Uracil-Guanine
Bak	Bcl2 Antagonist/Killer 1
Bax	Apoptosis Regulator BCL2 Associated X Protein
BRCA	Breast Cancer Susceptibility
BSA	Bovine Serum Albumin
Cas9	CRISPR Associated Protein 9
CBP	CREB Binding Protein
CCNA	Cyclin A
CCNK	Cyclin K
CDH	Cadherin
CDK	Cyclin Dependent Kinase
CDKN2A	Cyclin Dependent Kinase Inhibitor 2A, (P16, INK4)
CDKN2B	Cyclin Dependent Kinase Inhibitor 2B, (P15)
CHOP	C/EBP Homologous Protein, (GADD153, DDIT3)
CI	Confidence Interval
CIS	Carcinoma *in situ*
CNA	Copy-Number Alteration
CO_2	Carbon Dioxide

CpG-5'	Cytosine-Phosphate-Guanine-5'
CREP	cAMP response element-binding protein 3-like protein 1, (GADD34)
CRISPR	Clustered Regularly Interspaced Short Palindromic Repeats
CTLA-4	Cytotoxic T-Lymphocyte Associated Protein 4
cTNM	Clinical TNM Staging
D	Dysplasia
DAPK	Death-Associated Protein Kinase
DDIT3	DNA Damage-Inducible Transcript 3
DFS	Disease-Free Survival
dH_2O	Distilled Water
DMEM	Dulbecco Modified Eagle Medium
DMSO	Dimethyl Sulfoxide
DNA	Deoxyribonucleic Acid
DNMT	DNA Methyltransferases
dNTP	Deoxynucleotide Triphosphate
DOI	Depth of Invasion
dsRNA	Double-Strand RNA
E1-E7	HPV Early Capsid Proteins
E2F	Elongation Factor 2
E2F1	E2F Transcription Factor 1
EBNA1	Epstein-Barr Nuclear Antigen 1
EBV	Epstein-Barr Virus, (HHV4)
EDTA	Ethylenediaminetetraacetic Acid
EGFR	Epidermal Growth Factor Receptor, (HER1, ERBB1)
eIF	Eukaryotic Intiation Factor
EIF2AK1	Eukaryotic Initiation Factor 2α Kinase 1, (HRI)
EIF2AK2	Eukaryotic Initiation Factor 2α Kinase 2, (PKR)
EIF2AK3	Eukaryotic Initiation Factor 2α Kinase 3, (PERK)
EIF2AK4	Eukaryotic Initiation Factor 2α Kinase 4, (GCN2)
EIF2S1-5	Eukaryotic Intiation Factor 2 Subunits 1-5
EMA	European Medicines Agency

EMT	Epithelial Mesenchymal Transition
ENE	Extracapsular Nodal Extension
EP300	E1A-binding Protein p300, (Histone Acetylotransferase P300)
ER	Endoplasmic Reticulum
FAT1	Fat Atypical Cadherin 1
FBS	Fetal Bovine Serum
FDA	Food And Drug Agency
FDR	False Detection Rate
FdUMP	Fluorodeoxyuridine Monophosphate
FdUTP	Fluorodeoxyuridine Triphosphate
FFPE	Formalin-Fixed Paraffin-Embedded
FUTP	Fluorouridine Triphosphate
GADD	Growth Arrest and DNA-Damage-Inducible
GAPDH	Glyceraldehyde-3-Phosphate Dehydrogenase
GCN2	General Control Nonderepressible 2
GEPIA	Gene Expression Profiling and Interactive Analysis
GISTIC	Genomic Identification of Significant Targets in Cancer
GTP	Guanosine Triphosphate
H&E	Hematoxylin and Eosin
HAS	Highest Single Agent
HCV	Hepatitis C Virus
HER2	Human Epidermal Growth Factor Receptor 2, (ERBB2)
HHV4	Human Herpesvirus 4
HIER	Heat-Induced Epitope Retrieval
HLA	Human Leukocyte Antigens
HNSCC	Head and Neck Squamous Cell Carcinoma
HPV	Human Papillomavirus
HR	Hazard Ratio
HRAS	Harvey Rat Sarcoma Viral Oncogene Homolog
hrHPV	High-Risk Human Papillomavirus
HRI	Heme-Regulated Eukaryotic Initiation Factor 2 Kinase

HRP	Horse-Radish Peroxidase
hTERT	Human Telomerase Reverse Transcriptase
IARC	International Agency for Research on Cancer
IC_{50}	Half-Maximal Inhibitory Concentration
ICD	Immunogenic Cell Death
ICI	Immune Checkpoint Inhibitors
IGRT	Image-Guided Radiotherapy
IHC	Immunohistochemistry
IMRT	Intensity-Modulated Radiotherapy
IRES	Internal Ribosome Entry Site
IS	Intensity Score
ISR	Integrated Stress Response
IUAC	International Union Against Cancer
JNK	C-Jun N-Terminal Kinase, MAPK Family Member
KEAP1	Kelch-Like ECH-Associated Protein 1
KMT2D	Lysine (K)-Specific Methyltransferase 2d
L1, L2	HPV Late Capsid Proteins
LL4	Logistic Regression 4
LMP1	Latent Membrane Protein 1
MAPK	Mitogen-Activated Protein Kinase
Met-tRNAi	Methionine Transfer RNA for Initiation
META	Metastasis
MGMT	O-6-Methylguanine-Dna Methyltransferase
MT	Microtubule
mTOR	Mechanistic Target of Rapamycin Kinase
MTT	3-(4,5-Dimethylthiazol-2-Yl)-2,5-Diphenyltetrazolium Bromide
N/D	Not Disclosed
NFE2L2	Nuclear Factor Erythroid 2-Related Factor 2
NFκB	Nuclear Factor Kappa B
NFKBIA	Nf-Kappa-B Inhibitor α
NNPL	Non-Neoplastic Lesion

NOTCH1	Notch Receptor 1
ns	Not Significant
NSD1	Nuclear Receptor Binding Set Domain Protein 1
Nu/Nu	Homozygous Nude Strain
OPMD	Oral Potentially Malignant Disorders
OPSCC	Oropharyngeal Squamous Cell Carcinoma
OS	Overall Survival
P	Phosphate group
P/S	Penicillin/Streptomycin
P16	Cyclin-Dependent Kinase Inhibitor 2A, ($P16^{ink4a}$)
P21	Cyclin Dependent Kinase Inhibitor 1A, (CIP1, WAF1)
P38	Protein 38, MAPK Family Member
PARP	Poly-ADP Ribose Polymerase
PBS	Phosphate-Buffered Saline
PCR	Polymerase-Chain Reaction
PD-1	Programmed Death 1
PD-L1	Programmed Cell Death Ligand 1
PD3DS	Patient-Derived 3D Spheroids
PERK	Protein Kinase RNA-Like Endoplasmic Reticulum Kinase
PFS	Progression-Free Survival
PI	Proteasome Inhibitor
PIC	Pre-Initiation Complex
PIK3	Phosphatidylinositol-3-Kinase
PIK3CA	PIK3 Catalytic Subunit α
PKB	Protein Kinase B, (AKT1)
PKR	Protein Kinase R
PMSF	Phenylmethylsulfonyl Fluoride
PP1c	Protein Phosphatase Catalytic Subunit
PPP1R15A/B	Protein Phosphatase 1 Regulatory Subunit 15A/B
PS	Proportion Score
PTEN	Phosphatase and Tensin Homolog

pTNM	Pathological TNM Staging
PVDF	Polyvinylidene Difluoride
RB1	Retinoblastoma 1
RNA	Ribonucleic Acid
RNASeq V2	RNA Sequencing Version 2
ROS	Reactive Oxygen Species
RSEM	RNA-Seq by Expectation Maximization
rTNM	TNM Staging of Recurrent Disease
SD	Standard Deviation
Ser	Serine
siRNA	short-interfering RNA
TBST	Tris-Buffered Saline, Tween®
TC	Ternary Complex
TCGA	The Cancer Genome Atlas
TGF-β	Transforming Growth Factor β
TGFB2R	TGF- β Receptor Type 2
Tis	Tumor (Carcinoma) *In Situ*
TIS	Total Immunostaining Score
TNFα	Tumor Necrosis Factor α
TNM	Tumor, Nodes, Metastasis Staging System
TP53	Tumor Protein 53
TPF	Docetaxel (Taxotere), Cisplatin (Platinol), 5-Fluorouracil
TRAF3	TNF Receptor Associated Factor 3
tRNA	transfer RNA
TSS	Transcription Start Site
UALCAN	University Of Alabama at Birmingham Cancer
uORF	Upstream Open Reading Frame
VLP	Virus-Like Particles
WHO	World Health Organization
WNT	Wingless/Int Family Member
ZNF750	Zinc Finger Protein 750

References:

Aaltonen, L.-M., Rautiainen, N., Sellman, J., et al. (2014). Voice quality after treatment of early vocal cord cancer: a randomized trial comparing laser surgery with radiation therapy. International Journal of Radiation Oncology Biology Physics, 90(2), 255–260. https://doi.org/https://doi.org/10.1016/j.ijrobp.2014.06.032

Adomavicius, T., Guaita, M., Zhou, Y., et al. (2019). The structural basis of translational control by eIF2 phosphorylation. *Nature Communications*, *10*(1), 2136. https://doi.org/10.1038/s41467-019-10167-3

Aguirre-Urizar, J. M., Lafuente-Ibáñez de Mendoza, I., Warnakulasuriya, S. (2021). Malignant transformation of oral leukoplakia: systematic review and meta-analysis of the last 5 years. *Oral Diseases*, *27*(8), 1881–1895. https://doi.org/https://doi.org/10.1111/odi.13810

Alamoud, K. A., & Kukuruzinska, M. A. (2018). Emerging insights into wnt/β-catenin signaling in head and neck cancer. *Journal of Dental Research*, *97*(6), 665–673. https://doi.org/10.1177/0022034518771923

Amin, M. B., Greene, F. L., Edge, S. B., et al. (2017). The eighth edition ajcc cancer staging manual: continuing to build a bridge from a population-based to a more "personalized" approach to cancer staging. *CA: A Cancer Journal for Clinicians*, *67*(2), 93–99. https://doi.org/https://doi.org/10.3322/caac.21388

Anderson, G., Ebadi, M., Vo, K., et al. (2021). An updated review on head and neck cancer treatment with radiation therapy. *Cancers*, *13*(19), 4912. https://doi.org/10.3390/cancers13194912

Argiris, A., Karamouzis, M. V, Raben, D., et al. (2008). Head and neck cancer. *Lancet, 371*(9625), 1695–1709. https://doi.org/10.1016/S0140-6736(08)60728-X

Bader, A. G., Kang, S., Zhao, L., et al. (2005). Oncogenic PI3K deregulates transcription and translation. *Nature Reviews Cancer*, *5*(12), 921–929. https://doi.org/10.1038/nrc1753

Bagnardi, V., Rota, M., Botteri, E., et al. (2013). Light alcohol drinking and cancer: a meta-analysis. *Annals of Oncology*, *24*(2), 301–308. https://doi.org/https://doi.org/10.1093/annonc/mds337

Baker, K. S., Leisenring, W. M., Goodman, P. J., et al. (2019). Total body irradiation dose and risk of subsequent neoplasms following allogeneic hematopoietic cell transplantation. *Blood*, *133*(26), 2790–2799. https://doi.org/10.1182/blood.2018874115

Barul, C., Fayossé, A., Carton, M., et al. (2017). Occupational exposure to chlorinated solvents and risk of head and neck cancer in men: a population-based case-control study in France. *Environmental Health*, *16*(1), 77. https://doi.org/10.1186/s12940-017-0286-5

Bernier, J., Cooper, J. S., Pajak, T. F., et al. (2005). Defining risk levels in locally advanced head and neck cancers: a comparative analysis of concurrent postoperative radiation plus chemotherapy trials of the EORTC (#22931) and RTOG (# 9501). *Head & Neck*, *27*(10), 843–850. https://doi.org/https://doi.org/10.1002/hed.20279

Berthiller, J., Straif, K., Agudo, A., et al. (2016). Low frequency of cigarette smoking and the risk of head and neck cancer in the INHANCE consortium pooled analysis. *International Journal of Epidemiology*, *45*(3), 835–845. https://doi.org/10.1093/ije/dyv146

Berton, T. R., Mitchell, D. L., Guo, R., et al. (2005). Regulation of epidermal apoptosis and DNA repair by E2F1 in response to ultraviolet B radiation. *Oncogene*, *24*(15), 2449–2460. https://doi.org/10.1038/sj.onc.1208462

Beynon, R. A., Lang, S., Schimansky, S., et al. (2018). Tobacco smoking and alcohol drinking at diagnosis of head and neck cancer and all-cause mortality: results from head and neck 5000, a prospective observational cohort of people with head and neck cancer. *International Journal of Cancer*, *143*(5), 1114–1127. https://doi.org/https://doi.org/10.1002/ijc.31416

Bezu, L., Gomes-de-Silva, L. C., Dewitte, H., et al. (2015). Combinatorial strategies for the induction of immunogenic cell death. *Frontiers in Immunology*, *6*, 187. https://doi.org/10.3389/fimmu.2015.00187

Bhat, M., Robichaud, N., Hulea, L., et al. (2015). Targeting the translation machinery in cancer. *Nature Reviews Drug Discovery*, *14*(4), 261–278. https://doi.org/10.1038/nrd4505

Boehnke, K., Iversen, P. W., Schumacher, D., et al. (2016). Assay establishment and validation of a high-throughput screening platform for three-dimensional patient-derived colon cancer organoid cultures. *Journal of Biomolecular Screening*, *21*(9), 931–941. https://doi.org/10.1177/1087057116650965

Boffetta, P., Hayes, R. B., Sartori, S., et al. (2016). Mouthwash use and cancer of the head and neck: a pooled analysis from the International Head and Neck Cancer Epidemiology Consortium. *European Journal of Cancer Prevention*, *25*(4), 344–348. https://doi.org/10.1097/CEJ.0000000000000179

Bond, S., Lopez-Lloreda, C., Gannon, P. J., et al. (2020). The integrated stress response and phosphorylated eukaryotic initiation factor 2α in neurodegeneration. *Journal of Neuropathology and Experimental Neurology*, *79*(2), 123–143. https://doi.org/10.1093/jnen/nlz129

Borsetto, D., Fussey, J., Fabris, L., et al. (2020). HCV infection and the risk of head and neck cancer: a meta-analysis. *Oral Oncology*, *109*, 104869. https://doi.org/https://doi.org/10.1016/j.oraloncology.2020.104869

Boyce, M., Bryant, K. F., Jousse, C., et al. (2005). A selective inhibitor of eIF2alpha dephosphorylation protects cells from ER stress. *Science*, *307*(5711), 935–939. https://doi.org/10.1126/science.1101902

Braakhuis, B. J. M., Brakenhoff, R. H., & René Leemans, C. (2012). Treatment choice for locally advanced head and neck cancers on the basis of risk factors: biological risk factors. *Annals of Oncology*, *23*(Suppl 10), x173–x177. https://doi.org/https://doi.org/10.1093/annonc/mds299

Brewer, J. W., Hendershot, L. M., Sherr, C. J., et al. (1999). Mammalian unfolded protein response inhibits cyclin D1 translation and cell-cycle progression. *Proceedings of the National Academy of Sciences of the United States of America*, *96*(15), 8505–8510. https://doi.org/10.1073/pnas.96.15.8505

Brouns, E., Baart, J. A., Karagozoglu, K. H., et al. (2014). Malignant transformation of oral leukoplakia in a well-defined cohort of 144 patients. *Oral Diseases*, *20*(3), e19–e24. https://doi.org/https://doi.org/10.1111/odi.12095

Brown, A., Kumar, S., & Tchounwou, P. B. (2019). Cisplatin-based chemotherapy of human cancers. *Journal of Cancer Science & Therapy*, *11*(4), 97. https://pubmed.ncbi.nlm.nih.gov/32148661

Budach, V., & Tinhofer, I. (2019). Novel prognostic clinical factors and biomarkers for outcome prediction in head and neck cancer: a systematic review. *The Lancet Oncology*, *20*(6), e313–e326. https://doi.org/10.1016/S1470-2045(19)30177-9

Campbell, J. D., Yau, C., & Bowlby, R. (2018). Genomic, pathway network, and immunologic features distinguishing squamous carcinomas. *Cell Reports*, *23*(1), 194-212.e6. https://doi.org/10.1016/j.celrep.2018.03.063

Carton, M., Barul, C., Menvielle, G., et al. (2017). Occupational exposure to solvents and risk of head and neck cancer in women: a population-based case-control study in France. *BMJ Open*, *7*(1), e012833–e012833. https://doi.org/10.1136/bmjopen-2016-012833

Cerami, E., Gao, J., Dogrusoz, U., et al. (2012). The cBio cancer genomics portal: an open platform for exploring multidimensional cancer genomics data. *Cancer Discovery*, *2*(5), 401. https://doi.org/10.1158/2159-8290.CD-12-0095

Chalabi-Dchar, M., Fenouil, T., Machon, C., et al. (2021). A novel view on an old drug, 5-fluorouracil: an unexpected RNA modifier with intriguing impact on cancer cell fate. *NAR Cancer*, *3*(3), zcab032. https://doi.org/10.1093/narcan/zcab032

Chandrashekar, D. S., Bashel, B., Balasubramanya, S. A. H., et al. (2017). UALCAN: a portal for facilitating tumor subgroup gene expression and survival analyses. *Neoplasia*, *19*(8), 649–658. https://doi.org/https://doi.org/10.1016/j.neo.2017.05.002

Chandrashekar, D. S., Karthikeyan, S. K., Korla, P. K., et al. (2022). UALCAN: An update to the integrated cancer data analysis platform. *Neoplasia*, *25*, 18–27. https://doi.org/https://doi.org/10.1016/j.neo.2022.01.001

Chattaraj, A., Syed, M. P., Low, C. A., et al. (2023). Cisplatin-induced ototoxicity: a concise review of the burden, prevention, and interception strategies. *JCO Oncology Practice*, *19*(5), 278–283. https://doi.org/10.1200/OP.22.00710

Chaturvedi, A. K., Graubard, B. I., Broutian, T., et al. (2017). Effect of prophylactic human papillomavirus (HPV) vaccination on oral HPV infections among young adults

in the United States. *Journal of Clinical Oncology*, *36*(3), 262–267. https://doi.org/10.1200/JCO.2017.75.0141

Chen, L., He, J., Zhou, J., et al. (2019). EIF2A promotes cell survival during paclitaxel treatment in vitro and in vivo. *Journal of Cellular and Molecular Medicine*, *23*(9), 6060–6071. https://doi.org/10.1111/jcmm.14469

Choi, J.-H., Lee, B.-S., Jang, J. Y., et al. (2023). Single-cell transcriptome profiling of the stepwise progression of head and neck cancer. *Nature Communications*, *14*(1), 1055. https://doi.org/10.1038/s41467-023-36691-x

Chow, L. Q. M. (2020). Head and neck cancer. *New England Journal of Medicine*, *382*(1), 60–72. https://doi.org/10.1056/NEJMra1715715

Clemens, M. J., van Venrooij, W. J., & van de Putte, L. B. A. (2000). Apoptosis and autoimmunity. *Cell Death & Differentiation*, *7*(1), 131–133. https://doi.org/10.1038/sj.cdd.4400633

Clin, B., Gramond, C., Thaon, I., et al. (2022). Head and neck cancer and asbestos exposure. *Occupational and Environmental Medicine*, *79*(10), 690. https://doi.org/10.1136/oemed-2021-108047

Cogliano, V. J., Baan, R., Straif, K., et al. (2011). Preventable exposures associated with human cancers. *Journal of the National Cancer Institute*, *103*(24), 1827–1839. https://doi.org/10.1093/jnci/djr483

Curradi, M., Izzo, A., Badaracco, G., et al. (2002). Molecular mechanisms of gene silencing mediated by DNA methylation. *Molecular and Cellular Biology*, *22*(9), 3157–3173. https://doi.org/10.1128/MCB.22.9.3157-3173.2002

Cyran, A. M., Kleinegger, F., Nass, N., et al. (2023). Inhibition of EIF2α dephosphorylation decreases cell viability and synergizes with standard-of-care chemotherapeutics in head and neck squamous cell carcinoma. *Cancers*, *15*(22), 5350. https://doi.org/10.3390/cancers15225350

Dadey, D. Y. A., Kapoor, V., Khudanyan, A., et al. (2018). PERK regulates glioblastoma sensitivity to ER stress although promoting radiation resistance. *Molecular Cancer Research*, *16*(10), 1447–1453. https://doi.org/10.1158/1541-7786.MCR-18-0224

Dakubo, G. D., Jakupciak, J. P., Birch-Machin, M. A., et al. (2007). Clinical implications and utility of field cancerization. *Cancer Cell International*, *7*(1), 2. https://doi.org/10.1186/1475-2867-7-2

Darini, C., Ghaddar, N., Chabot, C., et al. (2019). An integrated stress response via PKR suppresses HER2+ cancers and improves trastuzumab therapy. *Nature Communications*, *10*(1), 2139. https://doi.org/10.1038/s41467-019-10138-8

Dasari, S., & Tchounwou, P. B. (2014). Cisplatin in cancer therapy: molecular mechanisms of action. *European Journal of Pharmacology*, *740*, 364–378. https://doi.org/10.1016/j.ejphar.2014.07.025

D'Cruz, A. K., Vaish, R., Kapre, N., et al. (2015). Elective versus therapeutic neck dissection in node-negative oral cancer. *New England Journal of Medicine*, *373*(6), 521–529. https://doi.org/10.1056/NEJMoa1506007

de Bakker, T., Journe, F., Descamps, G., et al. (2022). Restoring p53 function in head and neck squamous cell carcinoma to improve treatments. *Frontiers in Oncology*, *11*, 799993. https://doi.org/10.3389/fonc.2021.799993

de Sanjosé, S., Serrano, B., Tous, S., et al. (2018). Burden of human papillomavirus HPV-related cancers attributable to HPVs 6/11/16/18/31/33/45/52 and 58. *JNCI Cancer Spectrum*, *2*(4), pky045. https://doi.org/10.1093/jncics/pky045

Degli Esposti, D., Sklias, A., Lima, S. C., et al. (2017). Unique DNA methylation signature in HPV-positive head and neck squamous cell carcinomas. *Genome Medicine*, *9*(1), 33. https://doi.org/10.1186/s13073-017-0419-z

Dempster, J. M., Boyle, I., Vazquez, F., et al. (2021). Chronos: a cell population dynamics model of CRISPR experiments that improves inference of gene fitness effects. *Genome Biology, 22, 343*. https://doi.org/10.1186/s13059-021-02540-7

Dempster, J. M., Rossen, J., Kazachkova, M., et al. (2019). Extracting biological insights from the Project Achilles genome-scale CRISPR screens in cancer cell lines. *bioRxiv*. https://doi.org/10.1101/720243

Dietz, A., Ramroth, H., Urban, T., et al. (2004). Exposure to cement dust, related occupational groups and laryngeal cancer risk: results of a population-based case-control study. *International Journal of Cancer*, *108*(6), 907–911. https://doi.org/https://doi.org/10.1002/ijc.11658

Ding, Z., Liu, Y., Rubio, V., et al. (2016). OLA1, a translational regulator of p21, maintains optimal cell proliferation necessary for developmental progression. *Molecular and Cellular Biology*, *36*(20), 2568–2582. https://doi.org/10.1128/MCB.00137-16

Donnelly, N., Gorman, A. M., Gupta, S., et al. (2013). The eIF2α kinases: their structures and functions. *Cellular and Molecular Life Sciences*, *70*(19), 3493–3511. https://doi.org/10.1007/s00018-012-1252-6

Donzé, O., Jagus, R., Koromilas, A. E., et al. (1995). Abrogation of translation initiation factor eIF-2 phosphorylation causes malignant transformation of NIH 3T3 cells. *The EMBO Journal*, *14*(15), 3828–3834. https://doi.org/https://doi.org/10.1002/j.1460-2075.1995.tb00052.x

Drexler, H. C. A. (2009). Synergistic apoptosis induction in leukemic cells by the phosphatase inhibitor salubrinal and proteasome inhibitors. *PloS One*, *4*(1), e4161–e4161. https://doi.org/10.1371/journal.pone.0004161

Druesne-Pecollo, N., Tehard, B., Mallet, Y., et al. (2009). Alcohol and genetic polymorphisms: effect on risk of alcohol-related cancer. *The Lancet Oncology*, 10(2):173-80. https://doi.org/10.1016/S1470-2045(09)70019-1

Economopoulou, P., Kotsantis, I., & Psyrri, A. (2020). Special issue about head and neck cancers: HPV positive cancers. *International Journal of Molecular Sciences*, 21(9):3388. https://doi.org/10.3390/ijms21093388

Edge, S. B., & Compton, C. C. (2010). The American Joint Committee on Cancer: the 7th edition of the AJCC cancer staging manual and the future of TNM. *Annals of Surgical Oncology*, *17*(6), 1471–1474. https://doi.org/10.1245/s10434-010-0985-4

Edwards, N. J., Oberti, M., Thangudu, R. R., et al. (2015). The CPTAC data portal: a resource for cancer proteomics research. *Journal of Proteome Research*, *14*(6), 2707–2713. https://doi.org/10.1021/pr501254j

Ettl, T., Grube, M., Schulz, D., et al. (2022). Checkpoint inhibitors in cancer therapy: clinical benefits for head and neck cancers. *Cancers*, *14*(20), 4985. https://doi.org/10.3390/cancers14204985

European Medicines Agency (a). *Cervarix human papillomavirus vaccine [types 16, 18] (recombinant, adjuvanted, adsorbed)*. Summary of the European Public Assessment

Report (EPAR) for Gardasil 9. Retrieved October 28, 2023, from https://www.ema.europa.eu/en/medicines/human/EPAR/cervarix

European Medicines Agency (b). *Gardasil human papillomavirus vaccine [types 6, 11, 16, 18] (recombinant, adsorbed)*. Summary of the European Public Assessment Report (EPAR) for Gardasil. Retrieved October 28, 2023, from https://www.ema.europa.eu/en/medicines/human/EPAR/gardasil

European Medicines Agency (c). *Gardasil v9 human papillomavirus 9-valent vaccine (recombinant, adsorbed)*. Summary of the European Public Assessment Report (EPAR) for Gardasil 9. Retrieved October 28, 2023, from https://www.ema.europa.eu/en/medicines/human/EPAR/gardasil-9

Fields, A. P., Justilien, V., & Murray, N. R. (2016). The chromosome 3q26 OncCassette: a multigenic driver of human cancer. *Advances in Biological Regulation*, *60*, 47–63. https://doi.org/https://doi.org/10.1016/j.jbior.2015.10.009

Fitzgerald, A. L., Osman, A. A., Xie, T.-X., et al. (2015). Reactive oxygen species and p21Waf1/Cip1 are both essential for p53-mediated senescence of head and neck cancer cells. *Cell Death & Disease*, *6*(3), e1678–e1678. https://doi.org/10.1038/cddis.2015.44

Fucikova, J., Kepp, O., Kasikova, L., et al. (2020). Detection of immunogenic cell death and its relevance for cancer therapy. *Cell Death & Disease*, *11*(11), 1013. https://doi.org/10.1038/s41419-020-03221-2

Galluzzi, L., Humeau, J., Buqué, A., et al. (2020). Immunostimulation with chemotherapy in the era of immune checkpoint inhibitors. *Nature Reviews Clinical Oncology*, *17*(12), 725–741. https://doi.org/10.1038/s41571-020-0413-z

Gao, J., Aksoy, B. A., Dogrusoz, U., et al. (2013). Integrative analysis of complex cancer genomics and clinical profiles using the cBioPortal. *Science Signaling*, *6*(269), pl1–pl1. https://doi.org/10.1126/scisignal.2004088

Gatta, G., Botta, L., Sánchez, M.-J., et al. (2015). Prognoses and improvement for head and neck cancers diagnosed in Europe in early 2000s: The EUROCARE-5 population-based study. *European Journal of Cancer*, *51*(15), 2130–2143. https://doi.org/10.1016/j.ejca.2015.07.043

Gaździcka, J., Gołąbek, K., Strzelczyk, J. K., et al. (2020). Epigenetic modifications in head and neck cancer. *Biochemical Genetics*, *58*(2), 213–244. https://doi.org/10.1007/s10528-019-09941-1

Ghafouri-Fard, S., Abak, A., Tondro Anamag, F., et al. (2021). 5-fluorouracil: a narrative review on the role of regulatory mechanisms in driving resistance to this chemotherapeutic agent. *Frontiers in Oncology*, *11*, 658636. https://doi.org/10.3389/fonc.2021.658636

Ghittoni, R., Accardi, R., Chiocca, S., et al. (2015). Role of human papillomaviruses in carcinogenesis. *Ecancermedicalscience*, *9*:526. https://doi.org/10.3332/ecancer.2015.526

Gholap, D., Dikshit, R., Chaturvedi, P., et al. (2023). Exclusive use of different types of tobacco products, exposure to secondhand tobacco smoke and risk of subtypes of head and neck cancer among Indian males. *International Journal of Cancer*, *152*(3), 374–383. https://doi.org/https://doi.org/10.1002/ijc.34258

Giraldi, L., Leoncini, E., Pastorino, R., et al. (2017). Alcohol and cigarette consumption predict mortality in patients with head and neck cancer: a pooled analysis within the International Head and Neck Cancer Epidemiology (INHANCE) Consortium. *Annals of Oncology*, *28*(11), 2843–2851. https://doi.org/https://doi.org/10.1093/annonc/mdx486

Goon, P., Sauzet, O., Schuermann, M., et al. (2023). Recurrent respiratory papillomatosis (RRP)- meta-analyses on the use of the HPV vaccine as adjuvant therapy. *Npj Vaccines*, *8*(1), 49. https://doi.org/10.1038/s41541-023-00644-8

Goon, P., Schürmann, M., Oppel, F., et al. (2022). Viral and clinical oncology of head and neck cancers. *Current Oncology Reports*, *24*(7), 929–942. https://doi.org/10.1007/s11912-022-01263-7

Gordiyenko, Y., Llácer, J. L., & Ramakrishnan, V. (2019). Structural basis for the inhibition of translation through eIF2α phosphorylation. *Nature Communications*, *10*(1), 2640. https://doi.org/10.1038/s41467-019-10606-1

Gormley, M., Creaney, G., Schache, A., et al. (2022). Reviewing the epidemiology of head and neck cancer: definitions, trends and risk factors. *British Dental Journal*, *233*(9), 780–786. https://doi.org/10.1038/s41415-022-5166-x

Guan, J.-Y., Luo, Y.-H., Lin, Y.-Y., et al. (2023). Malignant transformation rate of oral leukoplakia in the past 20 years: a systematic review and meta-analysis. *Journal of Oral Pathology & Medicine*, 52(8):691-700. https://doi.org/https://doi.org/10.1111/jop.13440

Guigay, J., Tahara, M., Licitra, L., et al. (2019). The evolving role of taxanes in combination with cetuximab for the treatment of recurrent and/or metastatic squamous cell carcinoma of the head and neck: evidence, advantages, and future directions. *Frontiers in Oncology*, *9:668*. https://doi.org/10.3389/fonc.2019.00668

Guo, L., Chi, Y., Xue, J., et al. (2017). Phosphorylated eIF2α predicts disease-free survival in triple-negative breast cancer patients. *Scientific Reports*, *7*, 44674. https://doi.org/10.1038/srep44674

Hamamura, K., Minami, K., Tanjung, N., et al. (2014). Attenuation of malignant phenotypes of breast cancer cells through eIF2α-mediated downregulation of Rac1 signaling. *International Journal of Oncology*, *44*(6), 1980–1988. https://doi.org/10.3892/ijo.2014.2366

Hao, P., Yu, J., Ward, R., et al. (2020a). Eukaryotic translation initiation factors as promising targets in cancer therapy. *Cell Communication and Signaling*, *18*(1), 175. https://doi.org/10.1186/s12964-020-00607-9

Hao, P., Yu, J., Ward, R., et al. (2020b). Eukaryotic translation initiation factors as promising targets in cancer therapy. *Cell Communication and Signaling*, *18*(1), 175. https://doi.org/10.1186/s12964-020-00607-9

Harding, H. P., Zhang, Y., Scheuner, D., et al. (2009). Ppp1r15 gene knockout reveals an essential role for translation initiation factor 2 alpha (eIF2α) dephosphorylation in mammalian development. *Proceedings of the National Academy of Sciences of the United States of America*, *106*(6), 1832-7. https://doi.org/10.1073/pnas.0809632106

Hasegawa, Y., Tsukahara, K., Yoshimoto, S., et al. (2019). Neck dissections based on sentinel lymph node navigation versus elective neck dissections in early oral cancers: A randomized, multicenter, non-inferiority trial. *Journal of Clinical Oncology*, 39(18):2025-2036. https://doi.org/10.1200/JCO.20.03637

Hashibe, M., Brennan, P., Benhamou, S., et al. (2007). Alcohol drinking in never users of tobacco, cigarette smoking in never drinkers, and the risk of head and neck cancer: pooled analysis in the International Head and Neck Cancer Epidemiology Consortium. *Journal of the National Cancer Institute, 99*(10), 777–789. https://doi.org/10.1093/jnci/djk179

Hashibe, M., Brennan, P., Chuang, S.-C., et al. (2009). Interaction between tobacco and alcohol use and the risk of head and neck cancer: pooled analysis in the International Head and Neck Cancer Epidemiology Consortium. *Cancer Epidemiology, Biomarkers & Prevention*, *18*(2), 541–550. https://doi.org/10.1158/1055-9965.EPI-08-0347

Hashim, D., Sartori, S., Brennan, P., et al. (2016). The role of oral hygiene in head and neck cancer: results from International Head and Neck Cancer Epidemiology (INHANCE) consortium. *Annals of Oncology, 27*(8), 1619–1625. https://doi.org/10.1093/annonc/mdw224

Hayes, D. N., Van Waes, C., & Seiwert, T. Y. (2015). Genetic landscape of human papillomavirus-associated head and neck cancer and comparison to tobacco-related tumors. *Journal of Clinical Oncology, 33*(29), 3227–3234. https://doi.org/10.1200/JCO.2015.62.1086

Herrero, R., Quint, W., Hildesheim, A., et al. (2013). Reduced prevalence of oral human papillomavirus (HPV) 4 years after bivalent HPV vaccination in a randomized clinical trial in Costa Rica. *PloS One*, *8*(7), e68329–e68329. https://doi.org/10.1371/journal.pone.0068329

Hier, J., Vachon, O., Bernstein, A., et al. (2021). Portrait of DNA methylated genes predictive of poor prognosis in head and neck cancer and the implication for targeted therapy. *Scientific Reports*, *11*(1), 10012. https://doi.org/10.1038/s41598-021-89476-x

Hirth, J. M., Chang, M., Resto, V. A., et al. (2017). Prevalence of oral human papillomavirus by vaccination status among young adults (18–30years old). *Vaccine*, *35*(27), 3446–3451. https://doi.org/https://doi.org/10.1016/j.vaccine.2017.05.025

Huang, Z., Wu, Y., Zhou, X., et al. (2014). Efficacy of therapy with bortezomib in solid tumors: a review based on 32 clinical trials. *Future Oncology*, *10*(10), 1795–1807. https://doi.org/10.2217/fon.14.30

Hurwitz, B., Guzzi, N., Gola, A., et al. (2022). The integrated stress response remodels the microtubule-organizing center to clear unfolded proteins following proteotoxic stress. *ELife*, *11*, e77780. https://doi.org/10.7554/eLife.77780

Ianevski, A., Giri, A. K., & Aittokallio, T. (2022). SynergyFinder 3.0: an interactive analysis and consensus interpretation of multi-drug synergies across multiple samples. *Nucleic Acids Research*, *50*(W1), W739–W743. https://doi.org/10.1093/nar/gkac382

Iocca, O., Sollecito, T. P., Alawi, F., et al. (2020). Potentially malignant disorders of the oral cavity and oral dysplasia: A systematic review and meta-analysis of malignant transformation rate by subtype. *Head & Neck*, *42*(3), 539–555. https://doi.org/https://doi.org/10.1002/hed.26006

Isayeva, T., Li, Y., Maswahu, D., & Brandwein-Gensler, M. (2012). Human papillomavirus in non-oropharyngeal head and neck cancers: a systematic literature review. *Head and Neck Pathology*, *6*(1), 104–120. https://doi.org/10.1007/s12105-012-0368-1

Jeon, Y.-J., Kim, J. H., Shin, J.-I., et al. (2016). Salubrinal-mediated upregulation of eIF2α phosphorylation increases doxorubicin sensitivity in MCF-7/ADR cells. *Molecules and Cells*, *39*(2), 129–135. https://doi.org/10.14348/molcells.2016.2243

Johnson, D. E., Burtness, B., Leemans, C. R., et al. (2020). Head and neck squamous cell carcinoma. *Nature Reviews. Disease Primers*, *6*(1), 92. https://doi.org/10.1038/s41572-020-00224-3

Joshi, M., Kulkarni, A., & Pal, J. K. (2013). Small molecule modulators of eukaryotic initiation factor 2α kinases, the key regulators of protein synthesis. *Biochimie*, *95*(11), 1980–1990. https://doi.org/https://doi.org/10.1016/j.biochi.2013.07.030

Jousse, C., Oyadomari, S., Novoa, I., et al. (2003). Inhibition of a constitutive translation initiation factor 2alpha phosphatase, CReP, promotes survival of stressed cells. *The Journal of Cell Biology*, *163*(4), 767–775. https://doi.org/10.1083/jcb.200308075

Kazemi, S., Papadopoulou, S., Li, S., et al. (2004). Control of alpha subunit of eukaryotic translation initiation factor 2 (eIF2 alpha) phosphorylation by the human papillomavirus type 18 E6 oncoprotein: implications for eIF2 alpha-dependent gene expression and cell death. *Molecular and Cellular Biology*, *24*(8), 3415–3429. https://doi.org/10.1128/MCB.24.8.3415-3429.2004

Kepp, O., Semeraro, M., Bravo-San Pedro, J. M., et al. (2015). eIF2α phosphorylation as a biomarker of immunogenic cell death. *Seminars in Cancer Biology*, *33*, 86–92. https://doi.org/https://doi.org/10.1016/j.semcancer.2015.02.004

Khetan, P., Boffetta, P., Luce, D., et al. (2019). Occupations and the risk of head and neck cancer: a pooled analysis of the International Head and Neck Cancer Epidemiology (INHANCE) Consortium. *Journal of Occupational and Environmental Medicine*, *61*(5), 397–404. https://doi.org/10.1097/JOM.0000000000001563

Koizumi, M., Tanjung, N. G., Chen, A., et al. (2012). Administration of salubrinal enhances radiation-induced cell death of SW1353 chondrosarcoma cells. *Anticancer Research*, *32*(9), 3667–3673. https://pubmed.ncbi.nlm.nih.gov/22993304/

Kojima, E., Takeuchi, A., Haneda, M., et al. (2003). The function of GADD34 is a recovery from a shutoff of protein synthesis induced by ER stress-elucidation by GADD34-deficient mice. *The FASEB Journal*, *17*(11), 1–18. https://doi.org/https://doi.org/10.1096/fj.02-1184fje

Komar, A. A., & Merrick, W. C. (2020). A retrospective on eIF2A- and not the alpha subunit of eIF2. *International Journal of Molecular Sciences*, *21*(6), 2054. https://doi.org/10.3390/ijms21062054

Koneva, L. A., Zhang, Y., Virani, S., et al. (2018). HPV integration in HNSCC correlates with survival outcomes, immune response signatures, and candidate drivers. *Molecular Cancer Research: MCR*, *16*(1), 90–102. https://doi.org/10.1158/1541-7786.MCR-17-0153

Koromilas, A. E. (2015). Roles of the translation initiation factor eIF2α serine 51 phosphorylation in cancer formation and treatment. *Biochimica et Biophysica Acta* -

Gene Regulatory Mechanisms, *1849*(7), 871–880. https://doi.org/https://doi.org/10.1016/j.bbagrm.2014.12.007

Kostic, A. D., Ojesina, A. I., Pedamallu, C. S., et al. (2011). PathSeq: software to identify or discover microbes by deep sequencing of human tissue. *Nature Biotechnology*, *29*(5), 393–396. https://doi.org/10.1038/nbt.1868

Kreimer, A. R., Clifford, G. M., Boyle, P., et al. (2005). Human papillomavirus types in head and neck squamous cell carcinomas worldwide: a systematic review. *Cancer Epidemiology, Biomarkers & Prevention*, *14*(2), 467–475. https://doi.org/10.1158/1055-9965.EPI-04-0551

Kreimer, A. R., Johansson, M., Waterboer, T., et al. (2013). Evaluation of human papillomavirus antibodies and risk of subsequent head and neck cancer. *Journal of Clinical Oncology, 31*(21), 2708–2715. https://doi.org/10.1200/JCO.2012.47.2738

Krutz, M., Acharya, P., Chissoe, G., et al. (2022). Tobacco cessation after head and neck cancer diagnosis is an independent predictor of treatment response and long-term survival. *Oral Oncology*, *134*, 106072. https://doi.org/https://doi.org/10.1016/j.oraloncology.2022.106072

Kutler, D. I., Auerbach, A. D., Satagopan, J., et al. (2003). High incidence of head and neck squamous cell carcinoma in patients with Fanconi anemia. *Archives of Otolaryngology–Head & Neck Surgery*, *129*(1), 106–112. https://doi.org/10.1001/archotol.129.1.106

Langevin, S. M., O'Sullivan, M. H., Valerio, J. L., et al. (2013). Occupational asbestos exposure is associated with pharyngeal squamous cell carcinoma in men from the greater Boston area. *Occupational and Environmental Medicine*, *70*(12), 858–863. https://doi.org/10.1136/oemed-2013-101528

Lawrence, M. S., Sougnez, C., & Lichtenstein, L. et al. (2015). Comprehensive genomic characterization of head and neck squamous cell carcinomas. *Nature*, *517*(7536), 576–582. https://doi.org/10.1038/nature14129

Lechner, M., Liu, J., Masterson, L., et al. (2022). HPV-associated oropharyngeal cancer: epidemiology, molecular biology and clinical management. *Nature Reviews Clinical Oncology*, *19*(5), 306–327. https://doi.org/10.1038/s41571-022-00603-7

Lee, Y.-C. A., Boffetta, P., Sturgis, E. M., et al. (2008). Involuntary smoking and head and neck cancer risk: pooled analysis in the International Head and Neck Cancer Epidemiology Consortium. *Cancer Epidemiology, Biomarkers & Prevention, 17*(8), 1974–1981. https://doi.org/10.1158/1055-9965.EPI-08-0047

Leemans, C. R., Snijders, P. J. F., & Brakenhoff, R. H. (2018). The molecular landscape of head and neck cancer. *Nature Reviews Cancer*, *18*(5), 269–282. https://doi.org/10.1038/nrc.2018.11

Leonel, A.-C., Bonan, R.-F., Pinto, M.-B., et al. (2021). The pesticides use and the risk for head and neck cancer: A review of case-control studies. *Medicina Oral, Patologia Oral y Cirugia Bucal*, *26*(1), e56–e63. https://doi.org/10.4317/medoral.23962

Leprivier, G., Rotblat, B., Khan, D., et al. (2015). Stress-mediated translational control in cancer cells. *Biochimica et Biophysica Acta - Gene Regulatory Mechanisms*, *1849*(7), 845–860. https://doi.org/https://doi.org/10.1016/j.bbagrm.2014.11.002

Li, M.-H., Ito, D., Sanada, M., et al. (2004). Effect of 5-fluorouracil on G1 phase cell cycle regulation in oral cancer cell lines. *Oral Oncology*, *40*(1), 63–70. https://doi.org/https://doi.org/10.1016/S1368-8375(03)00136-2

Li, Q., Tie, Y., Alu, A., et al. (2023). Targeted therapy for head and neck cancer: signaling pathways and clinical studies. *Signal Transduction and Targeted Therapy*, *8*(1), 31. https://doi.org/10.1038/s41392-022-01297-0

Lichter, K., Krause, D., Xu, J., et al. (2020). Adjuvant human papillomavirus vaccine to reduce recurrent cervical dysplasia in unvaccinated women: a systematic review and meta-analysis. *Obstetrics and Gynecology*, *135*(5), 1070-1083. https://doi.org/10.1097/AOG.0000000000003833

Lobo, M. V. T., Martín, M. E., Pérez, M. I., et al. (2000). Levels, phosphorylation status and cellular localization of translational factor eIF2 in gastrointestinal carcinomas. *The Histochemical Journal*, *32*(3), 139–150. https://doi.org/10.1023/A:1004091122351

LoConte, N. K., Brewster, A. M., Kaur, J. S., et al. (2017). Alcohol and cancer: a statement of the American Society of Clinical Oncology. *Journal of Clinical Oncology*, *36*(1), 83–93.

https://doi.org/10.1200/JCO.2017.76.1155

Longley, D. B., Harkin, D. P., & Johnston, P. G. (2003). 5-Fluorouracil: mechanisms of action and clinical strategies. *Nature Reviews Cancer*, *3*(5), 330–338. https://doi.org/10.1038/nrc1074

Lorenzo-Pouso, A. I., Lafuente-Ibáñez de Mendoza, I., Pérez-Sayáns, M., et al. (2022). Critical update, systematic review, and meta-analysis of oral erythroplakia as an oral potentially malignant disorder. *Journal of Oral Pathology & Medicine, 51*(7), 585–593. https://doi.org/10.1111/jop.13304

Lu, W., Ni, K., Li, Z., et al. (2022). Salubrinal protects against cisplatin-induced cochlear hair cell endoplasmic reticulum stress by regulating eukaryotic translation initiation factor 2α signaling. *Frontiers in Molecular Neuroscience*, *15*, 916458. https://doi.org/10.3389/fnmol.2022.916458

Luo, J., Solimini, N. L., & Elledge, S. J. (2009). Principles of cancer therapy: oncogene and non-oncogene addiction. *Cell*, *136*(5), 823–837. https://doi.org/10.1016/j.cell.2009.02.024

Mahale, P., Sturgis, E. M., Tweardy, D. J., et al. (2016). Association between hepatitis c virus and head and neck cancers. *Journal of the National Cancer Institute*, *108*(8), djw035. https://doi.org/10.1093/jnci/djw035

Mandic, A., Hansson, J., Linder, S., et al. (2003). Cisplatin induces endoplasmic reticulum stress and nucleus-independent apoptotic signaling. *The Journal of Biological Chemistry*, *278*(110), 9100–9106. https://doi.org/10.1074/jbc.M210284200

Matthews, H. K., Bertoli, C., & de Bruin, R. A. M. (2022). Cell cycle control in cancer. *Nature Reviews Molecular Cell Biology*, *23*(1), 74–88. https://doi.org/10.1038/s41580-021-00404-3

Men, C., Chai, H., Song, X., et al. (2017). Identification of DNA methylation associated gene signatures in endometrial cancer via integrated analysis of DNA methylation and gene expression systematically. *Journal of Gynecologic Oncology*, *28*(6), e83–e83. https://doi.org/10.3802/jgo.2017.28.e83

Meyers, R. M., Bryan, J. G., McFarland, J. M., et al. (2017). Computational correction of copy number effect improves specificity of CRISPR-Cas9 essentiality screens in cancer cells. *Nature Genetics*, *49*(12), 1779-1784. https://doi.org/10.1038/ng.3984

Mohebbi, E., Hadji, M., Rashidian, H., et al. (2021). Opium use and the risk of head and neck squamous cell carcinoma. *International Journal of Cancer*, *148*(5), 1066–1076. https://doi.org/https://doi.org/10.1002/ijc.33289

Mroz, E. A., Tward, A. D., Hammon, R. J., et al. (2015). Intra-tumor genetic heterogeneity and mortality in head and neck cancer: analysis of data from the Cancer Genome Atlas. *PLoS Medicine*, *12*(2), e1001786. https://doi.org/10.1371/journal.pmed.1001786

Münger, K., Baldwin, A., Edwards, K. M., et al. (2004). Mechanisms of human papillomavirus-induced oncogenesis. *Journal of Virology*, *78*(21), 11451–11460. https://doi.org/10.1128/JVI.78.21.11451-11460.2004

Nagel, R., Semenova, E. A., & Berns, A. (2016). Drugging the addict: non-oncogene addiction as a target for cancer therapy. *EMBO Reports*, *17*(11), 1516–1531. https://doi.org/10.15252/embr.201643030

Nakagawa, T., Kurokawa, T., Mima, M., et al. (2021). DNA Methylation and HPV-associated head and neck cancer. *Microorganisms*, *9*(4), 801. https://doi.org/10.3390/microorganisms9040801

National Comprehensive Cancer Network. NCCN Clinical Practice Guidelines in Oncology for *Head and Neck Cancer Version 2.2023*. Retrieved May 15, 2023, from https://www.nccn.org

The Cancer Genome Atlas Research Network. Integrated genomic and molecular characterization of cervical cancer. *Nature*, *543*(7645), 378–384. https://doi.org/10.1038/nature21386

Nguyen, H. G., Conn, C. S., Kye, Y., et al. (2018). Development of a stress response therapy targeting aggressive prostate cancer. *Science Translational Medicine*, *10*(439), eaar2036. https://doi.org/10.1126/scitranslmed.aar2036

Nishiyama, A., & Nakanishi, M. (2021). Navigating the DNA methylation landscape of cancer. *Trends in Genetics*, *37*(11), 1012–1027. https://doi.org/10.1016/j.tig.2021.05.002

Novoa, I., Zhang, Y., Zeng, H., et al. (2003). Stress-induced gene expression requires programmed recovery from translational repression. *The EMBO Journal*, *22*(5), 1180–1187. https://doi.org/10.1093/emboj/cdg112

Obeid, M., Tesniere, A., Ghiringhelli, F., et al. (2007). Calreticulin exposure dictates the immunogenicity of cancer cell death. *Nature Medicine*, *13*(1), 54–61. https://doi.org/10.1038/nm1523

Osazuwa-Peters, N., Adjei Boakye, E., Chen, B. Y., et al. (2018). Association between head and neck squamous cell carcinoma survival, smoking at diagnosis, and marital status. *JAMA Otolaryngology- Head & Neck Surgery*, *144*(1), 43–50. https://doi.org/10.1001/jamaoto.2017.1880

Osazuwa-Peters, N., Simpson, M. C., Zhao, L., et al. (2018). Suicide risk among cancer survivors: head and neck versus other cancers. *Cancer*, *124*(20), 4072–4079. https://doi.org/https://doi.org/10.1002/cncr.31675

Pacini, C., Dempster, J. M., Boyle, I., et al. (2021). Integrated cross-study datasets of genetic dependencies in cancer. *Nature Communications*, *12*(1), 1661. https://doi.org/10.1038/s41467-021-21898-7

Paget-Bailly, S., Cyr, D., & Luce, D. (2012). Occupational exposures to asbestos, polycyclic aromatic hydrocarbons and solvents, and cancers of the oral cavity and pharynx: a quantitative literature review. *International Archives of Occupational and Environmental Health*, *85*(4), 341–351. https://doi.org/10.1007/s00420-011-0683-y

Pai, S. I., & Westra, W. H. (2009). Molecular pathology of head and neck cancer: implications for diagnosis, prognosis, and treatment. *Annual Review of Pathology*, *4*, 49–70. https://doi.org/10.1146/annurev.pathol.4.110807.092158

Pang, X., Tang, Y.-L., & Liang, X.-H. (2018). Transforming growth factor-β signaling in head and neck squamous cell carcinoma: Insights into cellular responses. *Oncology Letters*, *16*(4), 4799–4806. https://doi.org/10.3892/ol.2018.9319

Parker, T. M., Smith, E. M., Ritchie, et al. (2006). Head and neck cancer associated with herpes simplex virus 1 and 2 and other risk factors. *Oral Oncology*, *42*(3), 288–296. https://doi.org/https://doi.org/10.1016/j.oraloncology.2005.08.003

Payne, K. K. (2022). Cellular stress responses and metabolic reprogramming in cancer progression and dormancy. *Seminars in Cancer Biology*, *78*, 45–48. https://doi.org/https://doi.org/10.1016/j.semcancer.2021.06.004

Petti, S. (2003). Pooled estimate of world leukoplakia prevalence: a systematic review. *Oral Oncology*, *39*(8), 770–780. https://doi.org/https://doi.org/10.1016/S1368-8375(03)00102-7

Psyrri, A., Seiwert, T. Y., & Jimeno, A. (2013). Molecular pathways in head and neck cancer: EGFR, PI3K, and more. *American Society of Clinical Oncology Educational Book*, *33*, 246–255. https://doi.org/10.14694/EdBook_AM.2013.33.246

Pulte, D., & Brenner, H. (2010). Changes in survival in head and neck cancers in the late 20th and early 21st century: a period analysis. *The Oncologist*, *15*(9), 994–1001. https://doi.org/10.1634/theoncologist.2009-0289

Qi, J., Jin, F., Xu, X., et al. (2021). Combination cancer immunotherapy of nanoparticle-based immunogenic cell death inducers and immune checkpoint inhibitors. *International Journal of Nanomedicine*, *16*, 1435–1456. https://doi.org/10.2147/IJN.S285999

Rampias, T., Sasaki, C., & Psyrri, A. (2014). Molecular mechanisms of HPV induced carcinogenesis in head and neck. *Oral Oncology*, *50*(5), 356–363. https://doi.org/https://doi.org/10.1016/j.oraloncology.2013.07.011

Ranganathan, A. C., Ojha, S., Kourtidis, A., et al. (2008). Dual function of pancreatic endoplasmic reticulum kinase in tumor cell growth arrest and survival. *Cancer Research*, *68*(9), 3260–3268. https://doi.org/10.1158/0008-5472.CAN-07-6215

Ranganathan, K., & Kavitha, L. (2019). Oral epithelial dysplasia: classifications and clinical relevance in risk assessment of oral potentially malignant disorders. *Journal of Oral and Maxillofacial Pathology*, *23*(1), 19–27. https://doi.org/10.4103/jomfp.JOMFP_13_19

Riva, G., Albano, C., Gugliesi, F., et al. (2021). HPV meets APOBEC: new players in head and neck cancer. *International Journal of Molecular Sciences*, *22*(3), 1402.

https://doi.org/10.3390/ijms22031402

Rivera, F., García-Castaño, A., Vega, N., et al. (2009). Cetuximab in metastatic or recurrent head and neck cancer: the EXTREME trial. *Expert Review of Anticancer Therapy*, *9*(10), 1421–1428. https://doi.org/10.1586/era.09.113

Robichaud, N., Sonenberg, N., Ruggero, D., et al. (2018). Translational control in cancer. *Cold Spring Harbor Perspectives in Biology*, *11*(7), a032896. https://doi.org/10.1101/cshperspect.a032896

Rosenfeldt, M. T., Bell, L. A., Long, J. S., et al. (2014). E2F1 drives chemotherapeutic drug resistance via ABCG2. *Oncogene*, *33*(32), 4164–4172. https://doi.org/10.1038/onc.2013.470

Sabatini, M. E., & Chiocca, S. (2020). Human papillomavirus as a driver of head and neck cancers. *British Journal of Cancer*, *122*(3), 306–314. https://doi.org/10.1038/s41416-019-0602-7

Sabharwal, R., Mahendra, A., Moon, N. J., et al. (2014). Genetically altered fields in head and neck cancer and second field tumor. *South Asian Journal of Cancer*, *3*(3), 151–153. https://doi.org/10.4103/2278-330X.136766

Schewe, D. M., & Aguirre-Ghiso, J. A. (2009). Inhibition of eIF2alpha dephosphorylation maximizes bortezomib efficiency and eliminates quiescent multiple myeloma cells surviving proteasome inhibitor therapy. *Cancer Research*, *69*(4), 1545–1552. https://doi.org/10.1158/0008-5472.CAN-08-3858

Schrijvers, D., & Vermorken, J. B. (2000). Role of Taxoids in Head and Neck Cancer. *The Oncologist*, *5*(3), 199–208. https://doi.org/10.1634/theoncologist.5-3-199

Sengupta, S., Sevigny, C. M., Bhattacharya, P., et al. (2019). Estrogen-induced apoptosis in breast cancers is phenocopied by blocking dephosphorylation of eukaryotic initiation factor 2 alpha (eIF2α) protein. *Molecular Cancer Research*, *17*(4), 918–928. https://doi.org/10.1158/1541-7786.MCR-18-0481

Sharma, D. K., Bressler, K., Patel, H., et al. (2016). Role of eukaryotic initiation factors during cellular stress and cancer progression. *Journal of Nucleic Acids*, 2016:8235121. https://doi.org/doi:10.1155/2016/8235121

Shete, S., Liu, H., Wang, J., et al. (2020). A genome-wide association study identifies two novel susceptible regions for squamous cell carcinoma of the head and neck. *Cancer Research*, *80*(12), 2451–2460. https://doi.org/10.1158/0008-5472.CAN-19-2360

Shinawi, T., Hill, V. K., Krex, D., et al. (2013). DNA methylation profiles of long- and short-term glioblastoma survivors. *Epigenetics*, *8*(2), 149–156. https://doi.org/10.4161/epi.23398

Singh, G., Jaiswal, A., Goel, A. D., et al. (2021). Opium usage and risk of head and neck cancer: a systematic review and meta-analysis. *Asian Pacific Journal of Cancer Prevention*, *22*(3), 661–670. https://doi.org/10.31557/APJCP.2021.22.3.661

Slaughter, D. P., Southwick, H. W., & Smejkal, W. (1953). "Field cancerization" in oral stratified squamous epithelium. Clinical implications of multicentric origin. *Cancer*, *6*(5), 963–968. https://doi.org/https://doi.org/10.1002/1097-0142(195309)6:5<963::AID-CNCR2820060515>3.0.CO;2-Q

Smeets, S. J., Van Der Plas, M., Schaaij-Visser, T. B. M., et al. (2011). Immortalization of oral keratinocytes by functional inactivation of the p53 and pRb pathways. *International Journal of Cancer*, *128*(7)1596-1605. https://doi.org/10.1002/ijc.25474

Spilka, R., Ernst, C., Mehta, A. K., et al. (2013). Eukaryotic translation initiation factors in cancer development and progression. *Cancer Letters, 340*(1), 9–21. https://doi.org/10.1016/j.canlet.2013.06.019

Sung, H., Ferlay, J., Siegel, R. L., et al. (2021). Global Cancer Statistics 2020: GLOBOCAN estimates of incidence and mortality worldwide for 36 cancers in 185 countries. *CA: A Cancer Journal for Clinicians*, *71*(3), 209–249. https://doi.org/https://doi.org/10.3322/caac.21660

Szukalska, M., Szyfter, K., Florek, E., et al. (2020). Electronic cigarettes and head and neck cancer risk-current state of art. *Cancers*, *12*(11), 3274. https://doi.org/10.3390/cancers12113274

Szyfter, K., Wierzbicka, M., Hunt, J. L., et al. (2016). Frequent chromosomal aberrations and candidate genes in head and neck squamous cell carcinoma. *European Archives of Oto-Rhino-Laryngology*, *273*(3), 537–545. https://doi.org/10.1007/s00405-014-3339-1

Tabor, M. P., Brakenhoff, R. H., Ruijter-Schippers, et al. (2004). Genetically altered fields as origin of locally recurrent head and neck cancer: a retrospective study. *Clinical Cancer Research*, *10*(11), 3607–3613. https://doi.org/10.1158/1078-0432.CCR-03-0632

Tang, Z., Li, C., Kang, B., et al. (2017). GEPIA: a web server for cancer and normal gene expression profiling and interactive analyses. *Nucleic Acids Research*, *45*(W1), W98–W102.
https://doi.org/10.1093/nar/gkx247

Thakor, N., & Holcik, M. (2012). IRES-mediated translation of cellular messenger RNA operates in eIF2alpha- independent manner during stress. *Nucleic Acids Research*, *40*(2), 541–552.
https://doi.org/10.1093/nar/gkr701

Tian, S., Switchenko, J. M., Jhaveri, J., et al. (2019). Survival outcomes by high-risk human papillomavirus status in non-oropharyngeal head and neck squamous cell carcinomas: a propensity-scored analysis of the National Cancer Data Base. *Cancer*, *125*(16), 2782–2793.
https://doi.org/10.1002/cncr.32115

Tikhomirova, M. S., Kadosh, A., Saukko-Paavola, et al. (2022). A role for endoplasmic reticulum dynamics in the cellular distribution of microtubules. *Proceedings of the National Academy of Sciences*, *119*(15), e2104309119.
https://doi.org/10.1073/pnas.2104309119

Troy, J. D., Grandis, J. R., Youk, A. O., et al. (2013). Childhood passive smoke exposure is associated with adult head and neck cancer. *Cancer Epidemiology*, *37*(4), 417–423.
https://doi.org/https://doi.org/10.1016/j.canep.2013.03.011

Tsaytler, P., Harding, H. P., Ron, D., et al. (2011). Selective inhibition of a regulatory subunit of protein phosphatase 1 restores proteostasis. *Science*, *332*(6025), 91–94.
https://doi.org/10.1126/science.1201396

United States Centers for Disease Control and Prevention, National Center for Chronic Disease Prevention and Health Promotion, Office on Smoking and Health. (2010). How Tobacco Smoke Causes Disease: The Biology and Behavioral Basis for Smoking-Attributable Disease. A Report of the Surgeon General. PMID: 21452462.

United States Food and Drug Administration (a). *Vaccines Licensed for Use in the United States Cervarix*. Retrieved March 29, 2023, from https://www.fda.gov/vaccines-blood-biologics/vaccines/cervarix

United States Food and Drug Administration (b). *Vaccines Licensed for Use in the United States Gardasil*. Retrieved June 3, 2023, from https://www.fda.gov/vaccines-blood-biologics/vaccines/gardasil

Unites States Food and Drug Administration (c). *Vaccines Licensed for Use in the United States Gardasil v9.* Retrieved April 28, 2023, from https://www.fda.gov/vaccines-blood-biologics/vaccines/gardasil-9

Vajente, N., Norante, R., Redolfi, N., et al. (2019). Microtubules stabilization by mutant spastin affects ER morphology and Ca (2+) handling. *Frontiers in Physiology*, *10*, 1544. https://doi.org/10.3389/fphys.2019.01544

Walczak, A., Gradzik, K., Kabzinski, J., et al. (2019). The role of the ER-induced UPR pathway and the efficacy of its inhibitors and inducers in the inhibition of tumor progression. *Oxidative Medicine and Cellular Longevity*, *2019*, 5729710. https://doi.org/10.1155/2019/5729710

Wang, E. M., Akasaka, H., Zhao, J., et al. (2019). Expression and Clinical Significance of Protein Kinase RNA-Like Endoplasmic Reticulum Kinase and Phosphorylated Eukaryotic Initiation Factor 2α in Pancreatic Ductal Adenocarcinoma. *Pancreas*, *48*(3), 323–328. https://doi.org/10.1097/MPA.0000000000001248

Warnakulasuriya, S., Kujan, O., Aguirre-Urizar, J. M., et al. (2021). Oral potentially malignant disorders: A consensus report from an international seminar on nomenclature and classification, convened by the WHO Collaborating Centre for Oral Cancer. *Oral Diseases*, *27*(8), 1862–1880. https://doi.org/https://doi.org/10.1111/odi.13704

Weaver, B. A. (2014). How Taxol/paclitaxel kills cancer cells. *Molecular Biology of the Cell*, *25*(18), 2677–2681. https://doi.org/10.1091/mbc.e14-04-0916

Weinstein, G. S., Quon, H., Newman, H. J., et al. (2012). Transoral robotic surgery alone for oropharyngeal cancer: an analysis of local control. *Archives of Otolaryngology–Head & Neck Surgery*, *138*(7), 628–634. https://doi.org/10.1001/archoto.2012.1166

Wek, R. C. (2018). Role of eIF2α Kinases in Translational Control and Adaptation to Cellular Stress. *Cold Spring Harbor Perspectives in Biology*, *10*(7), a032870. https://doi.org/10.1101/cshperspect.a032870

Wen, Y., & Grandis, J. R. (2015). Emerging drugs for head and neck cancer. *Expert Opinion on Emerging Drugs*, *20*(2), 313–329. https://doi.org/10.1517/14728214.2015.1031653

Westra, W. H. (2012). The morphologic profile of HPV-related head and neck squamous carcinoma: implications for diagnosis, prognosis, and clinical management. *Head and Neck Pathology*, *6* (Suppl 1), S48–S54. https://doi.org/10.1007/s12105-012-0371-6

Wilson, G., & Conway, D. I. (2016). Mouthwash use and associated head and neck cancer risk. *Evidence-Based Dentistry*, *17*(1), 8–9. https://doi.org/10.1038/sj.ebd.6401146

Wołącewicz, M., Becht, R., Grywalska, E., et al. (2020). Herpesviruses in head and neck cancers. *Viruses*, *12*(2), 172. https://doi.org/10.3390/v12020172

Wong, C. F., Barnes, L. M., Dahler, A. L., et al. (2003). E2F modulates keratinocyte squamous differentiation: implications for E2F inhibition in squamous cell carcinoma. *Journal of Biological Chemistry*, *278*(31), 28516–28522. https://doi.org/10.1074/jbc.M301246200

Wong, K. C. W., Hui, E. P., Lo, K.-W., et al. (2021). Nasopharyngeal carcinoma: an evolving paradigm. *Nature Reviews Clinical Oncology*, *18*(11), 679–695. https://doi.org/10.1038/s41571-021-00524-x

Wooten, D. J., Meyer, C. T., Lubbock, A. L. R., et al. (2021). MuSyC is a consensus framework that unifies multi-drug synergy metrics for combinatorial drug discovery. *Nature Communications*, *12*(1), 4607. https://doi.org/10.1038/s41467-021-24789-z

Worden, F. P., & Ha, H. (2008). Controversies in the management of oropharynx cancer. *Journal of the National Comprehensive Cancer Network*, *6*(7), 707–714. https://doi.org/10.6004/jnccn.2008.0053

Worsham, M. J., Stephen, J. K., Chen, K. M., et al. (2014). Delineating an epigenetic continuum in head and neck cancer. *Cancer Letters*, *342*(2), 178–184. https://doi.org/10.1016/j.canlet.2012.02.018

Yan, L.-H., Wei, W.-Y., Cao, W.-L., et al. (2014). Overexpression of E2F1 in human gastric carcinoma is involved in anti-cancer drug resistance. *BMC Cancer*, *14*(1), 904.

https://doi.org/10.1186/1471-2407-14-904

Zhang, N., Yin, Y., Xu, S.-J., et al. (2008). 5-Fluorouracil: mechanisms of resistance and reversal strategies. *Molecules*, *13*(8), 1551–1569. https://doi.org/10.3390/molecules13081551

Zhao, S., Tang, Y., Wang, R., et al. (2022). Mechanisms of cancer cell death induction by paclitaxel: an updated review. *Apoptosis*, *27*(9), 647–667. https://doi.org/10.1007/s10495-022-01750-z

Zhou, C., Ye, M., Ni, S., et al. (2018). DNA methylation biomarkers for head and neck squamous cell carcinoma. *Epigenetics*, *13*(4), 398–409. https://doi.org/10.1080/15592294.2018.1465790

Zhou, J. Z., Jou, J., & Cohen, E. (2021). Vaccine strategies for human papillomavirus-associated head and neck cancers. *Cancers*, *14*(1), 33. https://doi.org/10.3390/cancers14010033

Zhu, Y., Xia, X., Gao, L., et al. (2019). Prognostic implications of human papillomavirus type 16 status in non-oropharyngeal head and neck cancer: a propensity score matching analysis. *Annals of Translational Medicine*, *7*(23), 759. https://doi.org/10.21037/atm.2019.11.72

Supplement List:

Supplement S1. List of Probes Used for *EIF2S1* Gene Promoter Methylation Analysis. ..... **ii**

Supplement S2. Heatmap and Dendrogram Source Code. ..... **ii**

Supplement S3. Buffers and Reagents Used for Protein Isolation, Gel Electrophoresis and Western Blotting. ..... **iii**

(A) NP-40 Lysis Buffer iii

(C) 5x Loading Buffer (Laemmli buffer) iv

(D) Running Buffer iv

(E) Transfer Buffer iv

(F) TBS-T Buffer v

Supplement S4. Polyacrylamide Gels ..... **v**

(A) Separation Gels v

(B) Stacking Gel vi

Supplement S5. EIF2S1 Expression in Relation to HPV Status Determined by P16 Detection and *in situ* Hybridization (P16&ISH) ..... **vi**

Supplement S6. List of Cell Lines Used in CRISPR-Cas9 Knockdown Experiments. ..... **vii**

Supplement S7. Original, Uncropped Western Blots Conforming eIF2α Phosphorylation by Salubrinal and Densitometric Raw Data. ..... **viii**

Supplement S8. Original, Uncropped Western Blots and Raw Densitometric Data for Analysis of Cell Cycle Protein Levels. ..... **ix**

Supplement S1. List of Probes Used for *EIF2S1* Gene Promoter Methylation Analysis.

Illumina Id	RefGene_group
cg22868346	TSS200
cg00924576	TSS1500
cg01838419	TSS1500
cg14286928	TSS1500
cg06889607	TSS1500
cg00496170	TSS200
cg20908993	TSS1500
cg21926698	TSS1500

Supplement S2. Heatmap and Dendrogram Source Code.

```
 import pandas as pd
from scipy import stats
import matplotlib.pyplot as plt
import seaborn as sns

# Read the data
df = pd.read_csv('data_RNA_Seq_v2_expression_median.csv', sep=';', index_col=0)
df = df.T

# Choose a list of EIFs
eif_list = ["EIF1", "EIF1AX", "EIF2A", ..., "EIF5"]
eif_list = [eif.lower() for eif in eif_list]

df = df[[c for c in df.columns.values if str(c).lower() in eif_list]]
df.rename(index={'Hugo_Symbol':'mRNA'},inplace=True)

# Calculate correlations
corr = df.iloc[1:].astype(float).corr(method="spearman")
corr.to_csv('Correlations_EIF_08-05-2023.csv')

# Draw a heatmap
sns.set(font="Arial", font_scale=2)
clustered_data = sns.clustermap(corr,
                center=0,
                cmap="vlag",
                linewidths=.75,
                figsize=(40, 20),
                annot = False,
                annot_kws={"size": 6},
                vmin=-1,
                vmax=1
                )
plt.savefig('Heatmap_eif_08-06-2023.eps')
plt.show()
```

Supplement S3. Buffers and Reagents Used for Protein Isolation, Gel Electrophoresis and Western Blotting.

(A) NP-40 Lysis Buffer

Reagent	Final concentration
Tris HCl (pH 7.5)	50 mM
NaCl	150 mM
NP-40	1%

Immediately before use add 10 µl phosphatase inhibitor.
(PhosSTOP, Millipore Sigma, Germany) per 1ml of buffer.

(B) SDS Lysis Buffer

Reagent	Final concentration
10% SDS	2%
Tris HCl (pH 6.8)	50 mM
100% glycerol	10%
dH_2O	To 1000 ml

Immediately before use add 10 µl phosphatase inhibitor.
(PhosSTOP, Millipore Sigma, Germany) and 10 µl PMSF per 1ml of buffer.

(C) 5x Loading Buffer (Laemmli buffer)

Reagent	Final concentration
Tris (pH 6.8)	250 mM
SDS	10%
Glycerol	50%
Bromophenol blue	0.5%
β-mercaptoethanol	25%

(D) Running Buffer

Reagent	Final concentration
Tris HCl (pH 8.4)	250 mM
Glycine	192 mM
SDS	1%

(E) Transfer Buffer

Reagent	Final concentration
Tris (pH 9.2)	25 mM
Glycine	190 mM
Methanol	20%

(F) TBS-T Buffer

Reagent	Final concentration
Tris (pH 8.0)	0.2 M
NaCl	1.4 M
Tween® -20	0.1%
HCl	(pH adjustment)

Supplement S4. Polyacrylamide Gels

(A) Separation Gels

Reagent	Volume (ml)		
	8% gel	**10% gel**	**12% gel**
dH_2O	4.6	4.0	3.3
TRIS 1.5 M (pH 8.8)	2.5	3.3	4.0
Acrylamide	2.7	2.5	2.5
10% SDS	0.1	0.1	0.1
Ammonium Persulfate	0.1	0.1	0.1
TEMED	0.006	0.004	0.004

(B) Stacking Gel

Reagent	Volume (ml)
dH_2O (Mq)	3.1
TRIS 1.5 M (pH 6.8)	1.25
Acrylamide	0.5
10% SDS	0.05
Ammonium Persulfate	0.025
TEMED	0.0075

Supplement S5. EIF2S1 Expression in Relation to HPV Status Determined by P16 Detection and *in situ* Hybridization (P16&ISH)

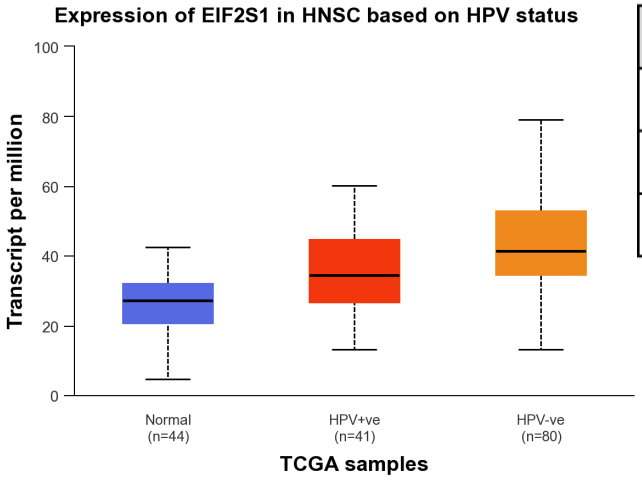

Comparison	Statistical significance
Normal-vs-HPV+ve	**4.25E-04**
Normal-vs-HPV-ve	**1.74E-12**
HPV+ve-vs-HPV-ve	6.42-02

Supplement S6. List of Cell Lines Used in CRISPR-Cas9 Knockdown Experiments.

1. A253
2. BB30HNC
3. BB49HNC
4. BHY
5. BICR10
6. BICR16
7. BICR18
8. BICR22
9. BICR31
10. BICR56
11. BICR6
12. BICR78
13. CA922
14. CAL27
15. CAL33
16. CGTHW1
17. DETROIT562
18. DOK
19. FADU
20. H103
21. H157
22. H3118
23. H357
24. H376
25. H413
26. HN
27. HO1N1
28. HO1U1
29. HSC2
30. HSC3
31. HSC4
32. HSQ89
33. JHU011
34. JHU022
35. JHU029
36. KON
37. KOSC2
38. LB771HNC
39. OSC19
40. OSC20
41. PCI15A
42. PCI30
43. PCI38
44. PCI4B
45. PCI6A
46. PECAPJ15
47. PECAPJ34 CLONEC12
48. PECAPJ41 CLONED2
49. PECAPJ49
50. RPMI2650
51. SAS
52. SAT
53. SCC15
54. SCC25
55. SCC4
56. SCC9
57. SKN3
58. SNU1041
59. SNU1066
60. SNU1076
61. SNU1214
62. SNU46
63. SNU899
64. SW579
65. T3M5
66. TR146
67. UPCISCC026
68. UPCISCC029A
69. UPCISCC040
70. UPCISCC074
71. UPCISCC090
72. UPCISCC111
73. UPCISCC116
74. UPCISCC131
75. UPCISCC152
76. UPCISCC154
77. UPCISCC200
78. YD10B
79. YD15
80. YD38
81. YD8

Supplement S7. Original, Uncropped Western Blots Conforming eIF2α Phosphorylation by Salubrinal and Densitometric Raw Data.

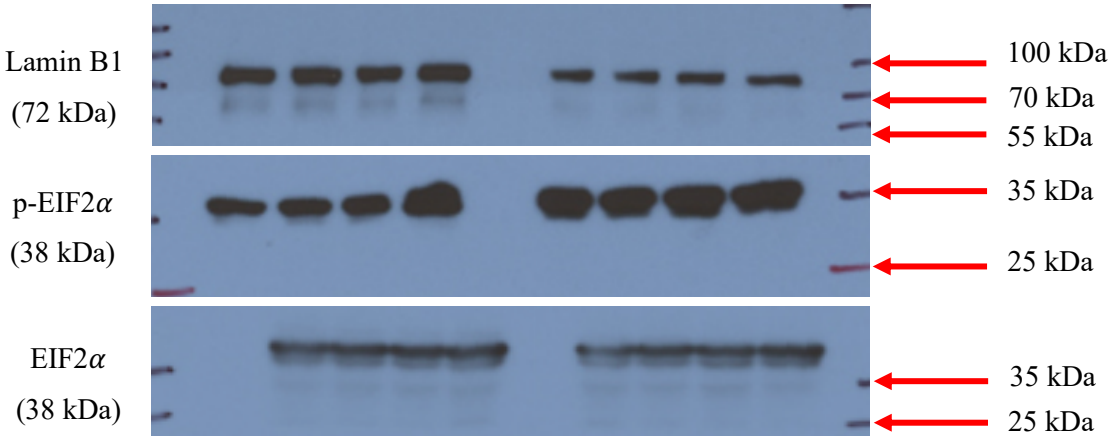

12h		Lamin B1	
			normalized
FaDu	NT	4386.527	1
	10	4093.648	0.93323214
	20	3269.87	0.74543483
	50	4419.406	1.00749545
SCC4	NT	3357.577	1
	10	3429.698	1.02148007
	20	3771.456	1.12326717
	50	3665.456	1.09169678

12h		p- eIF2a		
			normalized	norm to Lamin B1
FaDu	NT	5042.355	1	1
	10	5188.598	1.02900292	1.102622667
	20	5502.426	1.09124129	1.463898994
	50	9134.447	1.81154381	1.798066492
SCC4	NT	8344.083	1	1
	10	8448.912	1.01256327	0.991270706
	20	9450.447	1.13259264	1.008302099
	50	10076.912	1.20767159	1.106233538

12h		eIF2a		
			normalized	norm to Lamin B1
FaDu	NT	6696.669	1	1
	10	5762.376	0.86048392	0.922047023
	20	5712.205	0.85299199	1.144287811
	50	6539.983	0.9766024	0.969336781
SCC4	NT	6874.811	1	1
	10	5759.619	0.8377858	0.820168515
	20	6414.912	0.93310376	0.830705098
	50	7347.79	1.06879884	0.979025363

Supplement S8. Original, Uncropped Western Blots and Raw Densitometric Data for Analysis of Cell Cycle Protein Levels.

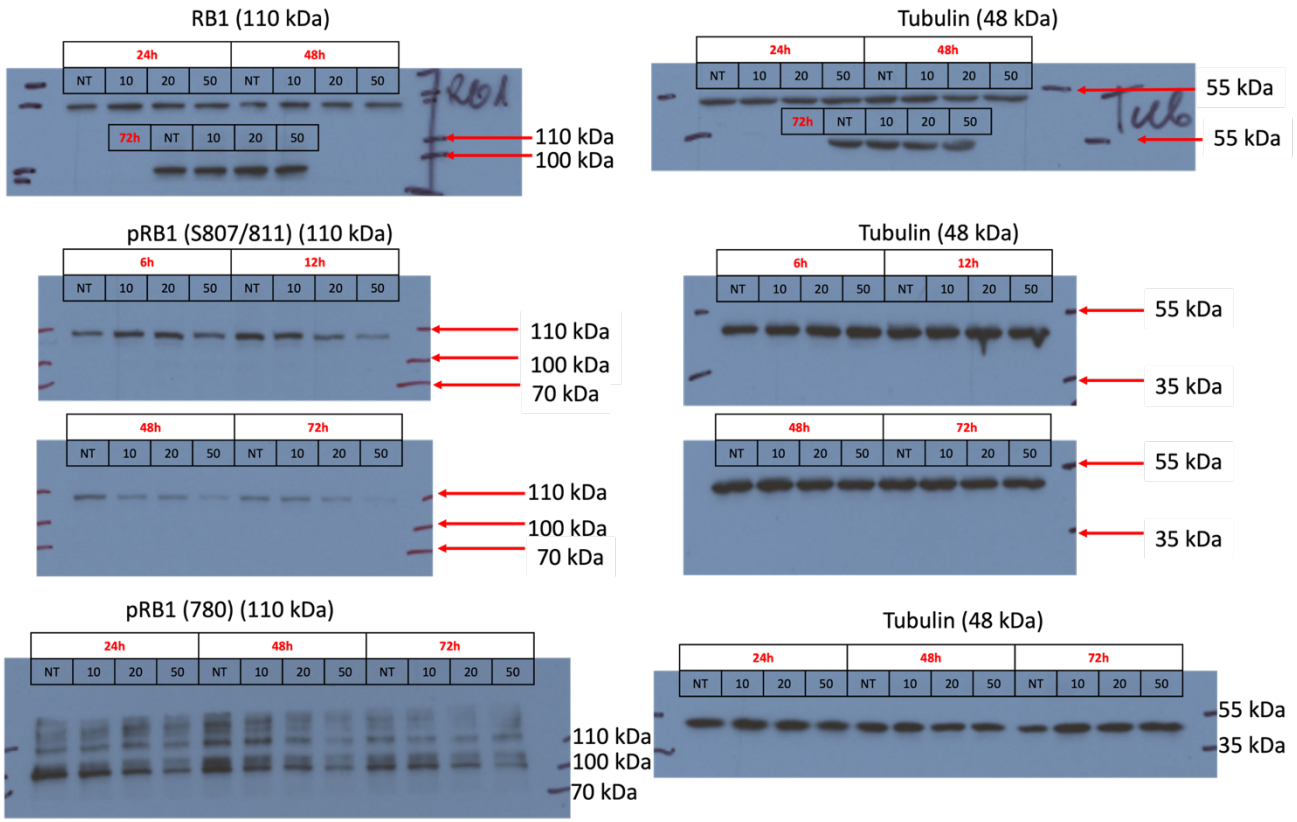

	RB1			normalized - tubulin
12h	NT	18281.915	1	1
	10	19026.329	1.0407186	1.00299327
	20	24757.371	1.35420009	1.37787475
	50	21346.886	1.16765043	1.02814504
24h	NT	8479.853	1	1
	10	15694.723	1.85082489	1.83542887
	20	11909.581	1.40445607	1.96115398
	50	11029.217	1.30063776	1.49700466
72h	NT	6853.903	1	1
	10	11660.995	1.70136563	1.47895513
	20	9570.51	1.39635913	1.50575698
	50	9757.752	1.42367816	1.75709369

	Tubulin for RB1		
12h	NT	6809.447	1
	10	7065.569	1.03761275
	20	6692.447	0.98281799
	50	7733.397	1.1356865
24h	NT	8141.518	1
	10	8209.811	1.00838824
	20	5830.447	0.71613758
	50	7073.569	0.8688268
72h	NT	8795.225	1
	10	10117.882	1.15038353
	20	8156.225	0.92734694
	50	7126.296	0.81024601

	pRB1 (807/811)			normalized - tubulin
12h	NT	34838.413	1	1
	10	33657.927	0.96611539	0.99826244
	20	24235.472	0.69565373	1.01330247
	50	15140.945	0.4346049	0.99967121
24h	NT	19551.622	1	1
	10	11589.53	0.59276565	0.99711047
	20	13077.187	0.66885433	1.00821872
	50	6043.681	0.30911405	1.00796556
72h	NT	15260.551	1	1
	10	15936.915	1.04432107	1.04506873
	20	9164.874	0.60055984	1.03780298
	50	2561.347	0.16784106	1.02077908

	Tubulin for pRB1 (807/811)		
12h	NT	103930.806	1
	10	103750.22	0.99826244
	20	105313.342	1.01330247
	50	103896.635	0.99967121
24h	NT	102700.978	1
	10	102404.22	0.99711047
	20	103545.049	1.00821872
	50	103519.049	1.00796556
72h	NT	99531.463	1
	10	104017.22	1.04506873
	20	103294.049	1.03780298
	50	101599.635	1.02077908

	pRB1 (780)			normalized - tubulin
12h	NT	15758.53	1	1
	10	12350.945	0.78376251	0.67465576
	20	8991.631	0.57058818	0.53518512
	50	5032.418	0.31934565	0.36845895
24h	NT	15285.702	1	1
	10	9944.924	0.65060303	0.64787285
	20	7552.681	0.49410102	0.56869988
	50	3655.175	0.23912379	0.2937009
72h	NT	9573.167	1	1
	10	9416.045	0.98358725	0.49775874
	20	5188.66	0.54200036	0.30619843
	50	3754.589	0.39219926	0.18715051

	Tubulin for pRB1 (780)		
12h	NT	9747.054	1
	10	11323.368	1.1617221
	20	10391.832	1.06615106
	50	8447.832	0.86670619
24h	NT	8641.054	1
	10	8677.468	1.00421407
	20	7507.569	0.86882561
	50	7035.326	0.81417452
72h	NT	5386.912	1
	10	10644.711	1.97603209
	20	9535.347	1.77009519
	50	11289.004	2.0956355

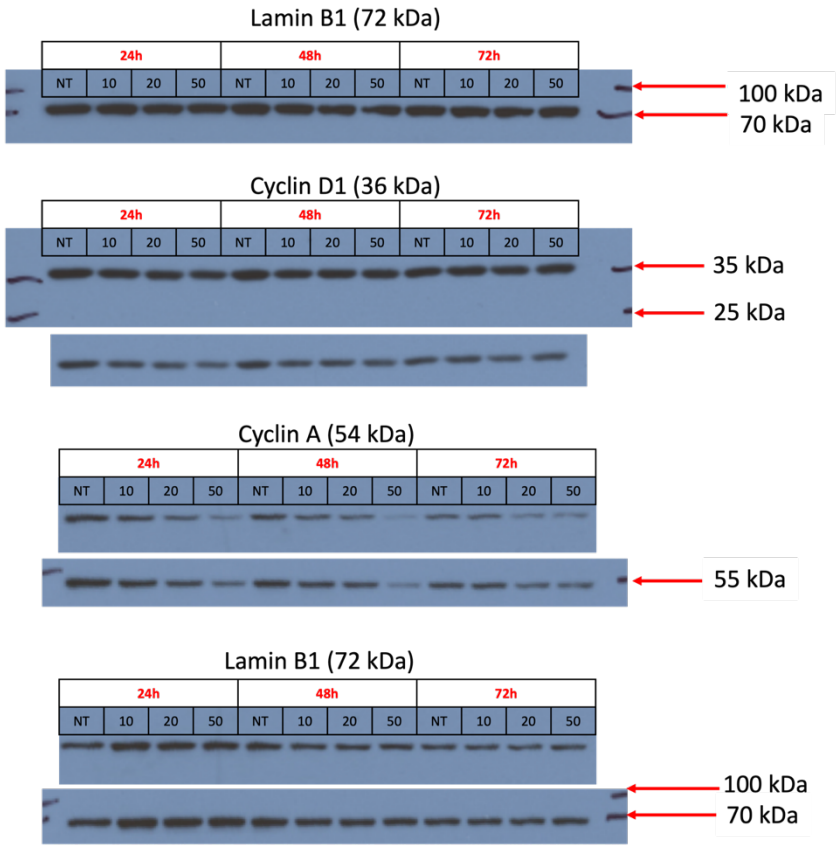

		Cyclin D1		normalized to lamin B1
24h	NT	8661.933	1	1
	10	5658.154	0.65322071	0.549761595
	20	4425.276	0.51088781	0.644875775
	50	3251.619	0.37539184	0.485000026
48h	NT	7154.104	1	1
	10	4774.154	0.66733081	0.72426685
	20	5348.447	0.74760543	1.311855507
	50	4344.74	0.60730736	1.271753148
72h	NT	5258.447	1	1
	10	5499.861	1.04590975	1.159733272
	20	3695.205	0.70271793	1.044944397
	50	4638.154	0.88203875	0.860293397

		lamin B1 for cyclin D1	
24h	NT	15280.217	1
	10	14976.439	0.98011952
	20	13354.024	0.87394204
	50	16032.501	1.04923255
48h	NT	14352.823	1
	10	12973.51	0.90389953
	20	11880.024	0.82771341
	50	10805.368	0.75283921
72h	NT	12452.246	1
	10	12690.731	1.01915197
	20	11657.489	0.93617561
	50	10829.167	0.86965572

		Cyclin A		normalized to lamin B1
24h	NT	7878.033	1	1
	10	4616.548	0.58600262	0.38940132
	20	2412.598	0.3062437	0.22409677
	50	889.941	0.11296487	0.08743681
48h	NT	4734.083	1	1
	10	2723.598	0.57531691	0.81761253
	20	1980.184	0.41828248	0.59591744
	50	311.678	0.06583704	0.0942296
72h	NT	2259.891	1	1
	10	2232.719	0.98797641	1.11925661
	20	831.406	0.3678965	0.47447439
	50	738.527	0.32679762	0.34071388

		lamin B1 for cyclin A	
24h	NT	6429.619	1
	10	9675.811	1.50488093
	20	8786.518	1.366569
	50	8306.811	1.29196007
48h	NT	7129.447	1
	10	5016.669	0.70365472
	20	5004.255	0.70191349
	50	4981.255	0.69868743
72h	NT	4039.719	1
	10	3565.891	0.88270768
	20	3132.305	0.77537695
	50	3874.719	0.95915557

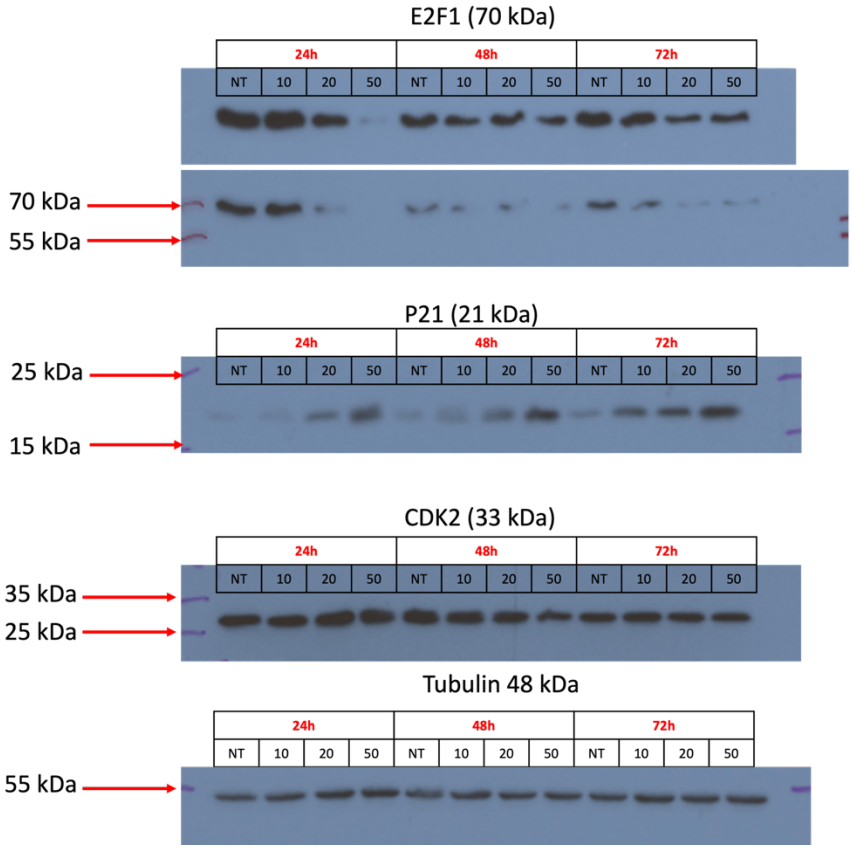

	P21			normalized to Tubulin
24h	NT	568.849	1	1
	10	875.678	1.53938567	1.53938567
	20	39776.765	69.9249977	69.9249977
	50	39800.869	69.967371	69.967371
48h	NT	1232.163	1	1
	10	39767.246	32.2743387	32.2743387
	20	39788.735	32.2917788	32.2917788
	50	39797.555	32.2989369	32.2989369
72h	NT	1537.548	1	1
	10	5317.539	3.45845398	3.45845398
	20	7211.66	4.69036414	4.69036414
	50	13522.631	8.79493258	8.79493258

	Tubulin for P21, E2F1, CDK2		
24h	NT	3298.326	1
	10	5074.347	1.53846133
	20	6508.882	1.97338953
	50	7618.468	2.30979836
48h	NT	5834.832	1
	10	4410.468	0.75588603
	20	3277.861	0.5617747
	50	2976.447	0.510117
72h	NT	3007.276	1
	10	4596.054	1.52831134
	20	4025.761	1.3386736
	50	4704.175	1.56426447

	E2F1			normalized to Tubulin
24h	NT	19750.459	1	1
	10	20130.51	1.01924264	0.66250781
	20	10673.539	0.54041979	0.27385358
	50	156.192	0.00790827	0.00342379
48h	NT	10515.368	1	1
	10	6797.811	0.64646439	0.85524056
	20	8488.368	0.80723452	1.4369364
	50	5014.569	0.47688003	0.93484442
72h	NT	13229.61	1	1
	10	10446.489	0.7896294	0.51666789
	20	5531.276	0.41809819	0.31232273
	50	7584.882	0.5733262	0.36651488

	CDK2			normalized to Tubulin
24h	NT	14661.338	1	1
	10	13936.681	0.95057361	0.61787293
	20	16696.752	1.13882867	0.57709269
	50	14046.095	0.95803637	0.41477056
48h	NT	14663.146	1	1
	10	13404.024	0.91413016	1.20934919
	20	11846.489	0.80790909	1.4381372
	50	8214.125	0.56018845	1.09815679
72h	NT	10730.075	1	1
	10	11830.782	1.10258148	0.72143774
	20	10068.832	0.9383748	0.70097356
	50	9654.589	0.89976901	0.57520261

Publications related to the presented dissertation:

Patent

Haybaeck J, Cyran AM, Arens C, Naumann M, *Eukaryotic translation initiation factors as novel biomarkers in head and neck squamous cell carcinoma.* US Patent US2020033334A1, EU Patent EP3725898B1

Publications in peer reviewed journals

1. Cyran AM, Kleinegger F, Nass N, Naumann M, Haybaeck J, Arens C. Inhibition of EIF2α Dephosphorylation Decreases Cell Viability and Synergizes with Standard-of-Care Chemotherapeutics in Head and Neck Squamous Cell Carcinoma, Cancers 2023; 15, 5350. https://doi.org/10.3390/cancers15225350.
2. Cyran AM, Nass N, Świerczyński P, Sprung S, Naumann M, Haybaeck J, Arens, Ch, Expression of eukaryotic initiation factors (eIFs) in head and neck squamous cell carcinoma (HNSCC) and its potential therapeutic implications, Laryngo-Rhino-Otologie. 2020 May;99.
3. Cyran AM, Nass N, Sprung S, Haybaeck J and Arens Ch, Expression and therapeutic potential of the eukaryotic initiation factor 2α (eIF2α) in head and neck squamous cell carcinomas (HNSCC), Laryngo-Rhino-Otologie. 2019 Apr; 98:11192.
4. Davaris N, Voigt-Zimmermann S, Cyran AM, Arens C, Endoskopische Frühdiagnostik von Karzinomen im oberen Aerodigestivtrakt (Endoscopic early diagnosis of carcinomas of upper respiratory and digestive tract), Laryngo-Rhino-Otologie. 2018 Apr;97(4):276-286, (in German).

Congress contributions

1. 4th Joint Annual Meeting of the Swiss and Austrian Societies of Pathology and 1st Joint Annual Meeting of the Swiss Societies of Pathology and Cytology, Luzern, Switzerland, 2019 *Expression levels of eukaryotic initiation factors (eIFs) are significantly altered in head and neck squamous cell carcinomas (HNSCC)* (oral presentation)
2. 90th Annual Meeting of the German Society of Oto-Rhino-Laryngology, Head and Neck Surgery, Berlin, Germany, 2018 *Expression and therapeutic potential of the eukaryotic initiation factor 2α (eIF2α) in head and neck squamous cell carcinomas (HNSCC)* (oral presentation)

Other publications by the author

1. Siewiera J, Smoleński M, Jermakow N, Kot J, Reichert TE, Miśkiewicz P, Zareba Ł, Cyran AM, Szczepański MJ, and Ludwig N. *Levels of small extracellular vesicles in patients treated with hyperbaric oxygenation*, Archives of Medical Science. 2024;20(1). doi:10.5114/aoms/169382.
2. Ursu M, Cyran AM, Zhitkovich A. *Mercury (II)-induced abnormalities in processing of topoisomerase I-mediated DNA damage*, Cancer Res 1 April 2023; 83 (7 Supplement): 1218. https://doi.org/10.1158/1538-7445.AM2023-1218.
3. Cyran AM, Zhitkovich A. *Heat Shock Proteins and HSF1 in Cancer* Frontiers in Oncology 2022 Mar 2;12:860320. doi: 10.3389/fonc.2022.860320. PMID: 35311075; PMCID: PMC8924369.
4. Cyran AM, Zhitkovich A. *HIF1, HSF1, and NRF2: Oxidant-Responsive Trio Raising Cellular Defenses and Engaging Immune System* Chemical research in toxicology 2022; 35, 10, 1690–1700.
5. Poślednik KB, Czerwaty K, Ludwig N, Molińska-Glura M, Jabłońska-Pawlak A, Miśkiewicz P, Kantor I, Dżaman K, Cyran AM, Szczepański MJ. *Treatment Results of Endoscopic Transnasal Orbital Decompression for Graves' Orbitopathy-A Single-Center Retrospective Analysis in 28 Orbits of 16 Patients*. Journal of Personalized Medicine. 2022 Oct 14;12(10):1714. doi: 10.3390/jpm12101714. PMID: 36294853; PMCID: PMC9605419.
6. Piszczatowska K, Czerwaty K, Cyran AM, Fiedler M, Ludwig N, Brzost J, Szczepański MJ, *The Emerging Role of Small Extracellular Vesicles in Inflammatory Airway Diseases*, Diagnostics (Basel). 2021 Feb 2;11(2):222.
7. Cyran AM, Kosla A, Kantor I, Szczepanski MJ, *Tympanometric Evaluation of Eustachian Tube Function in Polish Scuba-Divers*, Undersea Hyperb Med. 2018 Jul-Aug;45(4):437-443.
8. Brzost J, Cyran AM, Waniewska M, Szczepanski MJ, *Extracranial Internal Carotid Artery Aneurysm Mimicking Peritonsillar Abscess*, Case Rep Otolaryngol., 2015; 2015:389298. doi: 10.1155/2015/389298.

9. Szczepanski MJ, Cyran AM, Krzeski A, *Uraz ciśnieniowy uszu i zatok przynosowych zwiazany z nurkowaniem (Otic and paranasal sinus barotrauma in the population of Polish scuba-divers)*, Mag. Orl., 2014, Nr. 51, XIII, 114–122, (in Polish).

Other congress contributions by the author

1. American Association for Cancer Research Annual Meeting 2023, Orlando, FL, USA, 2023 *Mercury (II)-induced abnormalities in processing of topoisomerase I-mediated DNA damage* (poster presentation)
2. The Brazilian International Congress of Medical Students, Sao Paulo, Brazil, 2015 *Comparison of tympanometric parameters in scuba-divers and non-diving healthy volunteers* (oral presentation)
   *Prize for one of three best oral presentations
3. 9th Leiden International Medical Students' Conference, Leiden, Netherlands, 2015 *Preliminary evaluation of Nd:Yag laser surgery in recurrent respiratory papillomatosis* (poster presentation)
4. RhinoForum, Warsaw, Poland, 2014 *Spontaneous cerebrospinal fluid leak - case report and literature review* (oral presentation)
5. 10th Warsaw International Medical Students' Conference, Warsaw, Poland, 2014 *Extracranial internal carotid artery aneurysm mimicking peritonsillar abscess – case report* (oral presentation)

Ehrenwörtliche Erklärung

„Hiermit erkläre ich, dass ich die vorliegende Arbeit selbständig und ohne unzulässige Hilfe oder Benutzung anderer als der angegebenen Hilfsmittel angefertigt habe. Alle Textstellen, die wörtlich oder sinngemäß aus veröffentlichten oder nichtveröffentlichten Schriften entnommen sind, und alle Angaben, die auf mündlichen Auskünften beruhen, sind als solche kenntlich gemacht. Bei den von mir durchgeführten und in der Dissertation erwähnten Untersuchungen habe ich die Grundsätze guter wissenschaftlicher Praxis, wie sie in der „Satzung der Justus-Liebig-Universität Gießen zur Sicherung guter wissenschaftlicher Praxis“ niedergelegt sind, eingehalten sowie ethische, datenschutzrechtliche und tierschutzrechtliche Grundsätze befolgt. Ich versichere, dass Dritte von mir weder unmittelbar noch mittelbar geldwerte Leistungen für Arbeiten erhalten haben, die im Zusammenhang mit dem Inhalt der vorgelegten Dissertation stehen, und dass die vorgelegte Arbeit weder im Inland noch im Ausland in gleicher oder ähnlicher Form einer anderen Prüfungsbehörde zum Zweck einer Promotion oder eines anderen Prüfungsverfahrens vorgelegt wurde. Alles aus anderen Quellen und von anderen Personen übernommene Material, das in der Arbeit verwendet wurde oder auf das direkt Bezug genommen wird, wurde als solches kenntlich gemacht. Insbesondere wurden alle Personen genannt, die direkt und indirekt an der Entstehung der vorliegenden Arbeit beteiligt waren. Mit der Überprüfung meiner Arbeit durch eine Plagiatserkennungssoftware bzw. ein internetbasiertes Softwareprogramm erkläre ich mich einverstanden.“

Berlin, 26. Mai 2025

Anna M. Cyran

Dedication

I wish to dedicate this work to my husband, Piotr who relentlessly supported me throughout the years in all my endeavors. His assistance and encouragement throughout this project have been invaluable- from imparting the necessary programming and mathematical skills to ensuring there was always a hot cup of tea amidst the stacks of research papers on my desk. For him, no early morning hour was ever too late to collect me from work and inquire about my western blots.
The completion of this work has only been possible with your patience and steadfast belief in me. Thank you for standing behind me every step of the way.

Acknowledgements

First and foremost, I wish to sincerely thank Prof. Dr. med. Christoph Arens, whose unwavering support and mentorship have been instrumental throughout the years of my academic journey. I am truly grateful for the invaluable lessons learned under his mentorship at the very beginning of my career, both as a researcher and a clinician. Without any doubt, his direction and vision of translating scientific progress into patient care are what made this project possible.

I also want to express my deepest gratitude to Priv.-Doz. Norbert Naß for generously sharing his extensive research expertise and insights. Our fruitful discussions about translational oncology have gone beyond the immediate scope of my work, enriching my understanding of the field and contributing to my growth as a researcher.

I would like to express my appreciation to the entire team at the experimental laboratory at the Institute for Pathology, Otto-von-Guericke University, Magdeburg, for their generosity in sharing molecular biology techniques and providing me with technical support whenever needed. Your collaborative spirit has fostered a positive and enriching research environment.

Special thanks go to Susanne Sprung, Regina Moritz, and Piotr Czapiewski for their patience and assistance with microscopic evaluation of tissues.